



---

Masters Theses

Graduate School

---

5-2011

## Cross-Flow, Staggered-Tube Heat Exchanger Analysis for High Enthalpy Flows

Gary L. Hammock

*University of Tennessee Space Institute*, ghammock@utk.edu

Follow this and additional works at: [https://trace.tennessee.edu/utk\\_gradthes](https://trace.tennessee.edu/utk_gradthes)

 Part of the Aerodynamics and Fluid Mechanics Commons, Energy Systems Commons, and the Heat Transfer, Combustion Commons

---

### Recommended Citation

Hammock, Gary L., "Cross-Flow, Staggered-Tube Heat Exchanger Analysis for High Enthalpy Flows." Master's Thesis, University of Tennessee, 2011.  
[https://trace.tennessee.edu/utk\\_gradthes/877](https://trace.tennessee.edu/utk_gradthes/877)

---

This Thesis is brought to you for free and open access by the Graduate School at TRACE: Tennessee Research and Creative Exchange. It has been accepted for inclusion in Masters Theses by an authorized administrator of TRACE: Tennessee Research and Creative Exchange. For more information, please contact [trace@utk.edu](mailto:trace@utk.edu).

To the Graduate Council:

I am submitting herewith a thesis written by Gary L. Hammock entitled "Cross-Flow, Staggered-Tube Heat Exchanger Analysis for High Enthalpy Flows." I have examined the final electronic copy of this thesis for form and content and recommend that it be accepted in partial fulfillment of the requirements for the degree of Master of Science, with a major in Mechanical Engineering.

Basil Antar, Major Professor

We have read this thesis and recommend its acceptance:

Trevor Moulden, Alfonso Pujol

Accepted for the Council:  
Carolyn R. Hodges

Vice Provost and Dean of the Graduate School

(Original signatures are on file with official student records.)

# **Cross-Flow, Staggered-Tube Heat Exchanger Analysis for High Enthalpy Flows**

A Thesis Presented for  
the Master of Science Degree

The University of Tennessee, Knoxville

Gary L. Hammock  
May 2011

## **Acknowledgement**

The work reported herein was done at Arnold Engineering Development Center (AEDC) on the author's own time. This report was approved for public release on February 2, 2011 under AEDC PA Number: AEDC2011-006. Distribution of this document is unlimited.

## **Abstract**

Cross flow heat exchangers are a fairly common apparatus employed throughout many industrial processes. For these types of systems, correlations have been extensively developed. However, there have been no correlations done for very high enthalpy flows as produced by Arnold Engineering Development Center's (AEDC) H2 facility. The H2 facility uses a direct current electric arc to heat air which is then expanded through a converging-diverging nozzle to impart a supersonic velocity to the air. This high enthalpy, high temperature air must be cooled downstream by the use of a cross flow heat exchanger.

It is of interest to evaluate the actual performance of the air cooler to determine the effectiveness of possible facility upgrades. In order to characterize cooler effectiveness, a numerical model is built to calculate per-tube-row energy balances using real (temperature and pressure dependent) air and water properties and cross-flow Nusselt number calculations.

## Table of Contents

1.0 Introduction .....	1
1.1 Facility Description .....	1
1.2 Problem Description.....	4
2.0 Methodology.....	7
2.1 Analysis Technique .....	7
2.2 Heat Transfer Models .....	11
2.2.1 Grimison Model.....	17
2.2.2 Modified Grimison Model .....	21
2.2.3 Zhukauskas Model .....	23
2.2.4 Kays & London Model .....	27
2.2.5 First Law Analysis .....	29
2.2.6 Heat Exchanger Effectiveness .....	30
2.3 Pressure Drop Models.....	31
2.3.1 Holman-Jakob Model .....	31
2.3.2 Gunter-Shaw Model.....	32
2.3.3 Boucher and Lapple's Correction to the Gunter-Shaw Model .....	33
2.3.4 Zhukauskas Model .....	34
2.3.5 Kays & London Model .....	36
3.0 Results and Discussion.....	40
3.1 Group 1 .....	42
3.2 Group 2 .....	48
3.3 Group 3 .....	58
3.4 Group 4 .....	63
3.5 Possible Test Condition.....	69
3.6 Influence of Variables.....	72
3.7 Real Gas Effects .....	73
4.0 Conclusions .....	78
References .....	81
Appendices .....	84
Vita .....	95

## List of Tables

Table 1 - Constants of Equation 13 for airflow over a staggered tube bank <sup>[7][8]</sup> ....	18
Table 2 - Correction factor <i>C2</i> of equation 13 for staggered tubes with <i>NL</i> < 10 <sup>[7]</sup> .	18
Table 3 - Correction factor <i>C2</i> for staggered tubes with <i>NL</i> < 20 <sup>[9][11]</sup> for <i>Re</i> < 1000	24
Table 4 - Correction factor <i>C2</i> for staggered tubes with <i>NL</i> < 20 <sup>[7]</sup> for <i>Re</i> ≥ 1000 ...	24
Table 5 - Constants of equation 18 for airflow over a staggered tube bank <sup>[7]</sup> .....	24
Table 6 - Constants of equation 19 for airflow over a staggered tube bank <sup>[7]</sup> .....	25
Table 7 - Air Prandtl Number at Typical Tube Wall Temperatures .....	26
Table 8 - Zhukauskas Equation Prandtl Number Relative Error Considerations .....	26
Table 9 - Model Inputs for the H2 Air Cooler .....	42
Table 10 - Program Inputs for Run H2-031-024 .....	42
Table 11 - Program Inputs for Run H2-031-021 .....	49
Table 12 - Program Inputs for Run H2-031-023 .....	53
Table 13 - Program Inputs for Run H2-031-020 .....	58
Table 14 - Program Inputs for Run H2-031-019 .....	64
Table 15 - Input Conditions for Representative High Heat Flux Run .....	70
Table 16 - Static Thermodynamic Properties used in Original Model .....	74

## List of Figures

Figure 1 - Schematic of a Huels Arc Heater.....	1
Figure 2 - Aft View of the AEDC H <sub>2</sub> Arc Heater .....	2
Figure 3 - The Inlet of H <sub>2</sub> 's Cross Flow, Staggered Tube Heat Exchanger .....	3
Figure 4 - Cross Sectional View of the H <sub>2</sub> Cooler .....	4
Figure 6 - Thermodynamic Properties of air at 1.5 psia.....	5
Figure 7 - Program Overview Flowchart.....	8
Figure 8 - Row Solver Algorithm Overview Flowchart .....	9
Figure 9 - Air Thermodynamic Properties Solver Overview .....	10
Figure 10 - Single Tube Control Volume .....	11
Figure 11 - Equivalent Resistance Circuit Analogy .....	12
Figure 12 - Staggered Tube Free Body Diagram .....	16
Figure 13 - Comparison of the <i>c</i> <sub>1</sub> Coefficients with Fitted Data .....	20
Figure 14 - Comparison of the <i>m</i> Exponents with Fitted Data .....	20
Figure 15 – $\xi_H$ Correction to the Original Grimison Model ( <i>Pr</i> = 0.69) .....	22
Figure 16 - Kays & London influence of <i>N<sub>L</sub></i> variations in the heat transfer coefficient <sup>[12]</sup> .....	29
Figure 17 - Gunter-Shaw Crossflow Friction Factors .....	32
Figure 18 - Friction Factor for Zhukauskas Pressure Drop Model (Equation 39) ....	35
Figure 19 - Geometry Correction Factor for Zhukauskas Pressure Drop Model.....	35
Figure 20 - Control Volume of a Single Tube Row .....	37
Figure 21 - Heat Exchanger Flow Diagram .....	40
Figure 22 - H <sub>2</sub> -031 Run Conditions .....	41

Figure 23 - Air Temperature v. Axial Distance (Row Number) for Various Heat Transfer Models for H2-031-024 .....	43
Figure 24 - Inlet Water Manifold Temperature Comparisons by Heat Transfer Model for Run H2-031-024.....	44
Figure 25 - Tube Temperatures per Row as Calculated for H2-031-024 (Inset: Temperature of Tubes in the First Row) .....	45
Figure 26 - Calculated Reynolds Number by Heat Transfer Model for H2-031-024	45
Figure 27 - Pressure Drop Model Comparisons for H2-031-024.....	47
Figure 28 - Air Temperature v. Axial Distance (Row Number) for Various Heat Transfer Models for H2-031-021 .....	49
Figure 29 - Inlet Water Manifold Temperature Comparisons by Heat Transfer Model for Run H2-031-021.....	50
Figure 30 - Tube Temperatures per Row as Calculated for H2-031-021.....	51
Figure 31 - Comparison of Pressure Drop Models for H2-031-021 .....	52
Figure 32 - Air Temperature v. Axial Distance (Row Number) for Various Heat Transfer Models for H2-031-023 .....	53
Figure 33 - Inlet Water Manifold Temperature Comparisons by Heat Transfer Model for Run H2-031-023 .....	55
Figure 34 - Tube Temperatures per Row as Calculated for H2-031-023.....	55
Figure 35 - Calculated Reynolds Number by Heat Transfer Model for H2-031-023	56
Figure 36 - Comparison of Pressure Drop Models for H2-031-023 .....	57
Figure 37 - Air Temperature v. Axial Distance (Row Number) for Various Heat Transfer Models for H2-031-020 .....	59

Figure 38 - Inlet Water Manifold Temperature Comparisons by Heat Transfer Model for Run H2-031-020 .....	60
Figure 39 - Tube Temperatures per Row as Calculated for H2-031-020.....	61
Figure 40 - Calculated Reynolds Number by Heat Transfer Model for H2-031-020	61
Figure 41 - Comparison of Pressure Drop Models for H2-031-020 .....	63
Figure 42 - Air Temperature v. Axial Distance (Row Number) for Various Heat Transfer Models for H2-031-019 .....	65
Figure 43 - Inlet Water Manifold Temperature Comparisons by Heat Transfer Model for Run H2-031-019.....	66
Figure 44 - Tube Temperatures per Row as Calculated for H2-031-019.....	66
Figure 45 - Calculated Reynolds Number by Heat Transfer Model for H2-031-019	68
Figure 46 - Comparison of Pressure Drop Models for H2-031-019 .....	68
Figure 47 - Tube Temperatures of Representative High Heat Flux Condition .....	71
Figure 48 - Calculated Reynolds Number for Representative High Heat Flux Condition.....	71
Figure 49 - Influence Coefficients on the Nusselt Number Calculation for the Four Heat Transfer Models .....	72
Figure 50 - Air Temperature Comparisons Using Static Properties and Real Gas Properties for H2-031-020 .....	75
Figure 51 - Calculated Tube Wall Temperature Comparisons Using Static Properties and Real Gas Properties for H2-031-020 .....	75
Figure 52 - Air Temperature Comparison for High Enthalpy, Notional Condition....	76
Figure 53 - Calculated Tube Wall Temperature Comparison for High Enthalpy, Notional Condition .....	76

## List of Symbols / Nomenclature

$A_{min}$	Minimum free flow area
$A_f$	Individual fin surface area
$A_{FR}$	Flow entrance frontal area
$A_{surf,i}$	Tube wall inside surface area
$A_{surf,o}$	Tube wall outside surface area
$A_T$	Finned tube corrected area, $A_T = nA_f + A_{surf,o}$
$c_p$	Constant pressure specific heat
$C_f$	Kays & London pressure drop arrangement factor
$C_h$	Kays & London heat transfer arrangement factor
$d_{in}$	Inner diameter
$d_{out}$	Outer diameter
$D_v$	Volumetric Hydraulic Diameter, $D_v = \frac{4 \times (\text{Net Free Volume})}{(\text{Friction Surface})}$
$f$	Friction factor
$g$	Acceleration due to gravity
$g_c$	Unit conversion constant, $g_c \equiv \begin{cases} 32.17 \frac{\text{lb}_m \cdot \text{ft}}{\text{lbf} \cdot \text{s}^2} & \text{for English Units} \\ 1.0 & \text{for SI Units} \end{cases}$
$G$	Mass velocity, $G = \rho V$
$h$	Convective heat transfer coefficient
$H$	Heat exchanger height
$i$	Enthalpy
$j_H$	Colburn-j heat transfer factor, $j_H = StPr^{2/3}$
$k$	Thermal conductivity
$\ell$	Heat exchanger axial length
$L$	Tube length (equal to the heat exchanger width)
$\dot{m}$	Mass flow rate
$N_f$	Number of fins per tube
$N_L$	Number of tube rows in bank
$N_T$	Number of tubes per row

$Nu$	Nusselt Number, $Nu \equiv \frac{hd_{out}}{k}$
$P$	Pressure
$Pr$	Prandtl Number, $Pr = \frac{\mu c_p}{k}$
$\dot{q}$	Heat transfer rate
$r$	radius
$R$	Thermal resistance
$\mathbb{R}$	Gas constant
$Re$	Reynolds Number, $Re \equiv \frac{\rho V d}{\mu}$
$S_D$	Diagonal pitch, $S_D = \sqrt{S_L^2 + \left(\frac{S_T}{2}\right)^2}$
$S_L$	Longitudinal tube pitch
$S_T$	Transverse tube pitch
$St$	Stanton Number, $St \equiv \frac{h}{G c_p}$
$t$	Fin thickness
$T$	Temperature
$W$	Heat exchanger width (Equal to tube length)
$\nu$	Specific volume, $\nu = \frac{1}{\rho}$
$V$	Velocity
$z$	Elevation
$\gamma$	Ratio of specific heats, $\gamma \equiv \frac{c_P}{c_V}$ .
$\eta_f$	Fin Efficiency
$\mu$	Absolute viscosity
$\xi_H$	Correction factor to the Grimison model for low $Re$
$\rho$	Density
$\sigma$	Ratio of minimum free flow area to frontal area, $\sigma = \frac{A_{min}}{A_{FR}}$

# 1.0 Introduction

## 1.1 Facility Description

The H<sub>2</sub> arc heater is an N-4 Huels-type arc heated ground test facility used to simulate representative hypersonic heating environments for hypersonic materials testing. The facility uses a high-voltage, direct-current power supply to generate an electric arc discharge heating the working fluid to a total temperature of up to 5,300 K (9,600°R) at total pressures of up to 100 atm. The facility exhausts into a subatmospheric test cell providing high enthalpy flows at Mach numbers ranging from 3.4 to 7 in order to simulate hypersonic flight at simulated pressure altitudes ranging from 20 to 50 km (70 to 160 kft).<sup>[1][2]</sup>

The Huels-type arc heater is one of the simplest arc heater configurations available. The facility is usually configured to use dry air as the working fluid, but recent testing has successfully demonstrated that nitrogen is a viable test gas as well.<sup>[3]</sup> Figure 1 shows a notional schematic of a Huels arc heater. Figure 2 shows an aft view of the H<sub>2</sub> Huels heater at AEDC's High Temperature Lab.

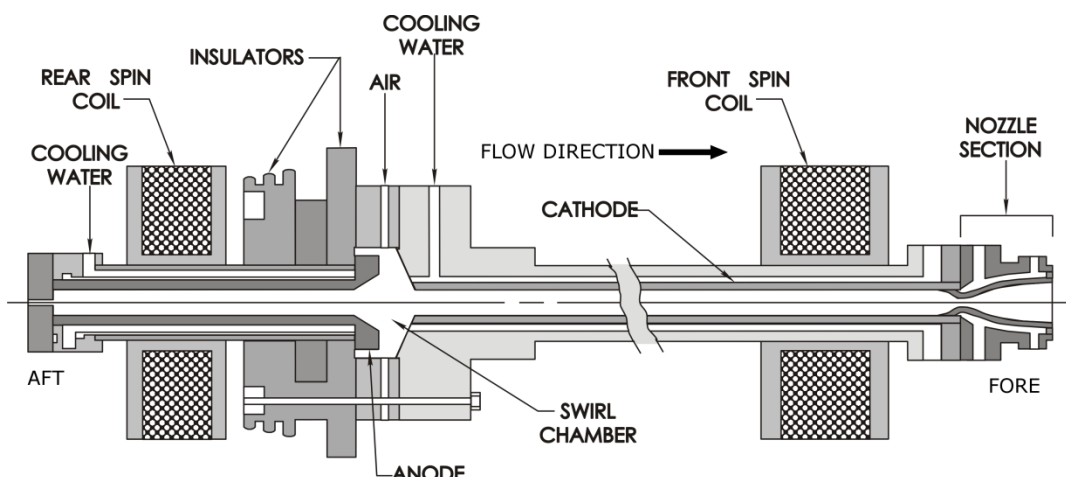


**Figure 1 - Schematic of a Huels Arc Heater**

As seen in figure 1, the H<sub>2</sub> arc heater consists of two coaxial electrodes separated by a swirl chamber. The working fluid (air or nitrogen) is injected circumferentially into the heater at the electrode interface. This injection causes the electric arc to be vortex stabilized—meaning that the test gas has a tangential velocity component that helps to fix the arc at the bore centerline<sup>[3]</sup>. This interaction with the arc causes the working fluid to be heated before expanding through the nozzle. The heated gas is used to subject material specimens to high temperature and high shear environments for survivability testing. After exposure on the test material coupons, this high temperature flow must be brought to a lower temperature before being forwarded to the exhaust air plant compressors, which are used to generate the subatmospheric condition in the test cell.

Downstream of the test cell, a 95 foot long diffuser is used for pressure recovery and removes some heat energy from the flow through its water cooled

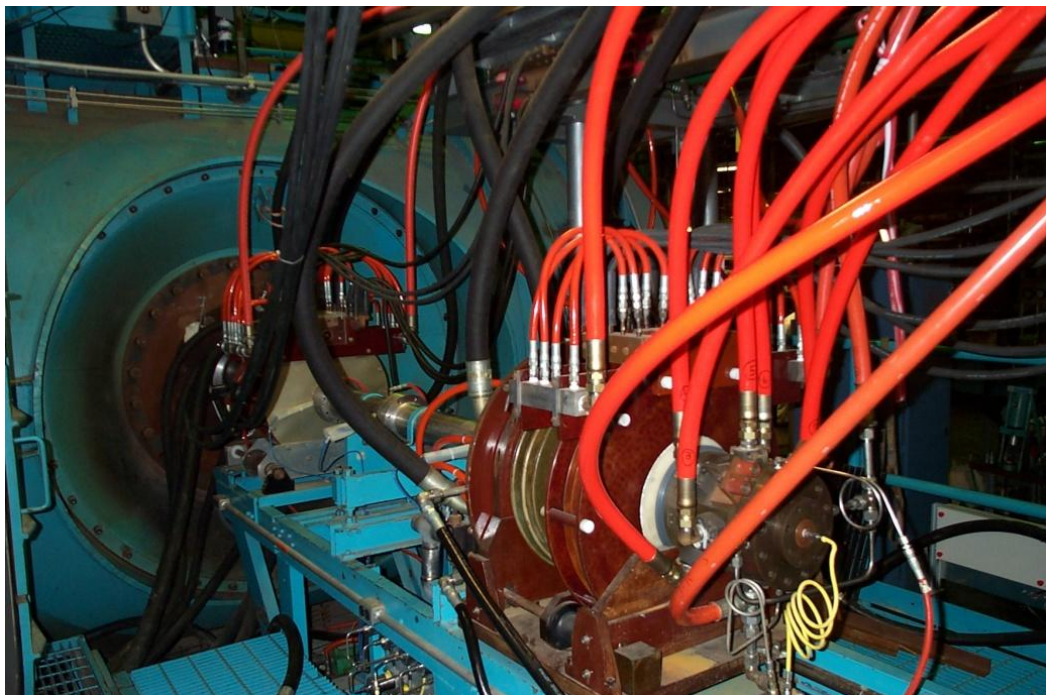


**Figure 2 - Aft View of the AEDC H<sub>2</sub> Arc Heater**

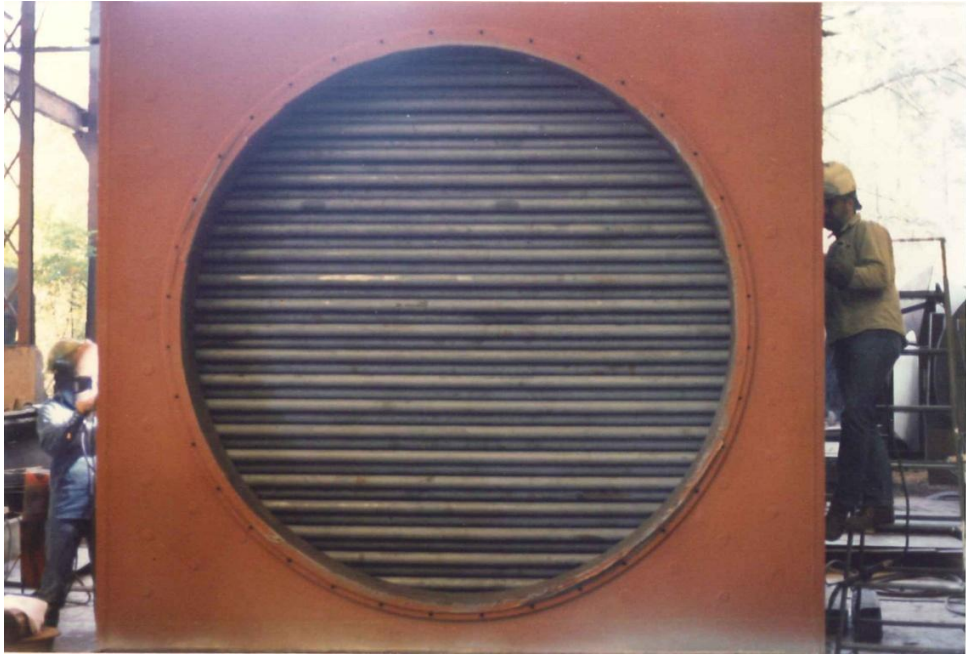


**Figure 3 - The Inlet of H2's Cross Flow, Staggered Tube Heat Exchanger**

walls. A water-cooled cross flow heat exchanger is used on the downstream side of the diffuser to further reduce the air temperature. The inlet of this heat exchanger may be seen in figure 3. Figure 4 shows a cross sectional view of the heat exchanger as installed in the H2 exhaust air system.

The objective of this study is the analysis of the heat transfer taking place within this water-cooled cross flow heat exchanger. Dry air will be considered the working fluid. As seen in figure 4, the air "cooler" consists of a series of varying-diameter staggered tubes. The geometry variation is due to strength requirements needed to prevent punctures should a material sample break during testing. The most downstream tube rows (consistent with topical literature, *row* is defined as a *vertical* series of tubes at the same axial location), are helically finned tubes.

The heat energy is removed from the system by untreated reservoir water at local ambient temperature. The water is screened and filtered upstream of the

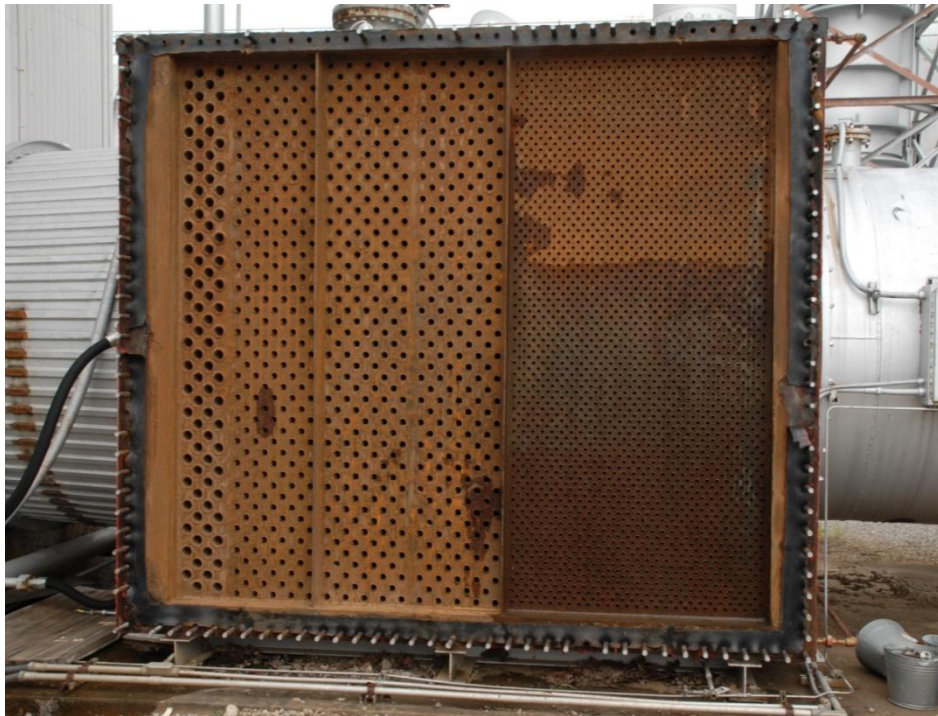


**Figure 4 - Cross Sectional View of the H2 Cooler**

water pumps to remove large particulates from the flow. High flow rate water pumps provide the pressure differential to flow this water at volumetric flow rates over 10,000 gallons per minute through the heat exchanger. For the analyses presented here, the cooling water is considered to be pure.

## **1.2 Problem Description**

In the interest of considering possible facility upgrades, it is vital to determine the thermal margin that is available within the existing cooler. When the current device was procured in 1987, a low fidelity model was developed using statically determined properties at standard temperature and pressure. To account for the higher temperatures of the flow, a  $\gamma$  value of 1.2 was used. The old model used the Grimison heat transfer model for banks of staggered tubes and the Gunter-Shaw relations to account for pressure drop through the tube banks.

It is necessary to use real gas (temperature and pressure dependent) properties to refine the calculated results. Coupled with this, higher fidelity heat transfer and pressure drop relations are needed to improve the numerical accuracy of the model. As will be shown later, these provide a significant improvement in the efficacy of the model at certain conditions.

As can be seen in figure 5, there is significant variation in the thermodynamic properties of air over the range of enthalpies and temperatures seen throughout the heat exchanger. The curves used in figure 5 are generated from the property fit data presented by Gupta, et al. in reference [4]. These data are presented in Appendix D for a nominal air pressure of 1.5 psia.

Note the discontinuity in the Prandtl number curve. The Prandtl number is a calculated parameter using the specific heat, the thermal conductivity, and the

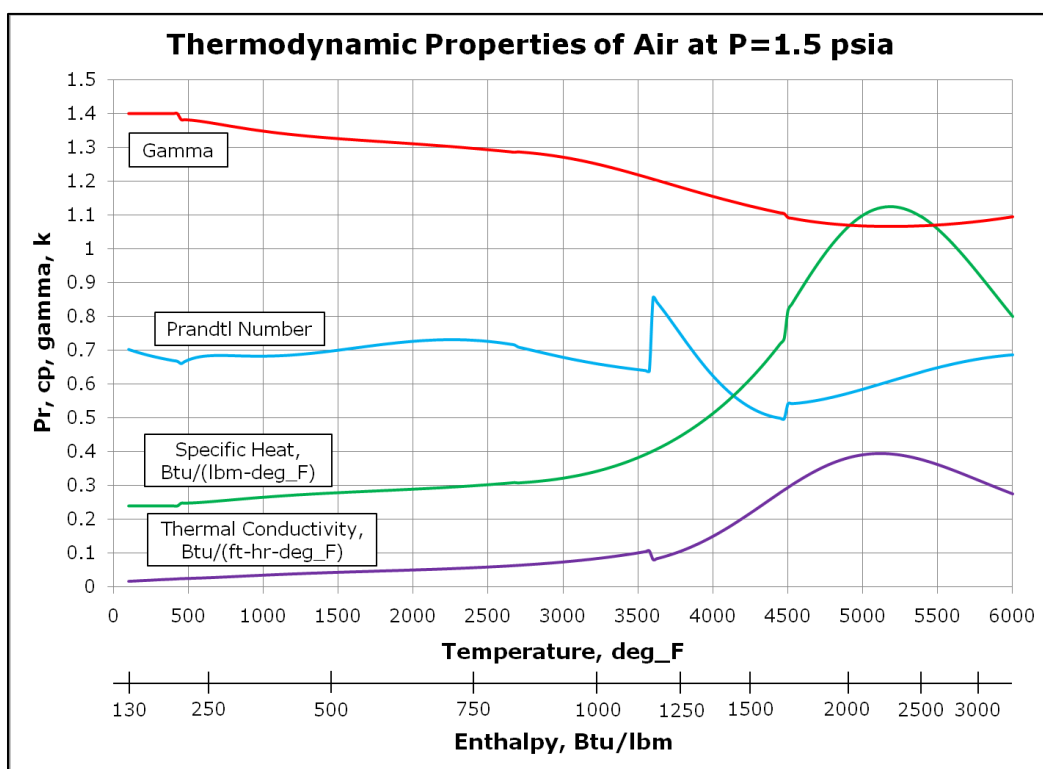


Figure 5 - Thermodynamic Properties of air at 1.5 psia

viscosity. The discontinuity lies on the boundary of a thermal calculation range and is due to having finite precision in the curve fit coefficients. Also, these data were interpolated for the given pressure regime. The program does not attempt to correct for these discontinuous regions in the curve, using only the discrete values calculated by the thermodynamic properties function. This may be improved upon in a later revision to the numeric model.

Total enthalpy is a facility-calculated parameter and is used as an input to the program. The other two air-side program inputs are the mass flow rate of the air and the diffuser exit / cooler inlet pressure. From the pressure and enthalpy, it is then possible to determine the remaining thermodynamic properties using the relations presented by Gupta, et al. in reference [4]. This is further detailed in the next chapter.

For the calculation of water-side heat transfer, the cooling water inlet temperature, inlet pressure, and volumetric flow rate (all measured parameters with the facility) are given as program inputs.

## **2.0 Methodology**

### **2.1 Analysis Technique**

A computer program was written to better model the heat transfer taking place within the H2 air cooler. The program, written in C++, calculates the heat transfer from the air to the cooling water on a row-by-row basis using convective relations for the air and water interfaces and conduction equations for the tube walls. The cooler inlet state is given for air and water, as well as the cooler geometry and material properties. The flowchart in figure 6 shows an overview of the program functionality.

The calculations that take place within the main calculation loop (labeled "Solve Row<sub>j</sub>" in the flowchart), are presented by figure 7. For each row, the thermodynamic properties of air and water are computed based on the inlet states. For the initial tube row, the cooler inlet properties are used. For successive downstream tube rows, the outlet state of the previous tube row is initialized as the inputs for the current row of interest.

In order to first begin a higher fidelity model, a better evaluation of air properties must be used. For this purpose, a function was developed to calculate real gas properties for equilibrium air at temperatures between 0-30,000 K (0-54,000°R) and pressures between  $10^{-4}$ -100 atm based on the curve fit data from Gupta, et al. in reference [4]. The thermodynamic properties calculated by these equations represent a three dimensional surface with temperature and pressure as the abscissae and the relevant thermodynamic property as the ordinate.

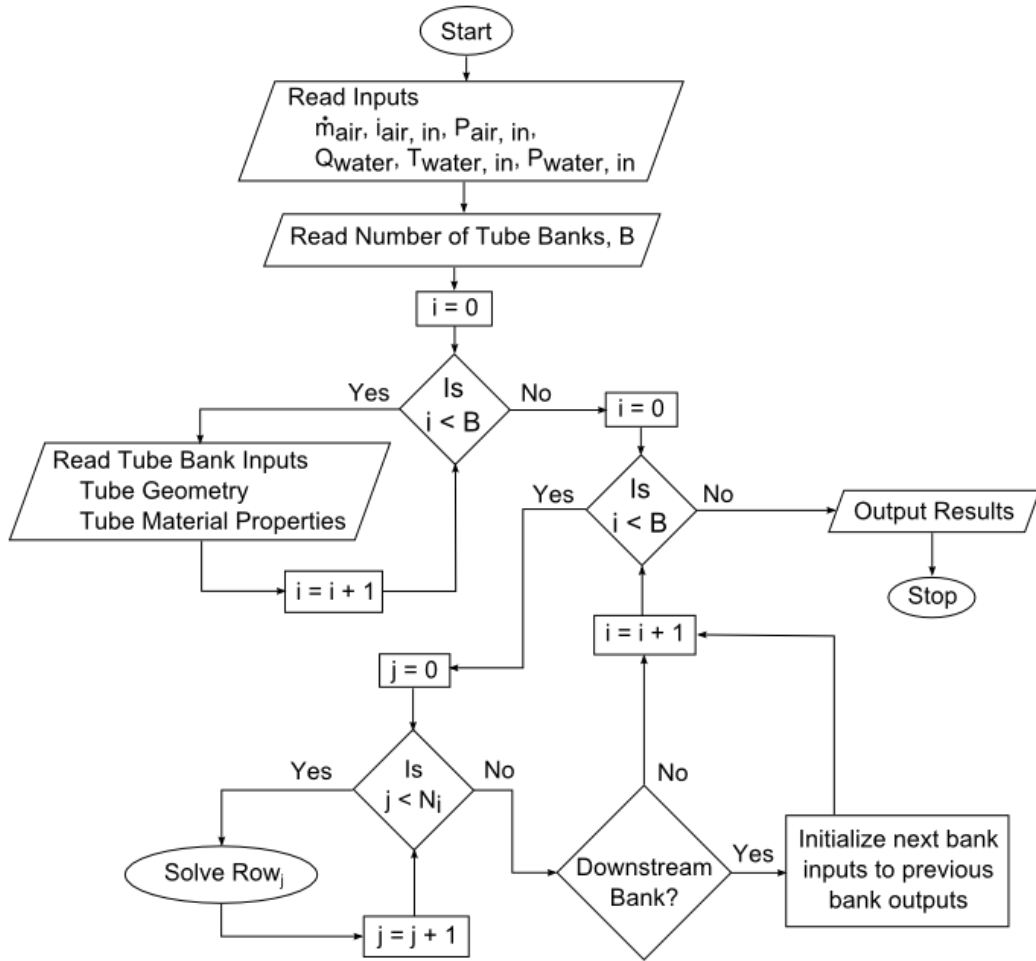


**Figure 6 - Program Overview Flowchart**

Because total enthalpy is given as the program input, an iterative loop is used to converge on the inlet air temperature for the given inlet pressure by minimizing the residual error in the enthalpy calculation. Once the temperature is calculated, the remaining thermodynamic properties are calculated using their respective surface fit equations, the calculated temperature, and the input pressure. This operation is notionally shown in the flowchart given in figure 8. Similarly, the thermodynamic properties of water are computed by data given by

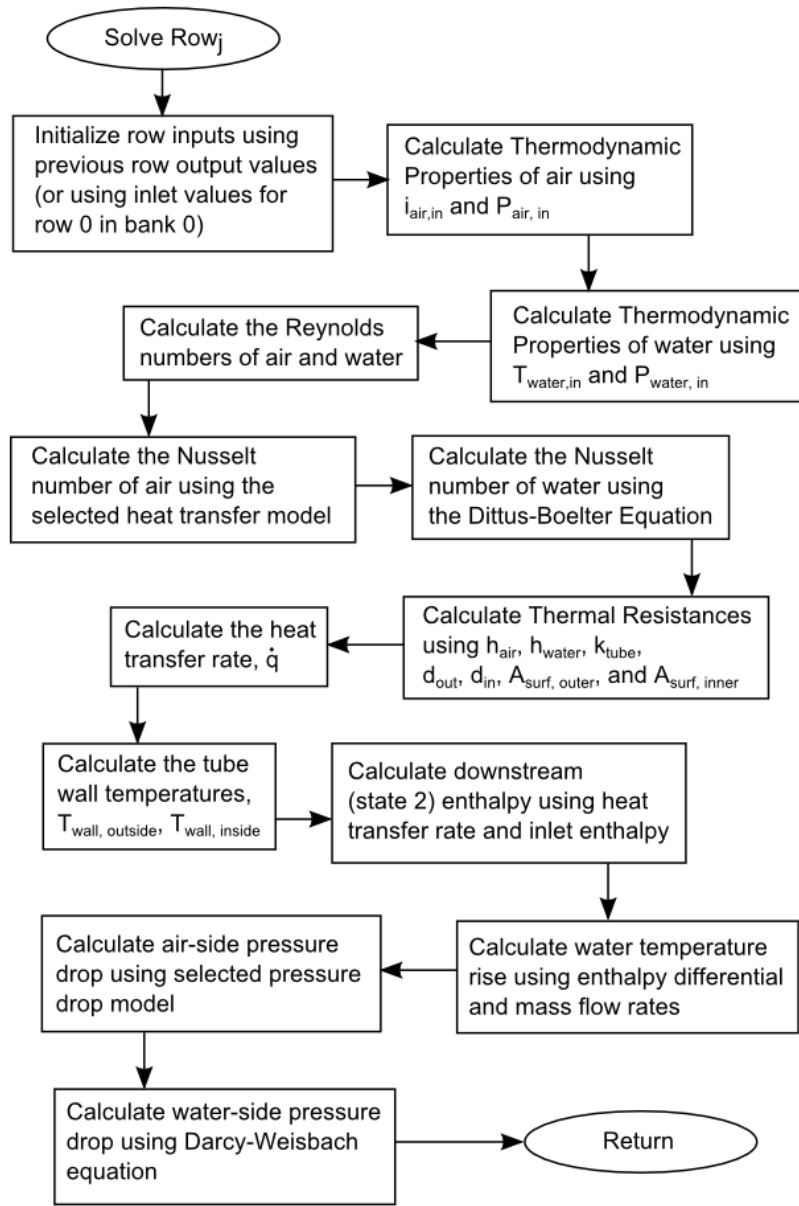


**Figure 7 - Row Solver Algorithm Overview Flowchart**

the International Association for the Properties of Water and Steam (IAPWS) in references [5] and [6].

The program compares four different heat transfer correlations to determine which has the smallest residual error when compared to the measured data. The heat transfer correlations are used to compute the Nusselt number characterizing

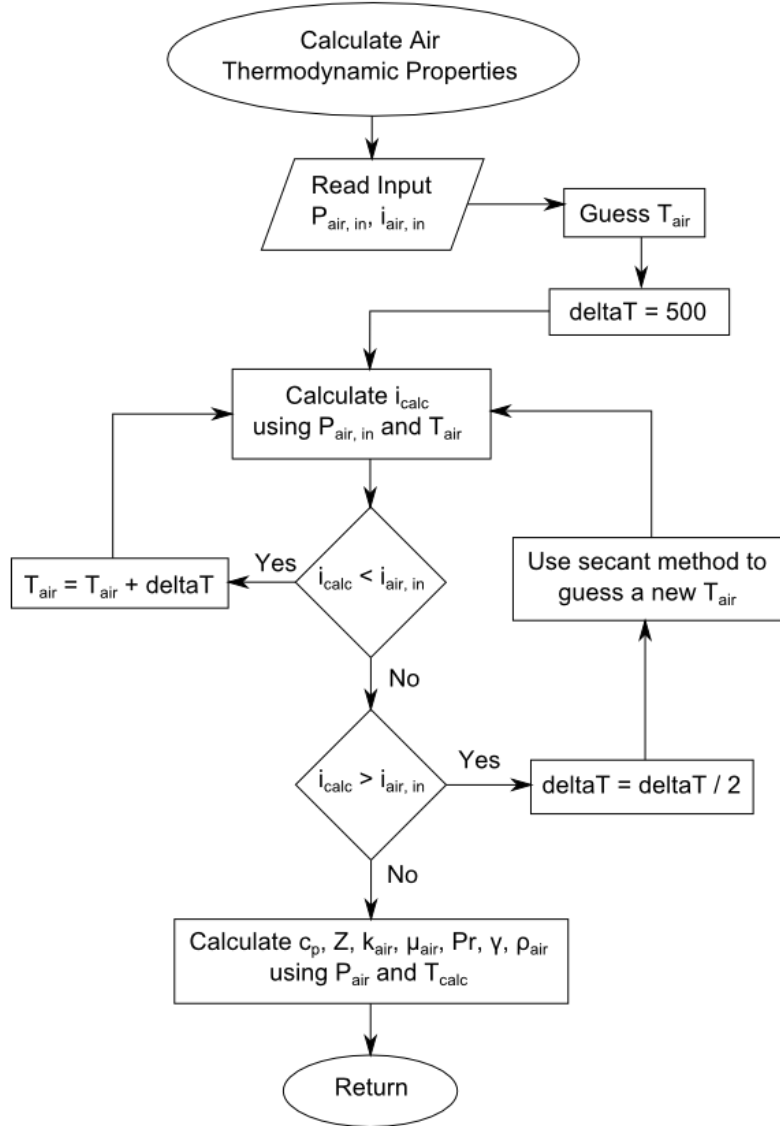


**Figure 8 - Air Thermodynamic Properties Solver Overview**

the convective strength of the flow. This is used to calculate the heat transfer from the air to the cooling water using the first law of thermodynamics. Then the water temperature rise is cumulatively fed forward through the discretized heat exchanger equations.

The program also compares several different pressure drop models to determine which relationship gives the best match to the measured data. For

completeness, the Darcy-Weisbach pressure drop equation is used to model the water-side pressure drop; though this varies the thermodynamic properties little.

## **2.2 Heat Transfer Models**

Traditional empirical methods for heat exchanger analysis typically specify a lower bound Prandtl number of 0.7 and a lower bound Reynolds number of 2000. For the inlet conditions of the H<sub>2</sub> cooler, the temperatures are high enough that the air may have a Prandtl number around 0.55 and the Reynolds number may be less than 150. These input conditions must be acceptable for the heat transfer models used by the program.

When evaluating the heat transfer from the air to the cooling water, the efficacy of the energy exchange is typically a function of the Reynolds number of the flow, the Prandtl number of the flow, and a coefficient that is empirically

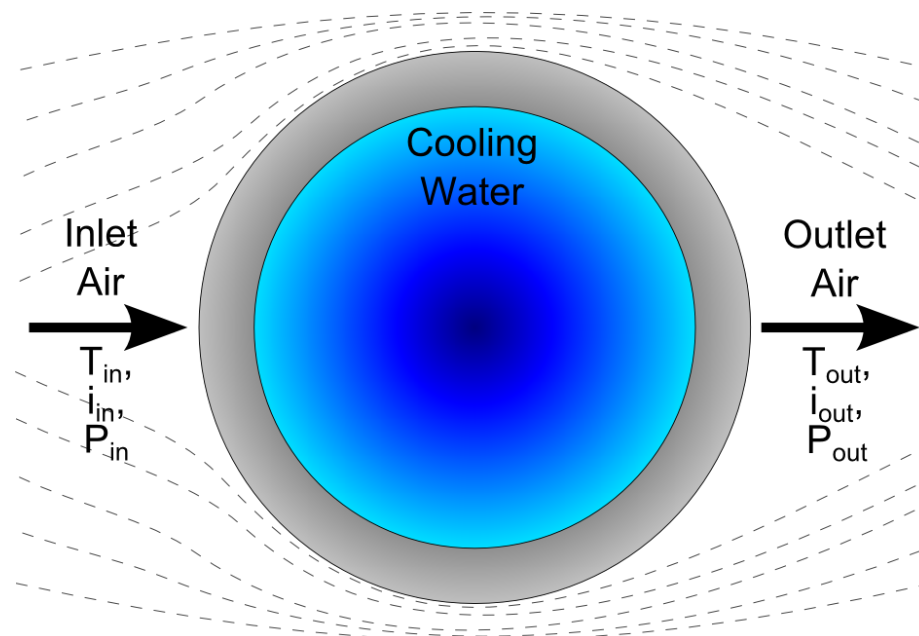


**Figure 9 - Single Tube Control Volume**

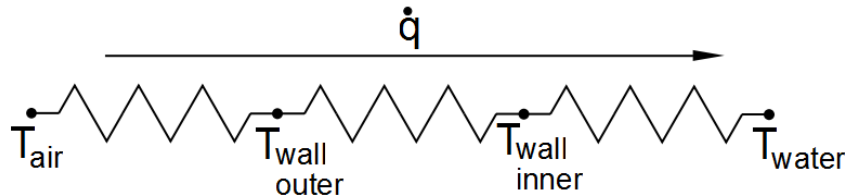


**Figure 10 - Equivalent Resistance Circuit Analogy**

determined based on the heat exchanger geometry and tube arrangement. These factors are used to evaluate the Nusselt number,  $Nu$ , and is typically expressed by a similarity equation of the form<sup>[8][9]</sup>:

$$Nu \propto \varphi(Re)^m(Pr)^n \quad (1)$$

where  $\varphi$  is a generic scalar variable

The Nusselt number is used to calculate the convective heat transfer coefficient ( $h$ ) which is used to quantify the heat energy transferred from the air to the tube wall ( $\dot{q}$ ).

Before it is possible to quantify the amount of heat transfer through the system, the control volume of interest must be defined and the analytic models for the calculation must be developed. Consider the control volume around a single tube as shown in figure 9. This control volume has elements of internal flow convection (the cooling water), external flow convection (cross flow of air over a body), and conduction heat transfer (through the tube wall).

It may be observed that the system may be modeled by use of a circuit analogy as applied to the heat transfer relations as shown in figure 10. By this analogy, the heat transfer may be computed directly using the known inlet air and water temperatures and a calculated equivalent thermal resistance using equation 2 below.

$$\dot{q} = \frac{T_{air} - T_{water}}{R_{eq}} \quad (2)$$

From the first law of thermodynamics, equation 2 can be expressed as:

$$\dot{q} = \frac{T_{air} - T_{water}}{R_{eq}} = \dot{m}_{air} \Delta i = \dot{m}_{air} (i_{in} - i_{out}) \quad (3)$$

where  $i_{in}$  is the inlet air enthalpy and  $i_{out}$  is the outlet air enthalpy as shown for the single tube control volume in figure 9.

The equivalent thermal resistance of this system is given as the sum of the individual resistances—these being the air-side convection term, the tube wall conduction term, and the water-side convection term.

$$R_{eq} = R_{air} + R_{wall} + R_{water} \quad (4)$$

The water-side thermal resistance is calculated based on the result of the Dittus-Boelter equation<sup>[7]</sup> for internal flow:

$$Nu = 0.023(Re)^{4/5}(Pr)^n$$

Where:  $n = 0.4$  (for heating) (5)  
 $n = 0.3$  (for cooling)

The operation of the heat exchanger is such that the air temperature is greater than the water temperature; thus, from an internal flow perspective, the cooling water will be heated and the exponent  $n = 0.4$  is used.

From equation 5, the convective coefficient was evaluated as:

$$h_{water} = \frac{(Nu) k_{water}}{d_{in}} = \frac{0.023 (Re)^{0.8} (Pr)^{0.4} k_{water}}{d_{in}} \quad (6)$$

The results of equation 6 were used to evaluate the water-side thermal resistance as:

$$R_{water} = \frac{1}{h_{water} A_{surf,i}} \quad (7)$$

Now, the tube wall thermal resistance must be evaluated. This is done by recognizing that the conduction equation in cylindrical coordinates is given by

$$\dot{q} = -kA \frac{dT}{dr} = -k(2\pi r L) \frac{dT}{dr} \quad (8)$$

For a hollow cylinder, this becomes<sup>[7]</sup>:

$$\dot{q} = \frac{2\pi L k (T_{s,1} - T_{s,2})}{\ln\left(\frac{r_2}{r_1}\right)} \quad (9)$$

Based on equation 9, it can be seen that the thermal resistance for a hollow cylinder is given by:

$$R_{wall} = \frac{\ln\left(\frac{d_{out}}{d_{in}}\right)}{2\pi k_{wall} L} \quad (10)$$

The air-side thermal resistance is of significant interest. The cross-flow environment in this particular application is such that the conditions are outside of the bounds of traditional heat transfer models. The air-side thermal resistance

follows the form of equation 11 for smooth-tubes with a modification for finned tubes to account for the increased surface area as shown in equation 11a. A derivation of equation 11a may be found in Appendix A.

$$R_{air} = \frac{1}{h_{air}A_{surf,o}} \quad (11)$$

$$\left(\text{for finned tubes}^{[7]}\right) \quad R_{air} = \frac{1}{h_{air}A_T \left[ 1 - \frac{N_f A_f}{A_T} (1 - \eta_f) \right]} \quad (11a)$$

Similar to equation 6, the air-side convective heat transfer coefficient is evaluated as:

$$h_{air} = \frac{(Nu) k_{air}}{d_{out}} \quad (12)$$

The air-side convective heat transfer coefficient cannot be determined without first calculating the Nusselt number. As mentioned previously, this calculation will be of the form given by equation 1 with variations to account for bank geometries.

Note that the equations presented thus far were developed from the perspective of flow over a single tube. The number of tubes per row ( $N_T$ ) must be taken into account to determine the total heat transfer through that tube row.

For the scope of this paper, only the heat transfer relations for a staggered array of tubes is examined; though, in practice, in-line arrays of tubes may be found in many applications. Heat transfer from banks of tubes depends on the flow conditions, tube geometries, and tube arrangements. Regarding the flow

conditions, the heat transfer from the shell-side fluid to a tube in the first row of the bank differs from that of a single tube due to the influence of other tubes within that row as well as any tubes in the transverse and diagonal planes.<sup>[7]</sup> It is for this reason that all four models presented have a correction for the number of tubes in the heat exchanger. This correction is to account for the front-row tube being coated by a relatively smooth boundary layer formed by an undisturbed freestream; however, successive downstream tubes benefit from augmented heat transfer due to the eddies of the turbulent wake created by upstream tubes<sup>[11]</sup>. It should be noted that a traditional critical transitional numbers for a turbulent wake of a cylindrical body in crossflow occur at  $Re \sim 40$ <sup>[11]</sup>. Since the heat transfer relations are based on empirical data, turbulent phenomena (such as vortex shedding) are thought to be included in the correlations.

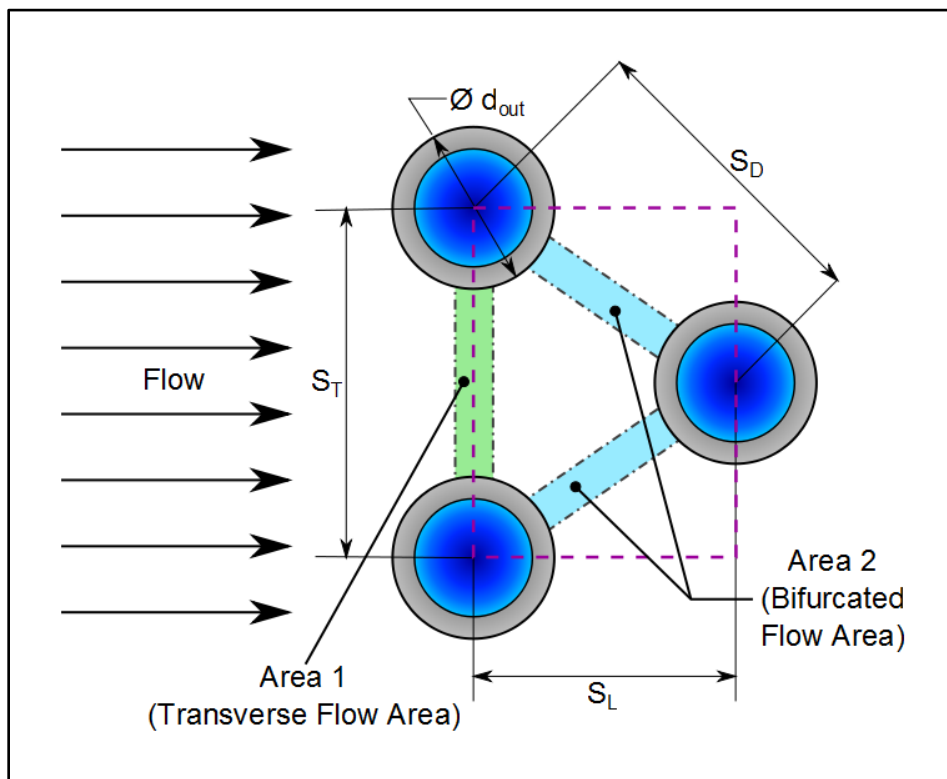


**Figure 11 - Staggered Tube Free Body Diagram**

The effect of natural convection at low Reynolds numbers was ignored in this study. Zhukauskas shows that the effect of natural convection becomes insignificant for  $Re_D \geq 200^{[9]}$ . For simplicity, radiation heat transfer is also ignored.

The calculated heat transfer rate may vary widely depending on the value of the thermal resistance. The conditions for the water side heat transfer are well within the bounds of the Dittus-Boelter equation and thus it is assumed that an analytic model based on equation 5 has merit. The thermal resistance calculation of the cylindrical wall is based on the conduction equation directly and is assumed to be exact within the uncertainty of the given dimensions and material properties. The air-side thermal resistances, however, present a wide range of uncertainty given the flow environment. Four heat transfer models are compared to determine the relative error between the calculation and the measured data. These models are used to compute the Nusselt number given the geometry and the air properties. The four heat transfer models used by the program are the Grimison model, a modified Grimison model, a Zhukauskas model, and the Kays & London model.

### 2.2.1 Grimison Model

The original Grimison model<sup>[7][8]</sup> for staggered tubes arrangements was developed in 1937. It computes the Nusselt number for a bank of tubes as

$$Nu = 1.13 C_1 C_2 Re_{D,max}^m Pr^{1/3}$$

(13)

$$\left[ \begin{array}{l} 2000 < Re_{D,max} < 40,000 \\ Pr \geq 0.7 \end{array} \right]$$

where  $C_1$  and  $m$  are listed in table 1 and  $C_2$  is a correction factor for tube banks having less than ten tubes ( $N_L < 10$ ) as listed in table 2.

**Table 1 - Constants of Equation 13 for airflow over a staggered tube bank<sup>[7][8]</sup>**

$S_L/d_{out}$	$S_T/d_{out}$							
	1.25		1.5		2.0		3.0	
	$C_1$	$m$	$C_1$	$m$	$C_1$	$m$	$C_1$	$m$
<b>0.600</b>	—	—	—	—	—	—	0.213	0.636
<b>0.900</b>	—	—	—	—	0.446	0.571	0.401	0.581
<b>1.000</b>	—	—	0.497	0.558	—	—	—	—
<b>1.125</b>	—	—	—	—	0.478	0.565	0.518	0.560
<b>1.250</b>	0.518	0.556	0.505	0.554	0.519	0.556	0.522	0.562
<b>1.500</b>	0.451	0.568	0.460	0.562	0.452	0.568	0.488	0.568
<b>2.000</b>	0.404	0.568	0.416	0.568	0.482	0.556	0.449	0.570
<b>3.000</b>	0.310	0.592	0.356	0.580	0.440	0.562	0.428	0.574

**Table 2 - Correction factor  $C_2$  of equation 13 for staggered tubes with  $N_L < 10$ <sup>[7]</sup>**

$N_L$	1	2	3	4	5	6	7	8	9
$C_2$	0.68	0.75	0.83	0.89	0.92	0.95	0.97	0.98	0.99

For implementation in the computer program, the coefficients  $C_1$  and  $m$  may be determined by the use of the following curve fits as evaluated in the present study:

$$\alpha_{coeff} = -0.066572 \left( \frac{S_T}{d_{out}} \right)^2 + 0.438619 \left( \frac{S_T}{d_{out}} \right) - 0.534414$$

$$\beta_{coeff} = 0.447806 \left( \frac{S_T}{d_{out}} \right)^2 - 2.867419 \left( \frac{S_T}{d_{out}} \right) + 3.482562$$

$$\gamma_{coeff} = -1.046594 \left( \frac{S_T}{d_{out}} \right)^2 + 6.359781 \left( \frac{S_T}{d_{out}} \right) - 7.686638$$

$$\delta_{coeff} = 0.803673 \left( \frac{S_T}{d_{out}} \right)^2 - 4.605252 \left( \frac{S_T}{d_{out}} \right) + 5.975412$$

$$\begin{aligned}\alpha_{exp} &= 0.009058 \left( \frac{S_T}{d_{out}} \right)^2 - 0.076068 \left( \frac{S_T}{d_{out}} \right) + 0.104510 \\ \beta_{exp} &= -0.071578 \left( \frac{S_T}{d_{out}} \right)^2 + 0.534418 \left( \frac{S_T}{d_{out}} \right) - 0.706706 \\ \gamma_{exp} &= 0.193359 \left( \frac{S_T}{d_{out}} \right)^2 - 1.270342 \left( \frac{S_T}{d_{out}} \right) + 1.608849 \\ \delta_{exp} &= -0.154482 \left( \frac{S_T}{d_{out}} \right)^2 + 0.934097 \left( \frac{S_T}{d_{out}} \right) - 0.585832\end{aligned}$$

$$\begin{aligned}C_1 &= \alpha_{coeff} \left( \frac{S_L}{d_{out}} \right)^3 + \beta_{coeff} \left( \frac{S_L}{d_{out}} \right)^2 + \gamma_{coeff} \left( \frac{S_L}{d_{out}} \right) + \delta_{coeff} \\ m &= \alpha_{exp} \left( \frac{S_L}{d_{out}} \right)^3 + \beta_{exp} \left( \frac{S_L}{d_{out}} \right)^2 + \gamma_{exp} \left( \frac{S_L}{d_{out}} \right) + \delta_{exp}\end{aligned}$$

These fitted data agree well with the data given from table 1 as shown in figures 12 and 13.

Note that equation 13 relies on the use of

$$Re_{D,max} \equiv \frac{\rho V_{max} d_{out}}{\mu} \quad (14)$$

where

$$V_{max} = \begin{cases} \frac{S_T}{S_T - d_{out}} V & \text{for } S_D \geq \frac{S_T + d_{out}}{2} \\ \frac{S_T}{2(S_D - d_{out})} V & \text{for } S_D < \frac{S_T + d_{out}}{2} \end{cases} \quad (15)$$

$$S_D \equiv \sqrt{S_L^2 + \left( \frac{S_T}{2} \right)^2}$$

The  $S_D$  criterion is used to determine if the maximum velocity occurs in the transverse plane (Area 1 in figure 11) or if the maximum velocity occurs in the

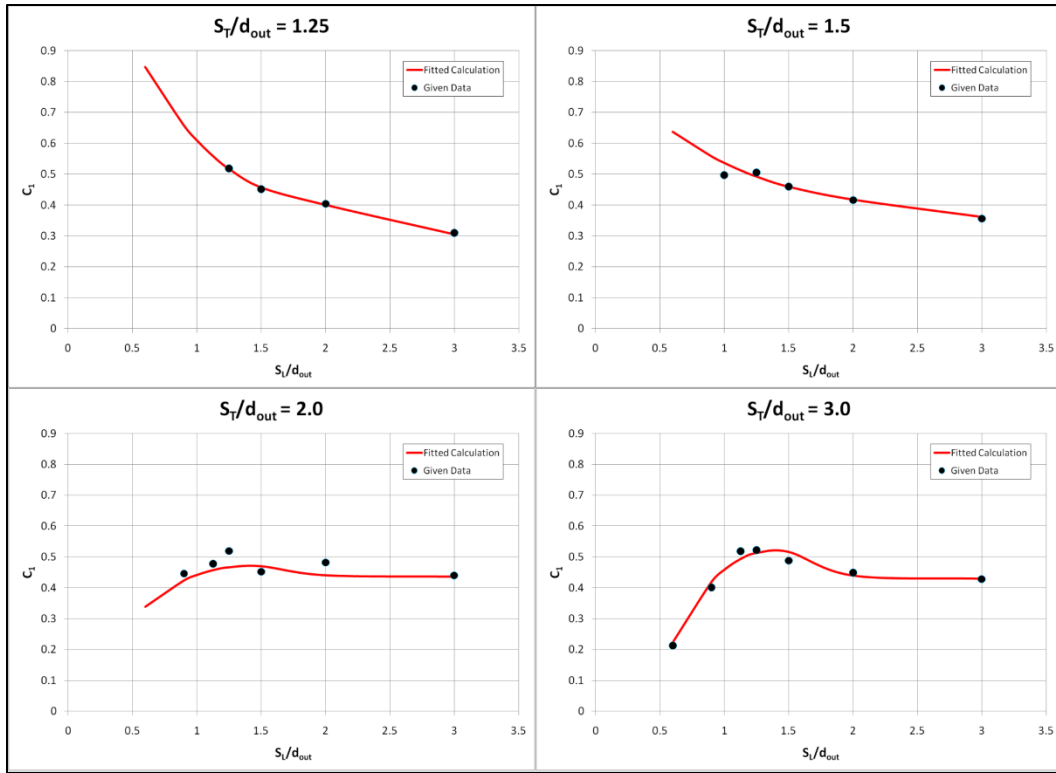


**Figure 12 - Comparison of the  $C_1$  Coefficients with Fitted Data**

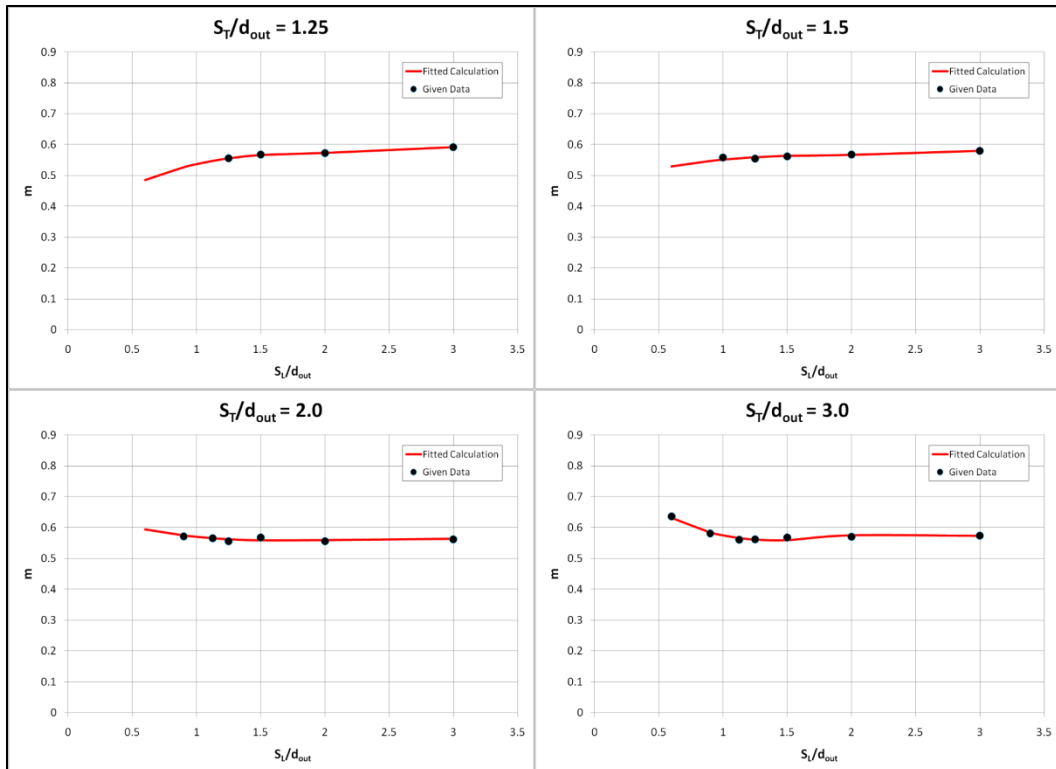


**Figure 13 - Comparison of the  $m$  Exponents with Fitted Data**

diagonal plane when the flow is bifurcated by the staggered tube arrangement (Area 2 in figure 11).

### 2.2.2 Modified Grimison Model

A few potential problems with the original Grimison model may be noted as relating to higher temperature cross-flows. Because of the higher temperatures on the air side,  $Pr < 0.7$ ; which is outside the domain of the valid Prandtl numbers given in the reference.

Another potential concern is the Reynolds number. For an input air mass flow rate and shell side area the flow velocity was computed as:

$$V = \frac{\dot{m}}{\rho A} = \frac{\dot{m}}{\rho(HW)}$$

For the typical conditions used in H2, the mass flow rate is low enough—and the heat exchanger area is large enough—that the Reynolds number calculated by equation 14 is typically much less than 2000.

Observe that equation 13 is more sensitive to the Reynolds number than the Prandtl number by comparing the magnitudes of the exponents of these two arguments. For all geometries given in table 1,  $m > 1/3$ ; also, for the cases presented herein,  $Re \sim O(100)$  while  $Pr \sim O(1)$ . These magnitudes also indicate that the Reynolds number has a larger influence on the relations than the Prandtl number. In order to correct the Grimison equation for the conditions beyond the lower bounds, the present study introduced a coefficient,  $\xi_H$ . This coefficient should allow for the specification of  $Nu = 0$  for  $Re_{D,max} = 0$  and, ideally, gives  $\xi_H = 1$  for

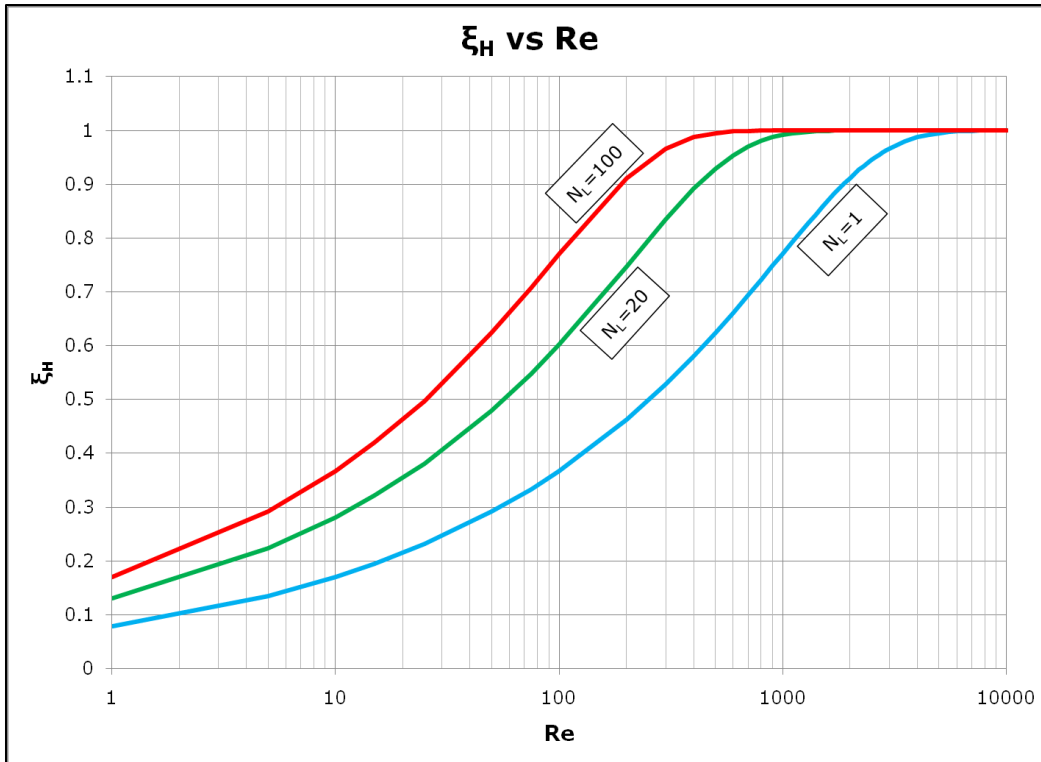


**Figure 14 –  $\xi_H$  Correction to the Original Grimison Model ( $Pr = 0.69$ )**

$Re_{D,max} = 2000$  and  $Pr = 0.71$ . For simplicity, consider a function that asymptotically approaches a value of 1 as its parameters increase. The hyperbolic tangent function is one such function and gives a steeper rise than a variant of  $1 - e^{-f(Re)}$ . Also use the standard temperature and pressure values for air as a reference  $Pr$  as well as the reference Reynolds number of 2000. For overall heat transfer analyses, a factor is also needed to account for the number of tube rows in the exchanger, otherwise the values of  $\xi_H$  will be too low when analyzing the entire non-discretized heat exchanger. Note that since the numerical model calculates the heat transfer by discrete rows,  $N_L = 1$  for each row heat transfer computation. By these criteria, a modified Grimison model may be represented by equations 16 with the correction factor equation 17 as proposed herein. Equation 17 is plotted in figure 14 for

various values of  $N_L$ . The coefficients  $C_1$  and  $C_2$  and the exponent  $m$  are all referenced from tables 1 and 2 or the previously discussed curve fits.

$$Nu = 1.13 \xi_H C_1 C_2 Re_{D,max}^m Pr^{1/3} \quad (16)$$

$$\xi_H = \left[ \tanh \left\{ \sqrt{N_L} \left( \frac{Re_{D,max}}{2000} \right) \left( \frac{Pr}{0.71} \right)^{1/3} \right\} \right]^{1/3} \quad (17)$$

Note that this is a simple alteration to the original Grimison model by solving for one additional scaling factor using the pre-computed Reynolds number and Prandtl number.

### 2.2.3 Zhukauskas Model

The Zhukauskas model, published in 1972, is given in equation 18<sup>[7][9][10]</sup>. The model has been used extensively since its publication and is presented in many textbooks on convection heat transfer such as those of Bejan<sup>[11]</sup> and Incropera & DeWitt<sup>[7]</sup>. The Zhukauskas model has been reported to be accurate to within ±15%<sup>[11]</sup>.

As can be observed, this model calculates the Nusselt number following the form of equation 1 with a correction for a thermal gradient due to the tube wall temperatures being cool relative to the hot air temperatures.

$$Nu = C_1 C_2 Re_{D,max}^m Pr^n \left( \frac{Pr}{Pr_s} \right)^{1/4} \quad (18)$$

$$\begin{bmatrix} 10 < Re_{D,max} < 2 \times 10^6 \\ 0.7 < Pr < 500 \end{bmatrix}$$

This equation uses  $Re_{D,max}$  as calculated using equations 14 and 15. The coefficient  $C_2$  is used to correct the Nusselt number for banks having less than 20 tubes as given in tables 3 (for  $Re < 1000$ ) and 4 (for  $Re \geq 1000$ ).

**Table 3 - Correction factor  $C_2$  for staggered tubes with  $N_L < 20^{[9][11]}$  for  $Re < 1000$**

$N_L$	1	2	3	4	5	7	10	13	16
$C_2$	0.83	0.88	0.91	0.94	0.95	0.97	0.98	0.99	1.0

**Table 4 - Correction factor  $C_2$  for staggered tubes with  $N_L < 20^{[7]}$  for  $Re \geq 1000$**

$N_L$	1	2	3	4	5	7	10	13	16
$C_2$	0.64	0.76	0.84	0.89	0.92	0.95	0.97	0.98	0.99

Note that the data presented in tables 3 and 4 can be numerically approximated by the conditional equation

$$C_2 = \begin{cases} 1 - e^{\left(-\frac{1}{N_L \sqrt{3}}\right)} & Re > 1000 \\ 1 - e^{-\sqrt{\frac{1}{3N_L}}} & Re \leq 1000 \end{cases} \quad (19)$$

The coefficient  $C_1$  and the exponents  $m$  and  $n$  are determined from table 5.

**Table 5 - Constants of equation 18 for airflow over a staggered tube bank<sup>[7]</sup>**

$Re_{D,max}$	$C_1$	$m$	$n$
10 – 100	0.90	0.40	0.36
100 – 1000	Approximate as an isolated cylinder		
$1000 - 2 \times 10^5$ $(S_T/S_L) < 2$	$0.35 \left(\frac{S_T}{S_L}\right)^{0.2}$	0.6	0.36
$1000 - 2 \times 10^5$ $(S_T/S_L) \geq 2$	0.40	0.6	0.36
$2 \times 10^5 - 2 \times 10^6$	0.022	0.84	0.36

Note that for the condition  $100 \leq Re_{D,max} < 1000$  Zhukauskas proposes that the tube bank be approximated by a single, isolated cylinder. For this case, Zhukauskas proposes that the Nusselt number be computed by equation 20 which differs from equation 18 only in that the Reynolds number used is based on the control volume freestream inlet velocity,  $V$ , rather than the maximum fluid velocity based on tube area constriction,  $V_{max}$  (i.e.  $Re_D \equiv \frac{\rho V d_{out}}{\mu}$  is used rather than  $Re_{D,max}$ ).

$$Nu = C_3 C_2 Re_D^m Pr^n \left( \frac{Pr}{Pr_s} \right)^{1/4} \quad (20)$$

$$n = \begin{cases} 0.36 & Pr > 10 \\ 0.37 & Pr \leq 10 \end{cases}$$

The coefficient  $C_3$  and the exponent  $m$  are given in table 6. Equation 20 also uses the correction factor  $C_2$  as read from tables 3 and 4.

**Table 6 - Constants of equation 19 for airflow over a staggered tube bank<sup>[7]</sup>**

$Re_D$	$C_3$	$m$
1–40	0.75	0.4
40–1000	0.51	0.5
$10^3$ – $2 \times 10^5$	0.26	0.6
$2 \times 10^5$ – $10^6$	0.076	0.7

Zhukauskas did publish an adjusted model in 1987 where the intervals and coefficients of table 5 were adjusted and the model no longer assumed an isolated cylinder for some flow regimes. When comparing the 1987 model to the 1972 model presented here, the results were little better than the original Grimison

model for the low Reynolds number cases seen by the H<sub>2</sub> heat exchanger. So for this analysis the 1972 model, as published in references [7] and [10], was used.

In both equations 18 and 20 the property  $Pr_s$  is evaluated using the tube wall temperature. Because the tube wall temperature will not initially be known at the time of the Nusselt number calculation, an initial film Prandtl number must be assumed.

Assume that the tube wall temperatures are typically in the range 100°F—600°F and having ambient air pressure of 1.5 psia. Using equilibrium air calculations, the following Prandtl number data is obtained.

**Table 7 - Air Prandtl Number at Typical Tube Wall Temperatures**

T	Pr
100°F	0.70
200°F	0.69
400°F	0.67
600°F	0.68

Averaging the data from table 7 produces  $Pr_{s,avg} = 0.69$  which, coincidentally, corresponds to a tube wall temperature of approximately 200°F. Because for most cases presented, the tube wall will be less than 200°F and this average Prandtl number value will be an acceptable approximation.

To prove this statement, the effect of the  $(Pr/Pr_s)^{1/4}$  term was examined:

**Table 8 - Zhukauskas Equation Prandtl Number Relative Error Considerations**

$Pr_s$	$Pr/Pr_s$	$(Pr/Pr_s)^{1/4}$
0.70	(1.43)Pr	(1.09)Pr <sup>0.25</sup>
0.69	(1.45)Pr	(1.10)Pr <sup>0.25</sup>
0.67	(1.49)Pr	(1.11)Pr <sup>0.25</sup>
0.68	(1.47)Pr	(1.10)Pr <sup>0.25</sup>

The absolute error of this is  $1.11Pr^{0.25} - 1.09Pr^{0.25} = 0.02Pr^{0.25}$  and the relative error of the spread is 1.8%. Using a  $Pr_{s,avg}$  of 0.69 has a calculation error of 1.4% to 1.5% for  $T_{wall} = 100^{\circ}\text{F}$  and  $T_{wall} = 600^{\circ}\text{F}$ , respectively.

It should be noted that iterating the heat transfer equation based on a feedback loop incorporating the Nusselt number and the tube wall temperature until a convergence criterion is reached would improve the fidelity of the model.

#### 2.2.4 Kays & London Model

The Kays & London model was introduced in 1984 to calculate the *overall* heat exchanger performance of so-called compact heat exchangers<sup>[12]</sup>. The authors recommended the use of the Colburn  $j$  factor as shown in equation 21 using the Stanton number,  $St$ , and the Prandtl number to compute the heat transfer of gas flow normal to an *infinite* bank of tubes.

$$j_H = StPr^{2/3} = h/Gc_p Pr^{2/3} \quad (21)$$

Rearranging equation 21 to solve for the convective heat transfer coefficient gives

$$h = j_H \frac{Gc_p}{Pr^{2/3}} \quad (22)$$

Recognizing that  $Nu \equiv \frac{hd_{out}}{k}$  and  $Re = \frac{Gd_{out}}{\mu}$  (for cylindrical tubes), the Nusselt number may be expressed as:

$$Nu_\infty = j_H \mu c_p k^{-1} Re Pr^{-2/3} \quad (23)$$

Recall that  $Pr \equiv \frac{\mu c_p}{k}$ . Using this definition, the previous relation simplifies to yield

$$Nu_{\infty} = j_H Re Pr^{1/3} \quad (24)$$

In their book *Compact Heat Exchangers*, Kays & London<sup>[12]</sup> present the relation

$$j_H = C_h Re^{-0.4} \quad (25)$$

for  $300 < Re < 15,000$

where the term  $C_h$  is a function of  $\left(\frac{S_T}{d_{out}}\right)$  and  $\left(\frac{S_L}{d_{out}}\right)$  and (for the geometries given) is bounded by  $0.2 \leq C_h \leq 0.425$ .

Observe that substituting equation 25 into equation 24 yields equation 26. Comparing equation 26 with equation 13 from the range of scalar coefficients from table 1 will show that the Kays & London heat transfer relation very closely resembles the Grimison heat transfer model; however, the coefficients used by the Kays & London model are meant for “compact” heat exchanger geometries (“compact” meaning  $1.5 \leq \frac{S_T}{d_{out}} \leq 2.5$  and  $0.75 \leq \frac{S_L}{d_{out}} \leq 1.5$ ). Notice that equation 26 mirrors equation 1 where  $m = 0.6$  and  $n = 1/3$ .

$$Nu_{\infty} = C_H Re^{0.6} Pr^{1/3} \quad (26)$$

Recall that equation 21 was developed with the assumption of an *infinite* bank of tubes. This is corrected by applying (as similar to both the Grimison and the Zhukauskas models) the relation:

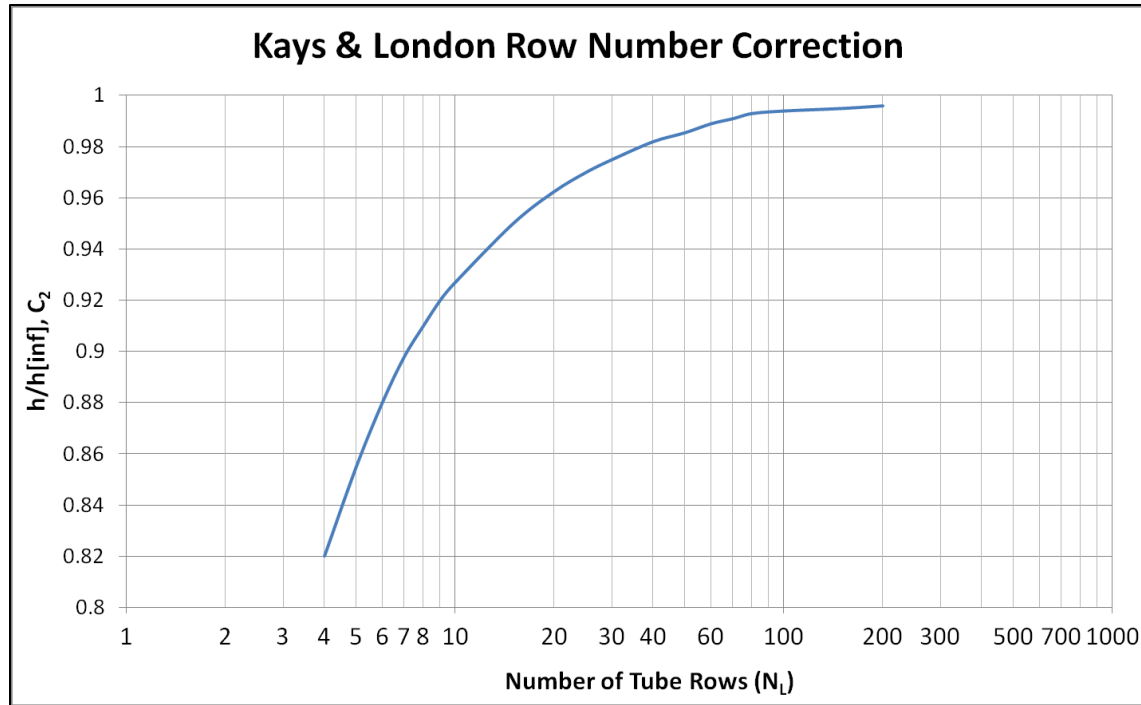


**Figure 15 - Kays & London influence of  $N_L$  variations in the heat transfer coefficient<sup>[12]</sup>**

$$Nu = C_2 Nu_\infty \quad (27)$$

Kays & London presented (graphically) a correction for finite tube banks duplicated in figure 15. The scaling may numerically be approximated using the equation:

$$C_2 \approx \frac{N_L^{0.728} + 1}{N_L^{0.72}} - \frac{N_L^{-0.2}}{\ln(N_L)} \quad (28)$$

### 2.2.5 First Law Analysis

The heat transfer rate through the air cooler may be quantified using the first law of thermodynamics. The first law being defined as

$$\dot{q} - \dot{w} = \dot{m}_{air} \left\{ \left( i_{air,inlet} + \frac{V_{inlet}^2}{2} + gZ_{inlet} \right) - \left( i_{air,outlet} + \frac{V_{outlet}^2}{2} + gZ_{outlet} \right) \right\} \quad (29)$$

Assuming that the potential energy of the system is negligible, the kinetic energy terms are much less than the enthalpy terms ( $\frac{V^2}{2} \ll i_{air}$ ,  $\frac{V^2}{2} \sim 0.1 \text{ Btu/lb}_m$ ), and that there is no component in the system to produce work, equation 29 reduces to

$$\dot{q} = \dot{m}_{air} (i_{air,inlet} - i_{air,outlet}) \quad (30)$$

### 2.2.6 Heat Exchanger Effectiveness

A common method of heat exchanger analysis is to determine the *effectiveness* of the exchanger. The heat exchanger effectiveness is defined as

$$\varepsilon \equiv \frac{\dot{q}}{\dot{q}_{max}} \quad (31)$$

where  $\dot{q}_{max}$  is the maximum possible heat transfer amount of the system in which the outlet temperature of the air (the hot fluid) is equal to the inlet temperature of the water (the cold fluid). As such, the maximum possible heat transfer rate may be defined as such:

$$\dot{q}_{max} = \dot{m}_{air} \{ i_{air,inlet} - i_{air}(T_{water,inlet}) \} \quad (32)$$

Therefore, the effectiveness of the exchanger may be represented in terms of the inlet and outlet enthalpies of the exchanger in addition to the enthalpy of air at the inlet temperature of the cooling fluid.

$$\varepsilon \equiv \frac{\dot{q}}{\dot{q}_{max}} = \frac{i_{air,inlet} - i_{air,outlet}}{i_{air,inlet} - i_{air}(T_{water,inlet})} \quad (33)$$

Note that in the case where the outlet air temperature is equal to the inlet water temperature, the effectiveness will be equal to unity.

## **2.3 Pressure Drop Models**

There are several models available that may be adopted to calculate the pressure drop across a bank of staggered tubes. In most models, the pressure drop is a function of the flow velocity, flow density, geometry conditions, and a scalar friction factor value that depends on the parameters of the tubes as well as the Reynolds number of the flow.

### 2.3.1 Holman-Jakob Model

The Holman-Jakob model<sup>[13]</sup>, introduced in 1938, relates the pressure drop across a bank of tubes by the relation:

$$\Delta p = \frac{G_{max}^2 N_L}{\rho(g/2)} \left( \frac{\mu_w}{\mu} \right)^{0.14} \left[ 0.25 + \frac{0.118}{\left( \frac{S_T - d_{out}}{d_{out}} \right)^{1.08}} \right] Re_{D,max}^{-0.16} \quad (34)$$

(English units only,  $[\Delta p] = \frac{l b_f}{ft^2}$ )

Note that equation 34 has no arguments to account for variations in tube material and thus the model would under predict the pressure drop for rough tubes while potentially over predicting the pressure drop for idealistically smooth tubes.

### 2.3.2 Gunter-Shaw Model

The Gunter-Shaw model<sup>[14]</sup> was published in 1945 and implements a piecewise friction factor correction based on the Reynolds number of the flow. Gunter and Shaw present the following friction relation<sup>[14]</sup>

$$\frac{f}{2} = \frac{\Delta p g D_v \rho}{G^2 \ell} \left( \frac{\mu}{\mu_w} \right)^{0.14} \left( \frac{D_v}{S_T} \right)^{-0.4} \left( \frac{S_L}{S_T} \right)^{-0.6} \quad (35)$$

Solving this relation in terms of the pressure drop yields the Gunter-Shaw pressure drop relation

$$\Delta p = \frac{f}{2} \frac{1}{g} \left( \frac{\mu_w}{\mu} \right)^{0.14} \left( \frac{D_v}{S_T} \right)^{0.4} \left( \frac{S_L}{S_T} \right)^{0.6} \left\{ \frac{G^2 \ell}{D_v \rho} \right\} \quad (36)$$

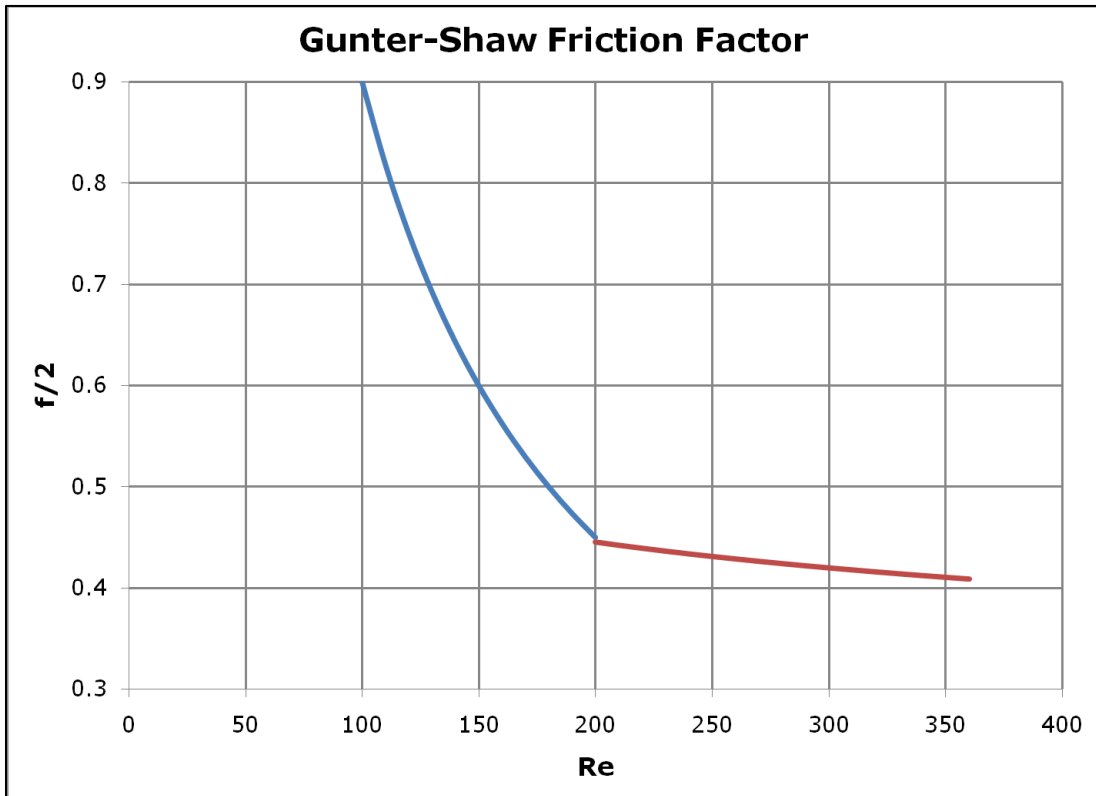


**Figure 16 - Gunter-Shaw Crossflow Friction Factors**

Gunter and Shaw assume a laminar-to-turbulent transition point at  $Re \cong 200$ . By their correlations, they present a piecewise friction factor relation of the form<sup>[14]</sup>:

$$\frac{f}{2} = \begin{cases} 90 Re^{-1} & \text{for } Re \leq 200 \\ 0.96 Re^{-0.145} & \text{for } Re > 200 \end{cases} \quad (37)$$

Notice that the values of both functions in equation 37 are equal at  $Re \cong 202.488$ .

Note that for the case of a staggered tube arrangement, the volumetric hydraulic diameter used in equation 36 may be expressed in terms of the heat exchanger's given dimensions as:

$$D_v \equiv \frac{4 \times (\text{Net Free Volume})}{(\text{Friction Surface})} = \frac{4 \times \left( S_T S_L - \frac{\pi}{4} d_{out}^2 \right)}{\pi d_{out}} \quad (38)$$

$$D_v = \frac{4 S_T S_L}{\pi d_{out}} - d_{out}$$

### 2.3.3 Boucher and Lapple's Correction to the Gunter-Shaw Model

In 1945, Boucher and Lapple<sup>[14]</sup> critiqued the Gunter-Shaw model by stating that the friction factors given by Gunter and Shaw are fairly good over a small range of configurations, but "become progressively worse as more extreme spacings are approached".

These authors continue their discussion of the Gunter-Shaw model and state that:

[The Gunter-Shaw] method of correlation does give a good representation of the data in the range of spacings commonly employed, but will yield low values for wide spacings.<sup>[15]</sup>

It will be shown that this comment by Boucher and Lapple appears to be correct. The present study found that the Gunter-Shaw model regularly underpredicts the pressure drop for the H<sub>2</sub> cooler.

For the geometries present in the H<sub>2</sub> cross flow heat exchanger, the friction factors calculated by equation 37 are too low and are thus corrected by multiplying by the scalar value of 1.75 to increase effect of the viscous losses. This factor was determined in the present study as Boucher and Lapple do not give an explicit correction to the Gunter-Shaw model, but they do specify that the friction factors as calculated by Gunter and Shaw give unduly low results at wide transverse spacings<sup>[15]</sup>.

#### 2.3.4 Zhukauskas Model

The Zhukauskas pressure drop model was included in Zhukauskas's work on an improved heat transfer model for crossflow tube banks. The Zhukauskas model is expressed as<sup>[10][11]</sup>

$$\Delta p = N_L \chi \left( \frac{\rho V_{max}^2}{2} \right) f \quad (39)$$

where the friction factor  $f$  and the correction factor  $\chi$  are presented graphically for staggered tube banks.

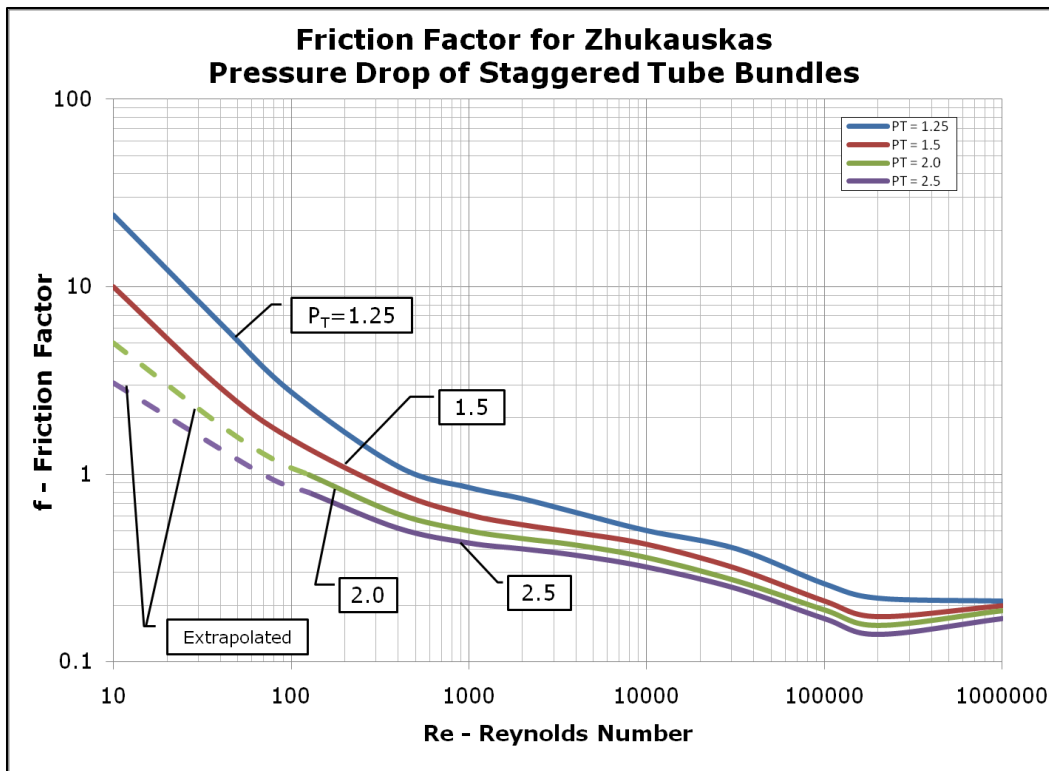


**Figure 17 - Friction Factor for Zhukauskas Pressure Drop Model (Equation 39)**

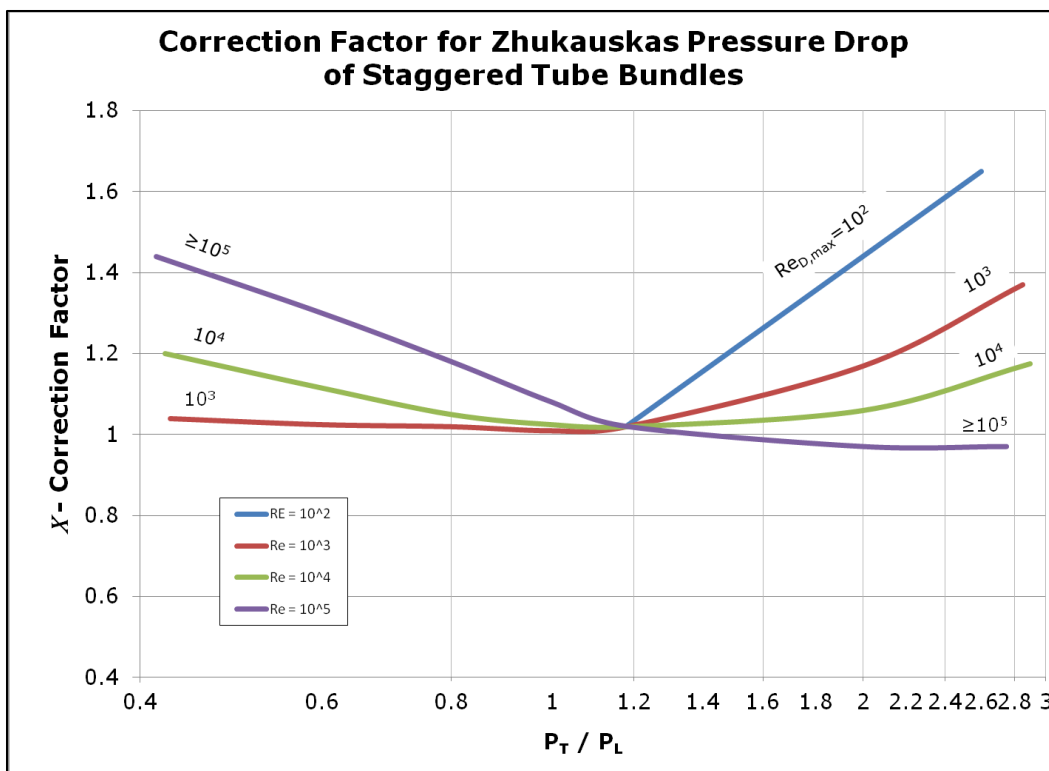


**Figure 18 - Geometry Correction Factor for Zhukauskas Pressure Drop Model**

These plots are reproduced using cubic splines in figures 17 and 18. Note that the data in figures 17 and 18 are presented in terms of dimensionless longitudinal and transverse pitches,  $P_L \equiv S_L/d_{out}$  and  $P_T \equiv S_T/d_{out}$ . The cubic spline coefficients that reproduce the curves shown in figures 17 and 18 are presented in Appendices B and C.

For the numerical model, the friction factor is logarithmically interpolated between the geometry curves. It is for this reason that the  $P_T = 2.0$  and  $P_T = 2.5$  curves are extrapolated into the low Reynolds number regime. This allows the  $P_T = 2.0$  and  $P_T = 2.5$  curves to have the same calculation domain as the  $P_T = 1.25$  and  $P_T = 1.5$  curves. The correction factor is linearly interpolated between the Reynolds number order of magnitude curves using the calculated Reynolds number at the correct geometry ratio.

### 2.3.5 Kays & London Model

The Kays & London pressure drop model was included in the 1984 publication *Compact Heat Exchangers* along with the heat transfer model. In this book, the following pressure drop relation<sup>[12]</sup> is proposed:

$$\frac{\Delta p}{p_1} = \frac{G^2}{2g_c} \frac{v_1}{p_1} \left[ (1 + \sigma^2) \left( \frac{v_2}{v_1} - 1 \right) + f \frac{A}{A_{min}} \frac{v_m}{v_1} \right] \quad (40)$$

where the subscripts 1 and 2 refer to the heat exchanger inlet and outlet, respectively, and  $A = A_{surf,o}$ . Equation 40 is a much improved form of the pressure drop model that Grimison suggested in reference [8]. Unlike Grimison's pressure

drop model, the Kays & London variant includes terms for tube arrangement spacing. Equation 40 can be rearranged by recognizing that  $\nu = 1/\rho$  and simplify as

$$\Delta p = \frac{G^2}{2g_c\rho_1} \left[ (1 + \sigma^2) \left( \frac{\rho_1}{\rho_2} - 1 \right) + f \frac{A}{A_{min}} \frac{\rho_1}{\rho_m} \right] \quad (41)$$

As discussed in the analytic model, the heat exchanger is numerically evaluated on a discretized row-by-row basis. With this discretization, use the control volume shown by figure 19, allowing that the aforementioned subscripts 1 and 2 now refer to the tube row inlet and outlet, respectively. Using this discretization, it can be assumed that the air-side density change over a *single* row of tubes is negligible. Under this assumption, allow  $\rho_1 = \rho_2 = \rho$  in which case equation 41 reduces to

$$\Delta p = \frac{G^2 f}{2g_c \rho} \frac{A_{surf,o}}{A_{min}} \quad (42)$$

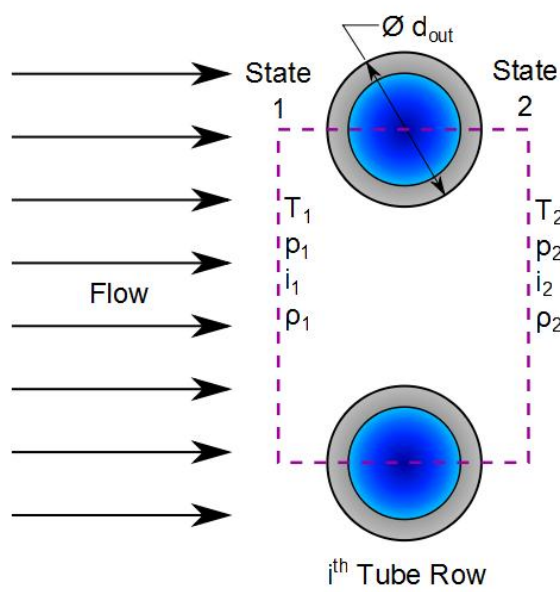


**Figure 19 - Control Volume of a Single Tube Row**

Kays and London specified a relation for determining the value of the friction factor  $f$  as a power law function of the Reynolds number given by the equation

$$f = C_f Re^{-0.18} \quad (43)$$

where the scalar term  $C_f$  is a function of  $(\frac{S_T}{d_{out}})$  and  $(\frac{S_L}{d_{out}})$  and (for the geometries given) is bounded by  $0.15 \leq C_f \leq 0.452$ .

The next difficulty is in the determination of the *minimum* free flow area,  $A_{min}$ . Refer to the areas given previously in figure 11. Assuming a unit length, recognize that the free flow area in the transverse plane is given by

$$A_{trans} = S_T - d_{out} \quad (44)$$

In the case of the bifurcated flow area, recognize that the diagonal pitch may be expressed as

$$S_D = \sqrt{S_L^2 + \left(\frac{S_T}{2}\right)^2} \quad (45)$$

Subtracting the diameter from the above equation to get the linear distance between diagonal tube walls and recalling that there are two interspatial areas gives the bifurcated flow area equation (again assuming unit length)

$$A_{bif} = 2 \left[ \sqrt{S_L^2 + \left(\frac{S_T}{2}\right)^2} - d_{out} \right] \quad (46)$$

Now, the minimum free flow area may be expressed by the conditional equation

$$A_{min} = \min \left\{ S_T - d_{out}, 2 \left[ \sqrt{S_L^2 + \left( \frac{S_T}{2} \right)^2} - d_{out} \right] \right\} \quad (47)$$

### 3.0 Results and Discussion

In order to get quantitative data to compare with numerical results, thermocouples were installed in the intra-bank water manifolds to measure the temperature rise of the cooling water. These manifolds represent the outlet of a water-side upstream bank and the inlet of a water-side downstream bank. As mentioned previously, water is fed into the most downstream bank (Bank 4 as seen in figure 20) and exits from the most upstream bank (Bank 0). This effectively makes the H<sub>2</sub> cooler a cross-flow, counter-flow heat exchanger.

Existing instrumentation included flowmeters on the cooling water inlet, pressure transducers on the upstream and downstream ends of the cooler, and the air mass flow rate is metered by venturis upstream of the arc heater.

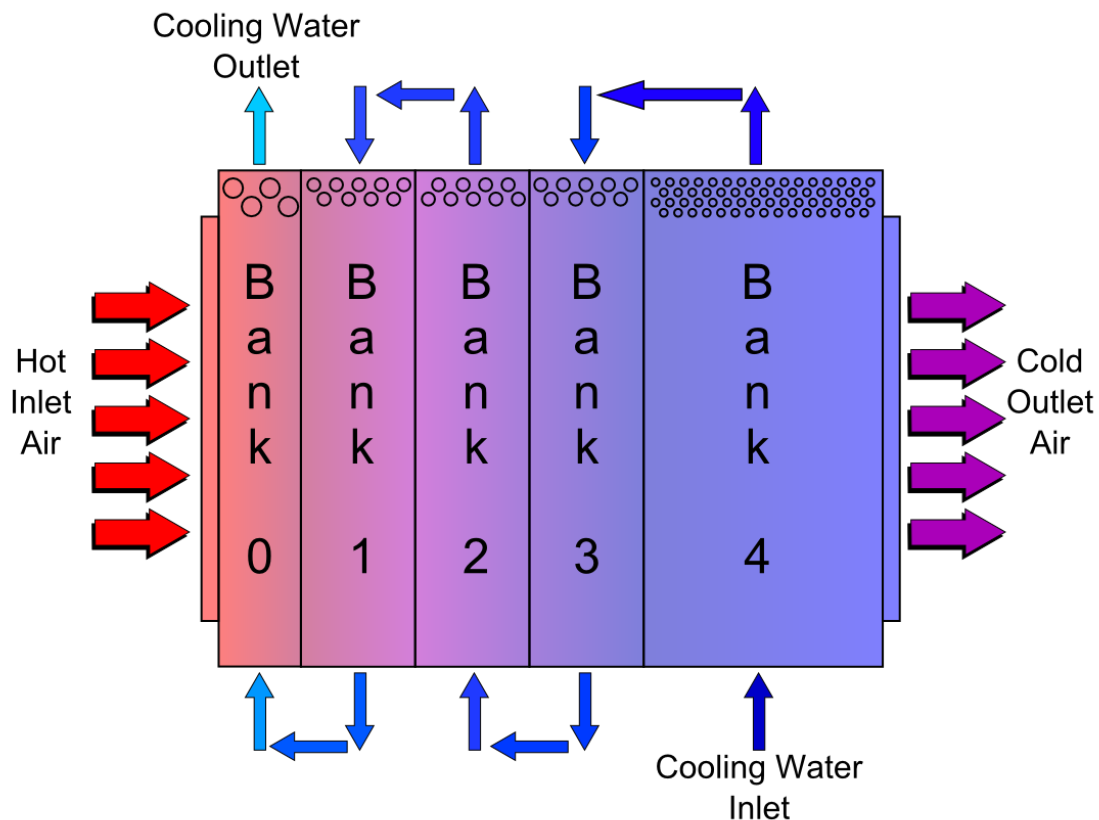
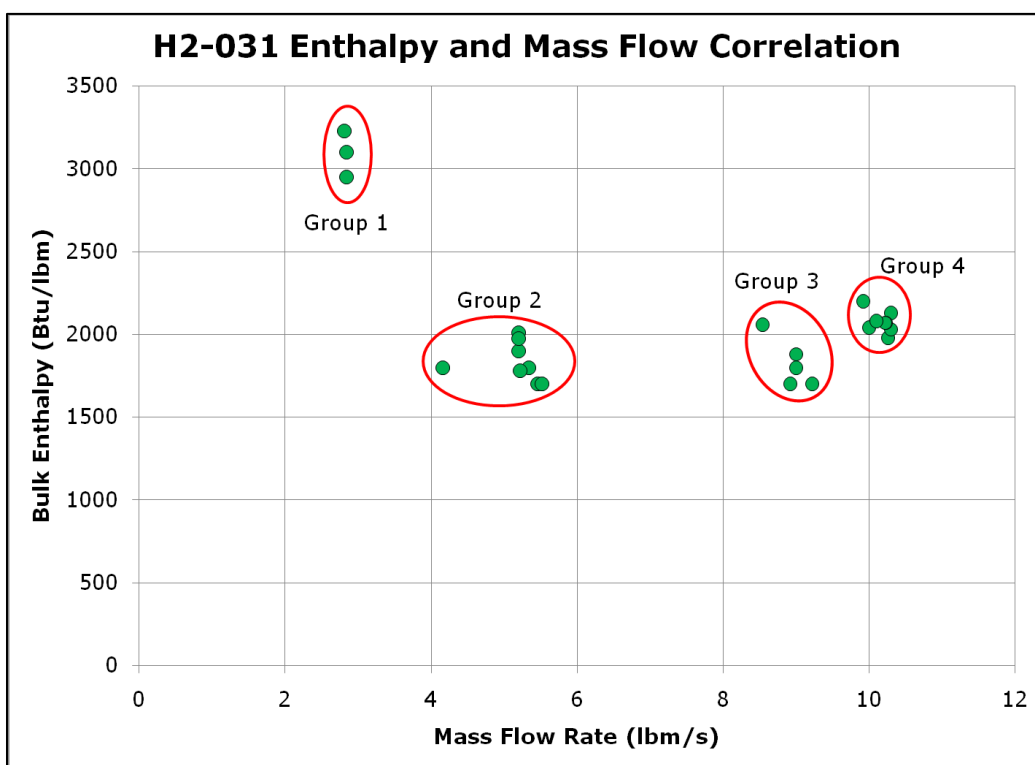


Figure 20 - Heat Exchanger Flow Diagram

All the data was collected during the H2-031 data series for which the data were aggregated into essentially four discrete groups as shown in figure 21. It could be argued that the data should be broken into as many as six groups, but taking into account the uncertainties of the measurements—as well as the assumptions of the model—there is little deviation between any subsets within the circled regions of figure 21.

As mentioned in the apparatus section, there is a 95-foot diffuser upstream of the air cooler. Measurements show that the water-cooled diffuser removes approximately 30% of the heat energy from the air stream. By this assumption, the total enthalpy input into the numerical model is 70% of the run condition total enthalpy.



**Figure 21 - H2-031 Run Conditions**

**Table 9 - Model Inputs for the H2 Air Cooler**

Bank Number	Tube Numbers	$d_{in}$	$d_{out}$	$S_T$	$S_L$	Tube Material	Tube Type
Bank 0	$0 \leq N \leq 3$	1.906	2.399	4.75	2.1875	Carbon Steel	Smooth
Bank 1	$4 \leq N \leq 12$	1.250	1.518	4.4375	1.9060	Cupronickel	Smooth
Bank 2	$13 \leq N \leq 21$	1.250	1.518	4.4375	1.9060	Cupronickel	Smooth
Bank 3	$22 \leq N \leq 30$	1.250	1.518	4.4375	1.9060	Cupronickel	Smooth
Bank 4	$31 \leq N \leq 82$	0.495	0.625	2.25	0.94	Cupronickel	Finned

Table 9 shows the H2 cooler inputs as given to the numerical model. Such inputs include the number of tubes, tube arrangement, tube material, and relevant fin geometry parameters. Using these inputs, consider the results from the four discrete groups as called out in figure 21.

### **3.1 Group 1**

Group 1 has three total data points within it, of which only one data point has intra-bank water manifold thermocouples. For this data point, the input conditions are as shown in table 10.

**Table 10 - Program Inputs for Run H2-031-024**

Run Number	H2-031-024
$\dot{m}_{air}$	2.84 lb <sub>m</sub> /s
$p_{air,inlet}$	1.47 psia
$i_{air,inlet}$	2170 Btu/lb <sub>m</sub>
$T_{water,inlet}$	75.4 °F
$P_{water,inlet}$	89 psia
$\dot{Q}_{water}$	9650 gpm

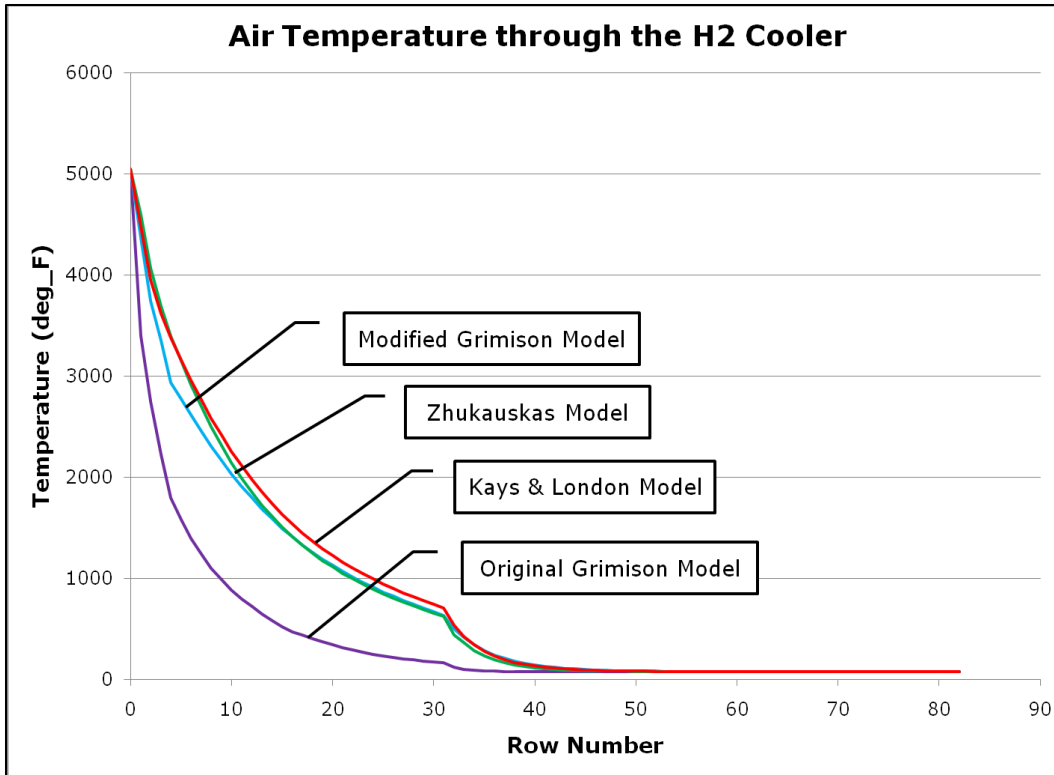


**Figure 22 - Air Temperature v. Axial Distance (Row Number) for Various Heat Transfer Models for H2-031-024**

Figure 22 shows the calculated air temperature comparing the four different heat transfer models. Note the changes in the curves at tube row number 31 due to the effect of the finned tubes in bank 4.

In figure 23, the black circle markers represent the measured water temperature at the intra-bank manifolds. As previously mentioned, the water moves counter-flow to the air flow and the program uses an iterative approach to solve the system until water temperatures at bank interfaces converge. Comparing figures 22, 23, and 24; it is evident that the original Grimison model over-predicts the convective heat transfer coefficient for the first row of tubes. Mathematically, this resolves itself by driving the tube wall temperatures in the first tube row over 40% higher than those predicted by the other models. This has the

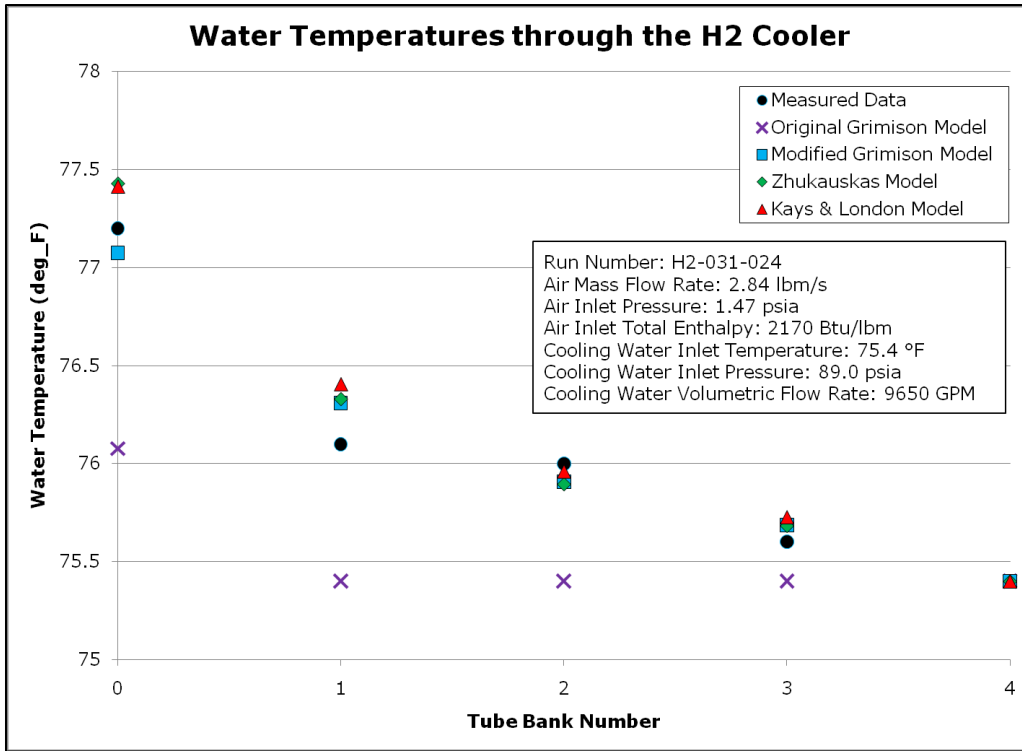


**Figure 23 - Inlet Water Manifold Temperature Comparisons by Heat Transfer Model for Run H2-031-024**

numerical effect of removing “too much” energy from the flow for which the remaining tube temperatures are less than those predicted by the other models. This is evidenced by the lower water temperatures calculated by the Grimison model as seen in figure 23.

The modified Grimison model predicts measured water temperature rise much better than the original Grimison model. The modified model also has better agreement with the other models in terms of tube temperatures along the axial length of the cooler. The maximum relative error of the calculated water temperatures of the modified Grimison model to the measured water temperatures is 0.27% which is well within the quoted uncertainty of the thermocouple measurement. Good agreement is observed in figure 23 between the calculated

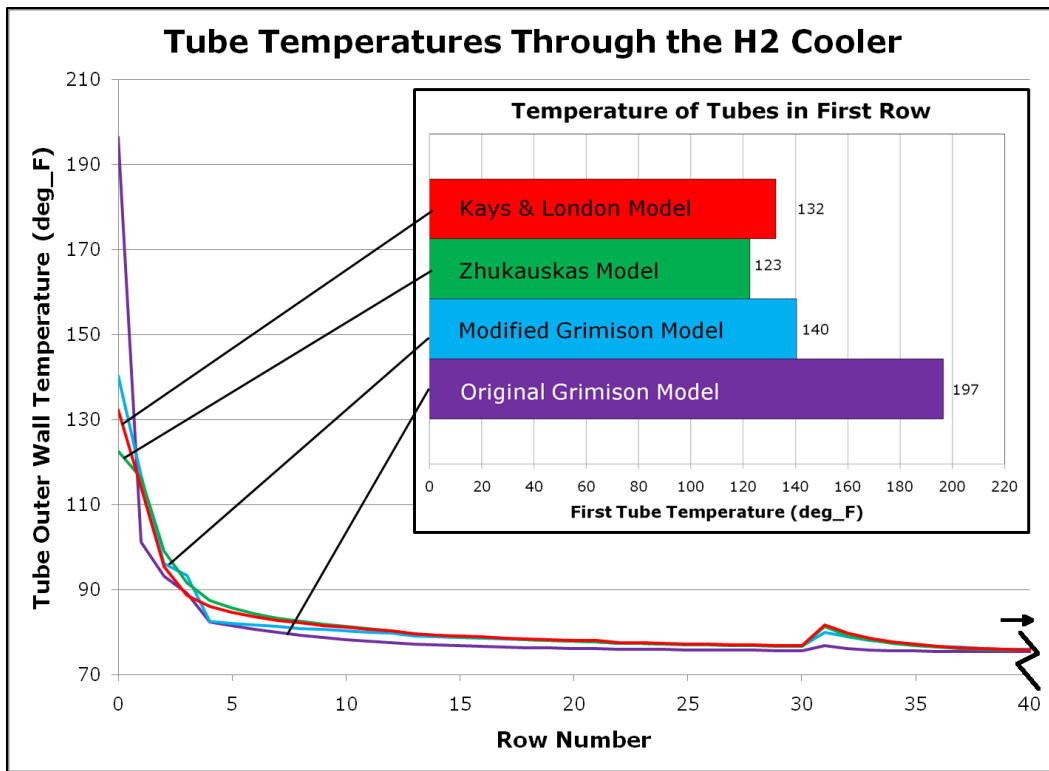


**Figure 24 - Tube Temperatures per Row as Calculated for H2-031-024 (Inset: Temperature of Tubes in the First Row)**

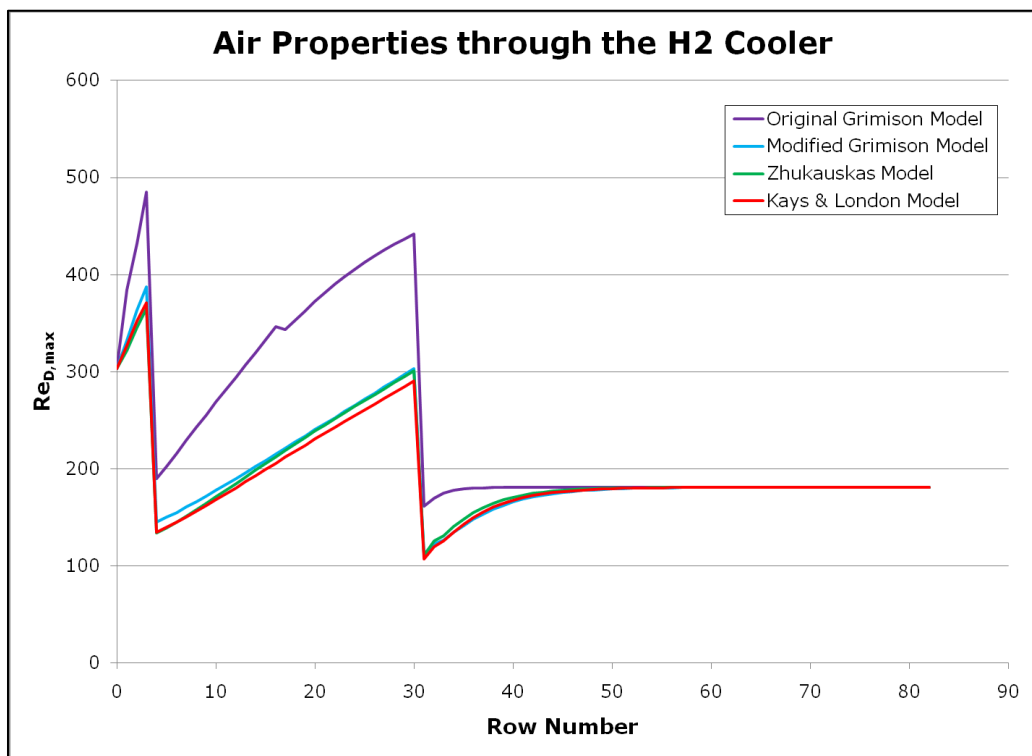


**Figure 25 - Calculated Reynolds Number by Heat Transfer Model for H2-031-024**

water temperatures of both the modified Grimison model and the well-established Zhukauskas model for these input conditions.

The Zhukauskas model gives a good prediction of the measured water temperature increases. The maximum relative error between calculated water temperatures and measured water temperatures are 0.30% using the Zhukauskas model and this run condition. The Zhukauskas model also predicts more reasonable tube wall temperatures than the original Grimison model and calculates the lowest first tube wall temperature amongst the heat transfer models.

The Kays & London heat transfer model fits the measured water temperatures well using an overall  $C_h = 0.3$ . The maximum relative error between the calculated water temperatures and the measured water temperatures for  $C_h = 0.3$  is 0.40%.

The numerical model shows that the air temperature does indeed reach the temperature of the inlet cooling water before exiting the heat exchanger. Due to this fact, the exchanger has  $\varepsilon = 1$ . In addition, by first law analysis

$$\begin{aligned}\dot{q} &= \dot{m}_{air}(i_{air,inlet} - i_{air,outlet}) \\ \dot{q} &= \left(2.84 \frac{lb_m}{s}\right) \left(2170 \frac{Btu}{lb_m} - 128.4 \frac{Btu}{lb_m}\right) \\ \dot{q} &= 5798 \frac{Btu}{s}\end{aligned}$$

Figure 24 shows the calculated tube outer wall temperatures for the four heat transfer models. Note that the abscissa is truncated in figure 24 to emphasize the temperature differences in the bank 0 tubes. Observe that the original Grimison model calculates a wall temperature that is almost 50% greater than the

average wall temperature of the other three models for the first tube in the exchanger. The small increase in wall temperature at row 31 is due to the increased surface area of the finned tubes in bank 4.

The calculated  $Re_{D,max}$  is plotted in figure 25. Recall that  $Re_{D,max}$  is the Reynolds number with respect to the maximum flow velocity consistent with equation 15. Observe that the calculated Reynolds numbers are much less than the recommended lower bound for the original Grimison model. The precipitous discontinuities in the curves are due to geometry changes between tube banks. The large difference between the calculated  $Re_{D,max}$  of the original Grimison model and the other three heat transfer models stems from the differences in the calculated air density because of the calculated air temperatures.

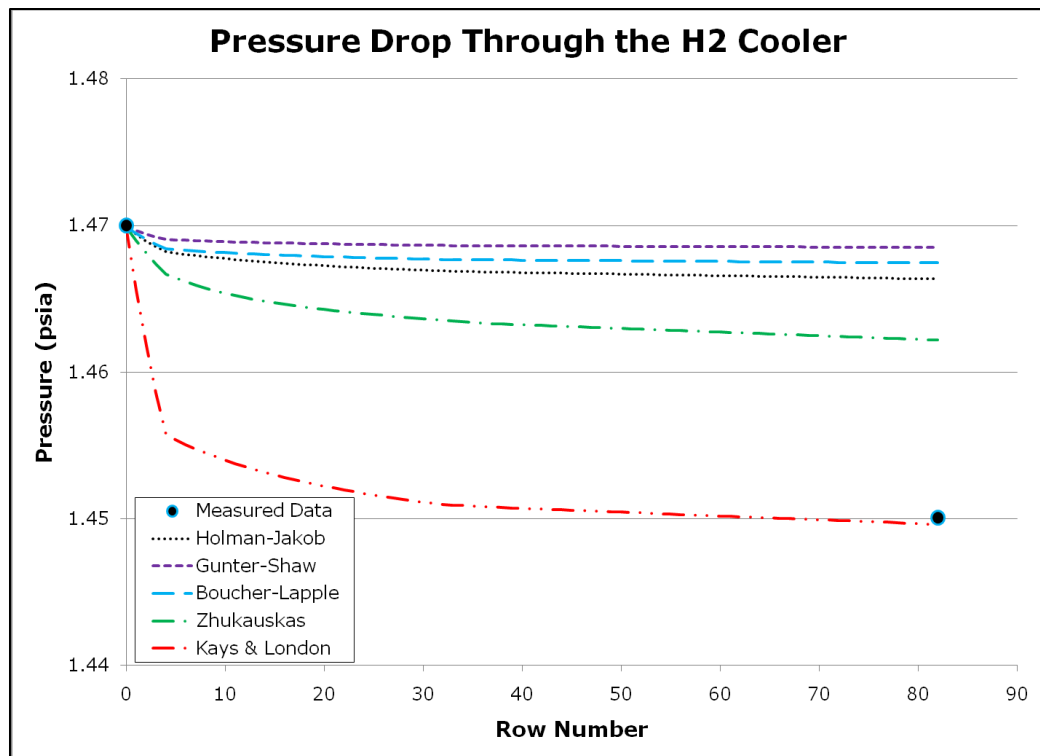


**Figure 26 - Pressure Drop Model Comparisons for H2-031-024**

Figure 26 compares the five pressure drop models of interest. For the purpose of comparison, the Zhukauskas heat transfer model is used to maintain a sense of *ceteris paribus*. For the conditions present, specifically the relatively low air mass flow rate, the pressure drop measured through the heat exchanger is admittedly low. As evidenced by figure 26, the Zhukauskas pressure drop model better predicts the pressure drop than the legacy models; however, the Kays & London model better predicts the pressure drop upon iterating to an overall  $C_f = 2.0$ . Note, however, this value is over five times the range presented in the reference.

The Gunter-Shaw pressure drop model predicts an almost negligible pressure drop across the heat exchanger. Taking into account the arguments of Boucher and Lapple, the calculated results of the Gunter-Shaw model are worse than the Holman-Jakob pressure drop model, which still underpredicts the pressure losses over the tube banks. It should be noted that the calculated pressure drop for all the models falls within the facility-quoted 1.6% uncertainty of the measured pressure for this condition.

### **3.2 Group 2**

Group 2 contains eight data points; of which, two test runs contain intra-bank water manifold temperature data. The first data point (H2-031-021) was compared to the numerical model using the program inputs given in table 11. Comparing figures 27, 28, and 29 observe that the four heat transfer models calculate a tube wall temperature spread of approximately 20% for the tubes in bank 0. Because the original Grimison model was designed to assume fully developed turbulent flow, the model removes the heat energy more quickly than

the other heat transfer models. This is, once again, manifested as a higher tube wall temperature in the first row and lower predicted water temperatures throughout the cooler.

**Table 11 - Program Inputs for Run H2-031-021**

Run Number	H2-031-021
$\dot{m}_{air}$	5.30 lb <sub>m</sub> /s
$p_{air,inlet}$	1.49 psia
$i_{air,inlet}$	1200 Btu/lb <sub>m</sub>
$T_{water,inlet}$	72.2 °F
$P_{water,inlet}$	86 psia
$\dot{Q}_{water}$	9020 gpm

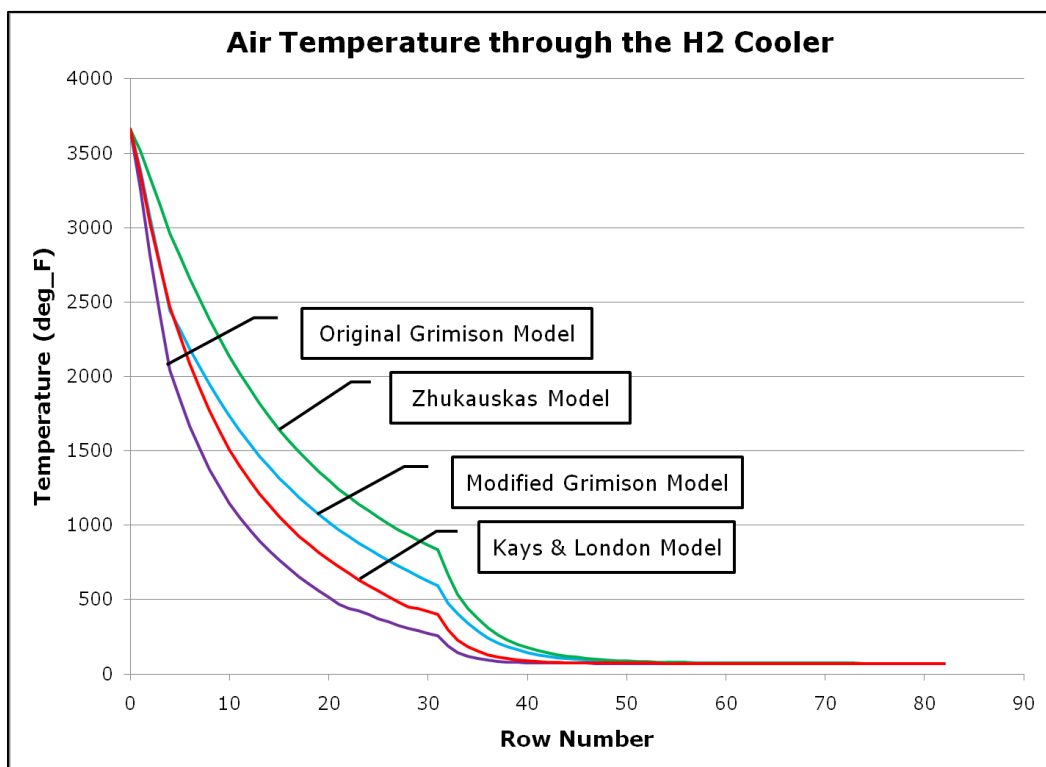


**Figure 27 - Air Temperature v. Axial Distance (Row Number) for Various Heat Transfer Models for H2-031-021**

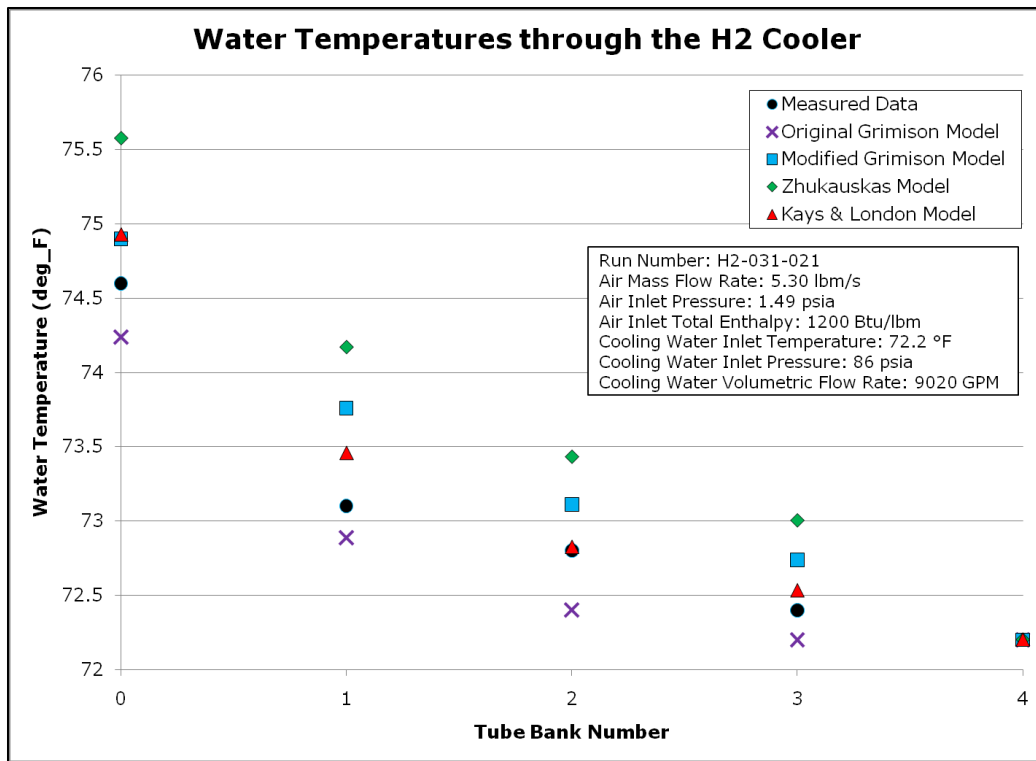


**Figure 28 - Inlet Water Manifold Temperature Comparisons by Heat Transfer Model for Run H2-031-021**

The modified Grimison model over-predicted the water temperature rise by a maximum relative error of 0.90%. For its simplicity, it performs rather well in predicting the water temperatures and presents a tube temperature profile that mirrors the best segments of the original Grimison model and the Zhukauskas model. It should be noted that the modified Grimison model was able to predict water temperature increases better than the Zhukauskas model and the original Grimison model without the need to iterate upon a  $C_h$  factor as in the case for the Kays & London model.

The Zhukauskas model predicts the measured water temperature increases somewhat well; over-predicting the water temperature rise by a maximum relative error of 1.46% from the measured temperatures. Curiously, the Zhukauskas model

calculates the lowest tube wall temperature for tubes in the first row, but calculates a large increase in the tube wall temperatures at the inlet of the finned tube section (beginning in tube row number 31) than the other models.

The Kays & London heat transfer model fits the measured water temperatures well using an overall  $C_h = 0.5$ . The maximum relative error between the calculated water temperatures and the measured water temperatures for  $C_h = 0.5$  is 0.49%. Note that the Kays & London model produces a tube temperature profile that appears similar in shape to the profile produced by the original Grimison model (figure 29). This is should not be a surprising result based on the similarities of equations 13 and 26 and the range of  $m$  exponent values presented in table 1.

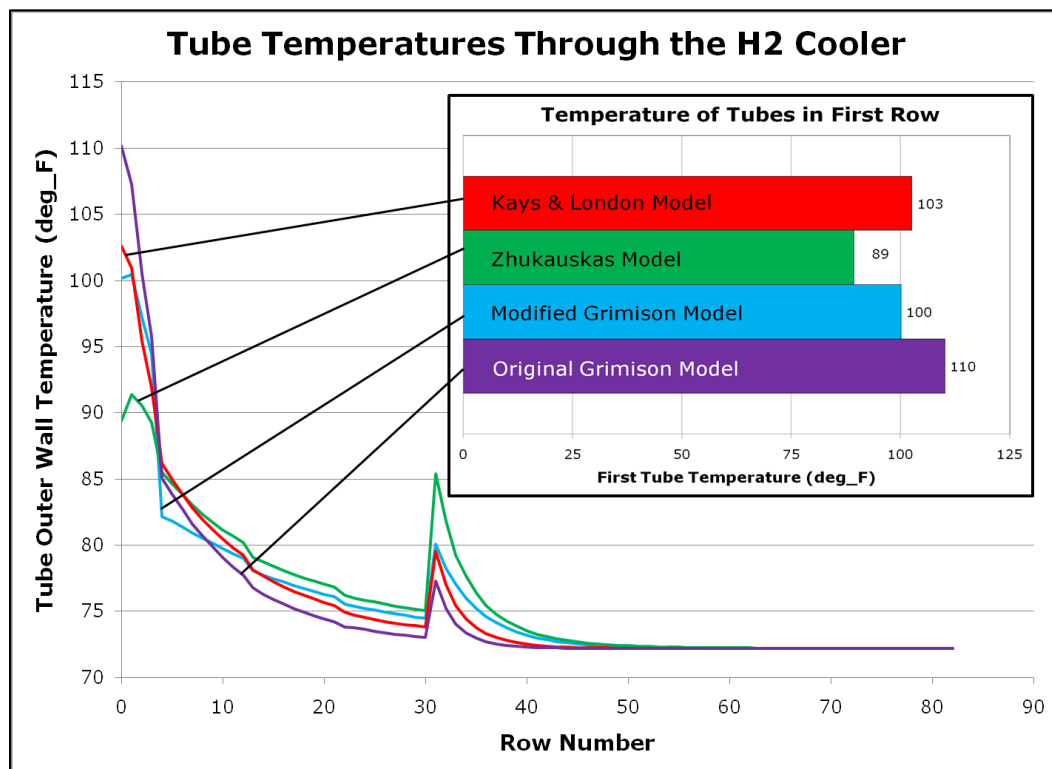


**Figure 29 - Tube Temperatures per Row as Calculated for H2-031-021**

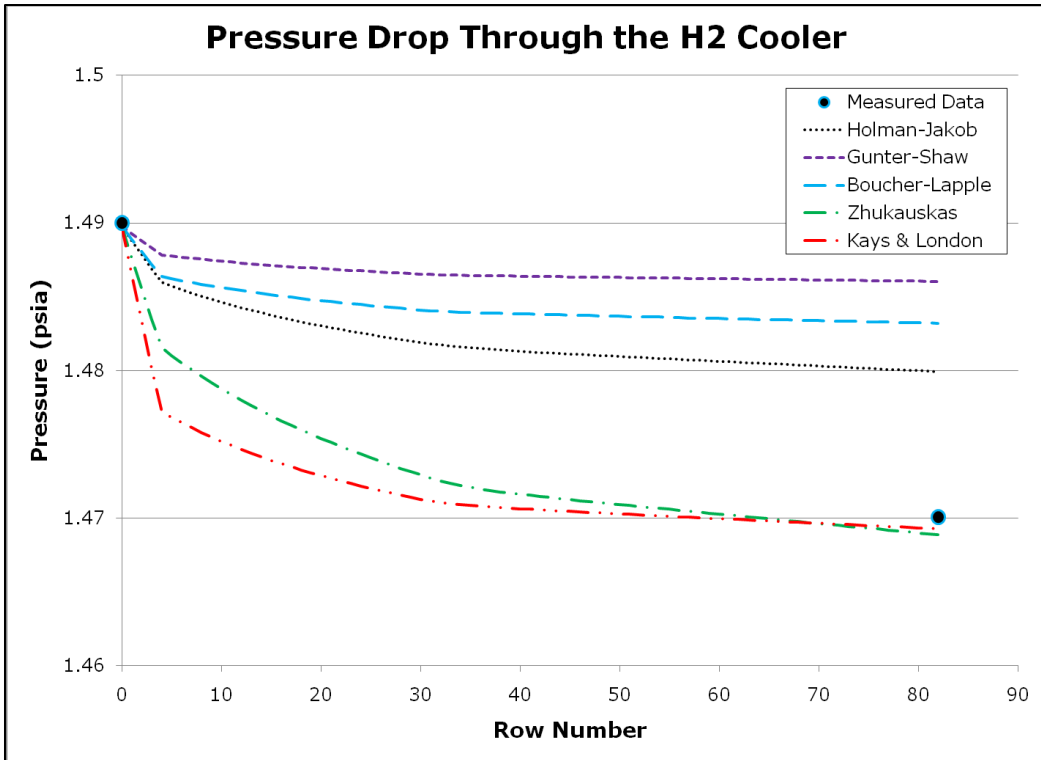


**Figure 30 - Comparison of Pressure Drop Models for H2-031-021**

For the case of run H2-031-021, the outlet air temperature is equal to the temperature of the inlet cooling water. Once again, the exchanger has  $\varepsilon = 1$ . By first law analysis

$$\begin{aligned}\dot{q} &= \dot{m}_{air}(i_{air,inlet} - i_{air,outlet}) \\ \dot{q} &= \left(5.30 \frac{lb_m}{s}\right) \left(1200 \frac{Btu}{lb_m} - 127.65 \frac{Btu}{lb_m}\right) \\ \dot{q} &= 5683.5 \frac{Btu}{s}\end{aligned}$$

Figure 30 compares the pressure drop models using the inputs given in table 11 for H2-031-021. The Zhukauskas model best predicts the pressure drop in advance by almost exactly calculating the measured pressure drop. The Kays & London model predicts the pressure drop using a  $C_f = 0.8$ , which was determined by

iteration. Neither the Holman-Jakob, Gunter-Shaw, nor the Boucher-Lapple correction models adequately model the pressure drop.

Now consider the second data point of interest within the Group 2 data set.

The numerical program inputs for H2-031-023 are given in table 12.

**Table 12 - Program Inputs for Run H2-031-023**

Run Number	H2-031-023
$\dot{m}_{air}$	5.51 lb <sub>m</sub> /s
$p_{air,inlet}$	1.56 psia
$i_{air,inlet}$	1190 Btu/lb <sub>m</sub>
$T_{water,inlet}$	72.6 °F
$P_{water,inlet}$	88.5 psia
$\dot{Q}_{water}$	9460 gpm

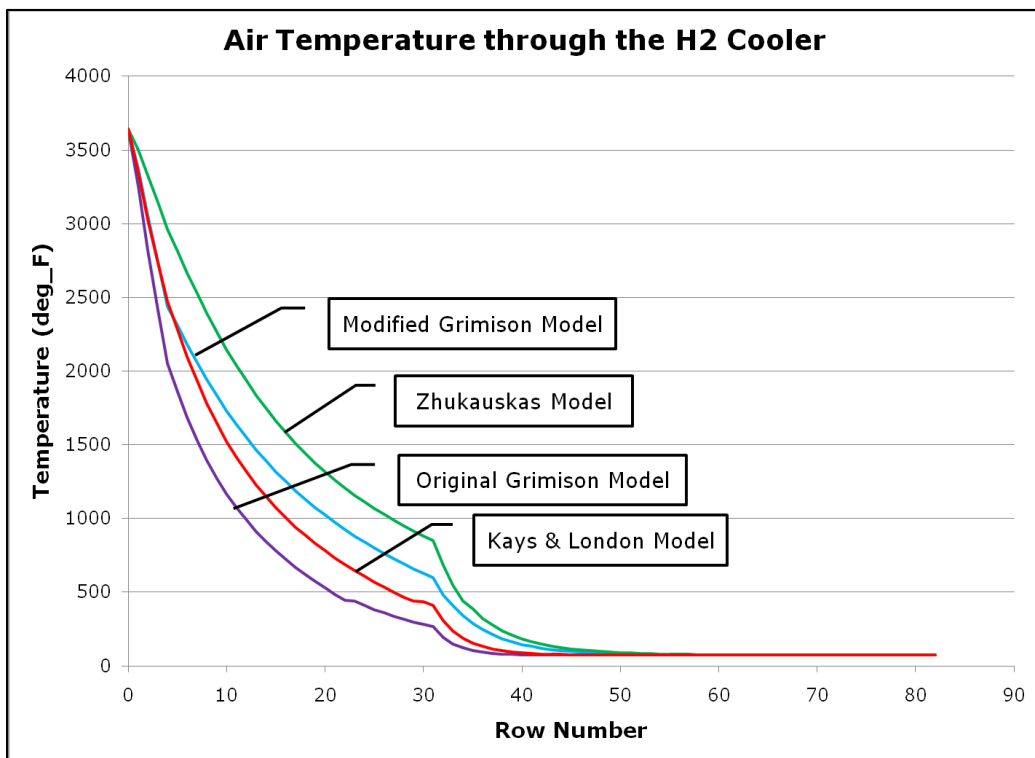


**Figure 31 - Air Temperature v. Axial Distance (Row Number) for Various Heat Transfer Models for H2-031-023**

It is interesting to note that for H2-031-023 (Figures 31-33) the original Grimison model predicts water temperatures that are very close to the measured values for bank 0 but then begins to deviate from the measured data. The calculated air and tube wall temperatures as calculated by the original Grimison model have profiles that are comparable to those calculated by the other heat transfer models as well. This is due to an increased mass flow rate for those data points within Group 2 as compared to those in Group 1. The increased mass flow rate increases the Reynolds number of the flow such that it begins to approach the lower Reynolds number limit of the original Grimison model as shown in figure 34. The change in geometry between banks 0 and 1 cause the flow velocity to decrease since, for the H2 cooler geometries, bank 1 has a 70% larger minimum free flow area than bank 0.

The modified Grimison model seems to underpredict the convective heat transfer coefficient, thus overpredicting the water temperature rise throughout the heat exchanger. Though the temperatures are overpredicted, the modified Grimison model better matches the water temperatures throughout the exchanger than the Zhukauskas model and better matches the water temperatures in banks 1-4 than the original Grimison model. The maximum relative error of the water temperature rise for this model is 1.17% for bank 0 tube manifold, but drops to as little as 0.01% for the bank 2 manifold.

The Zhukauskas model overpredicts the measured water temperature values for the run conditions of H2-031-023—having a maximum relative error of 2.08% from the measured results. It is interesting to note that the Zhukauskas model

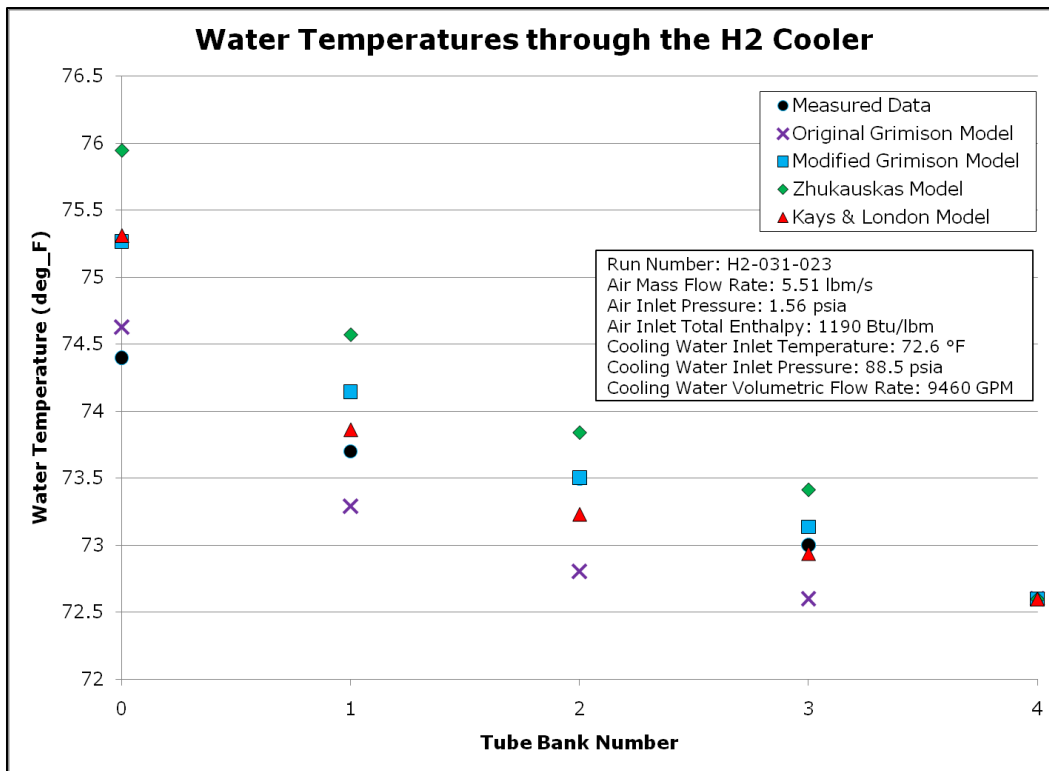


**Figure 32 - Inlet Water Manifold Temperature Comparisons by Heat Transfer Model for Run H2-031-023**

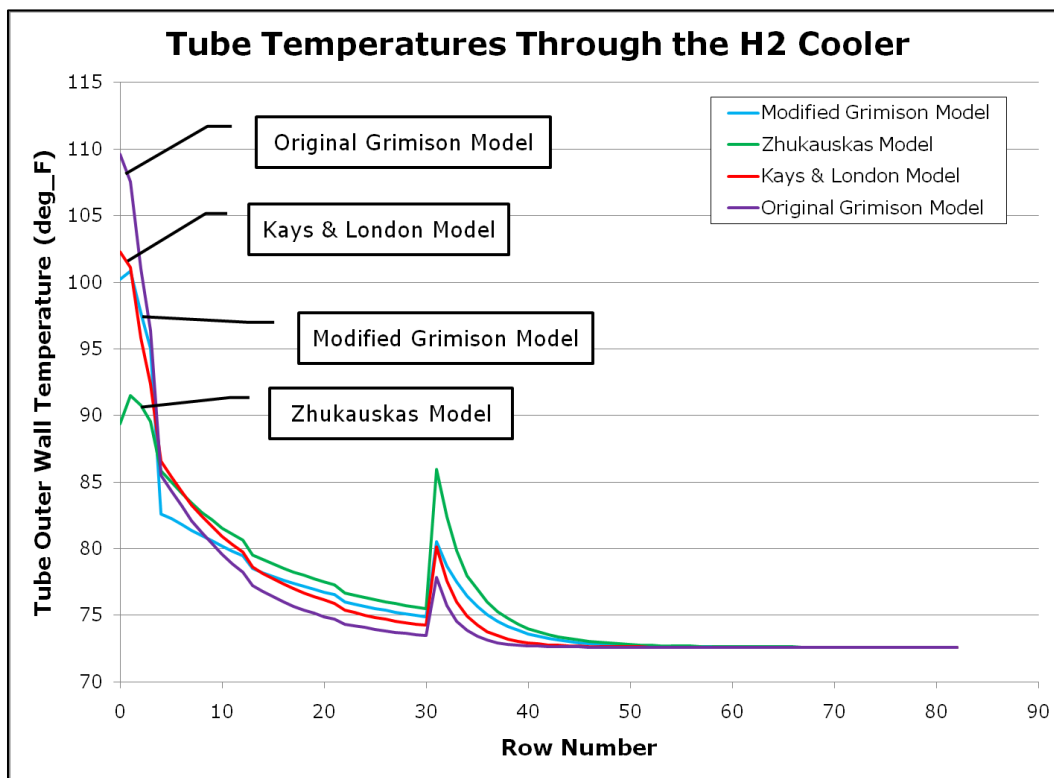


**Figure 33 - Tube Temperatures per Row as Calculated for H2-031-023**

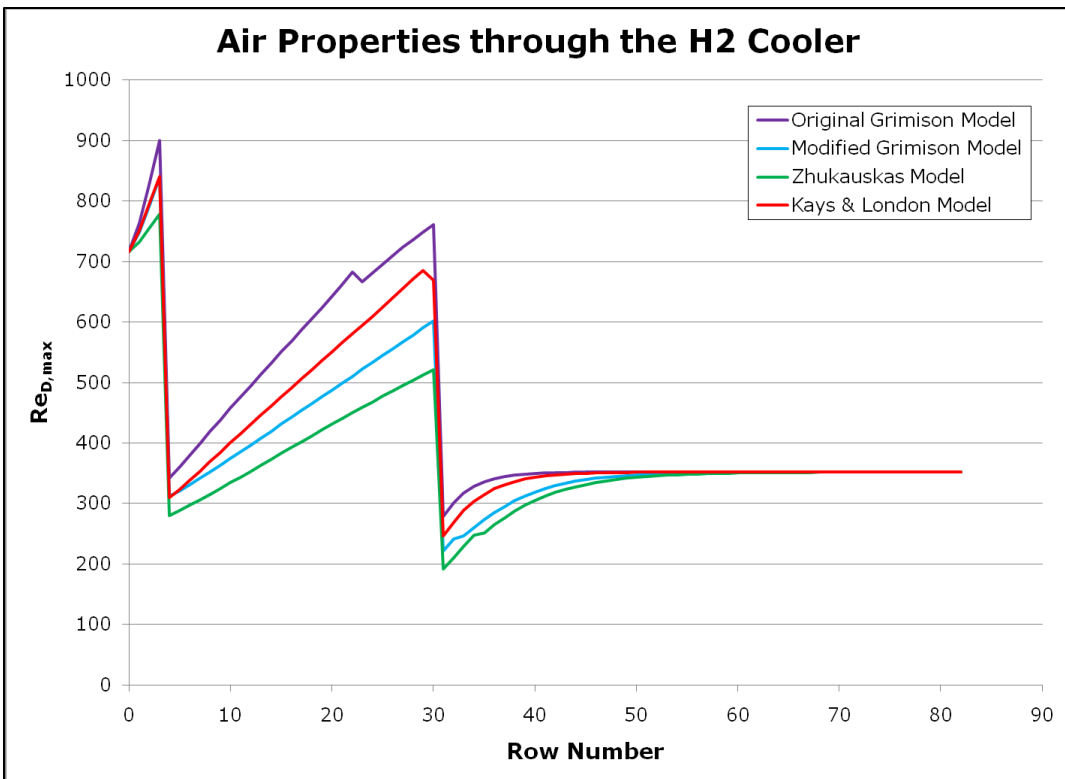


**Figure 34 - Calculated Reynolds Number by Heat Transfer Model for H2-031-023**

calculates almost half the energy extraction as the original Grimison model over the bank 0 tubes and approximately 40% of that calculated by the modified Grimison model; however, the model does calculate a much increased heat energy transfer than the original Grimison model and the modified Grimison model for the most downstream tube banks. This causes the large “spike” in the calculated tube wall temperatures at the bank 4 inlet as seen in figure 33 (starting with row 31). It is also interesting that the Zhukauskas model seems to predict profiles similar to those of the modified Grimison model (although differing in magnitude).

The Kays & London model best approximates the water temperatures for banks 1-4, though deviating somewhat largely for the bank 0 water temperature. For this run configuration, an overall  $C_h = 0.5$  gives the best match to the measured

water temperatures. With this  $C_h$ , the maximum relative error between the calculated water temperatures and the measured water temperatures is 1.23%.

For this test run, the outlet air temperature is once again equal to the temperature of the inlet cooling water as predicted by all the heat transfer models. Therefore the exchanger has  $\varepsilon = 1$  for this condition as well. By first law analysis

$$\dot{q} = \dot{m}_{air}(i_{air,inlet} - i_{air,outlet})$$

$$\dot{q} = \left(5.51 \frac{lb_m}{s}\right) \left(1190 \frac{Btu}{lb_m} - 127.75 \frac{Btu}{lb_m}\right)$$

$$\dot{q} = 5853 \frac{Btu}{s}$$

As with the pressure drop comparison of the previous data point, observe that the Zhukauskas model once again performs better than the Holman-Jakob,

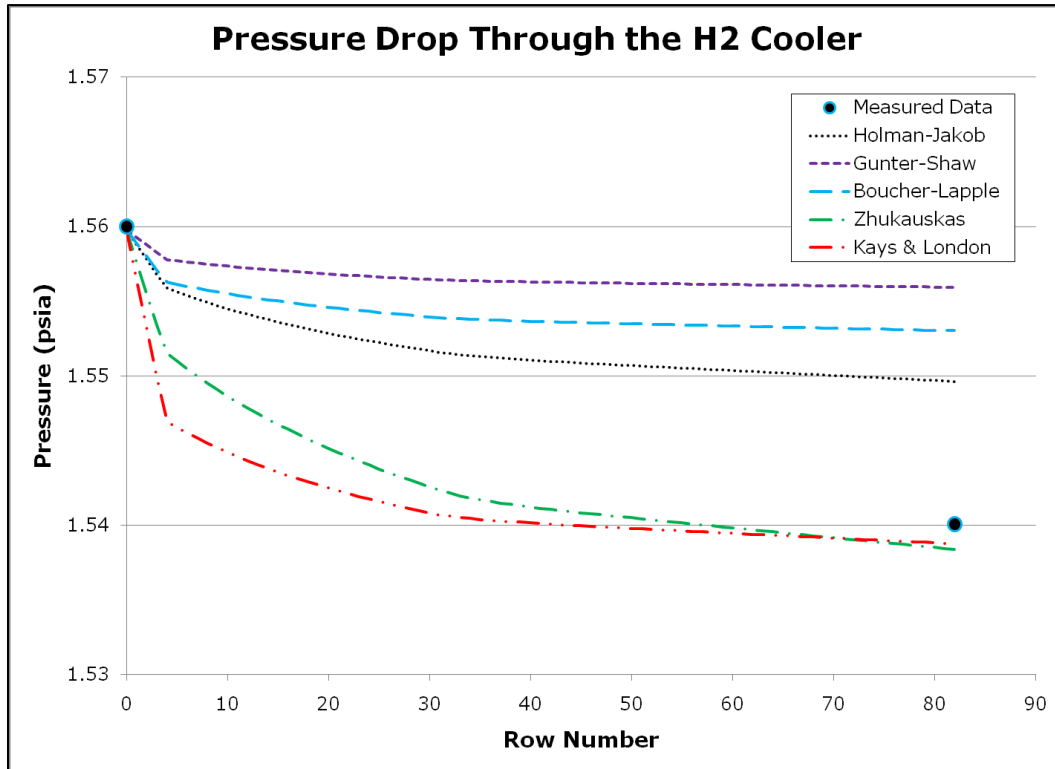


**Figure 35 - Comparison of Pressure Drop Models for H2-031-023**

the Gunter-Shaw, and the Boucher-Lapple correction models in terms of its predictive capability. As with the previous data, the Kays & London model calculates a pressure drop that very closely matches the measured the data using  $C_f = 0.8$ .

In comparing the data from the Group 1 representative data to that of the Group 2 set, it appears that the increased air mass flow rate seems to improve the calculation of the original Grimison model as well as closing the envelope of variability amongst the calculated air temperatures for all four of the heat transfer models as seen in figure 31. Next consider the data for the group 3 data from the dataset.

### **3.3 Group 3**

There are five test conditions within the cluster of Group 3, three of which have the more detailed instrumentation. Data point H2-031-020 within this subset will be considered. (All test runs in this group exhibit similar thermal data, temperature profiles, and deviate only slightly in the initial cooling water temperature measurement.)

**Table 13 - Program Inputs for Run H2-031-020**

<b>Run Number</b>	H2-031-020
$\dot{m}_{air}$	9.20 lb <sub>m</sub> /s
$p_{air,inlet}$	1.63 psia
$i_{air,inlet}$	1217 Btu/lb <sub>m</sub>
$T_{water,inlet}$	71.4 °F
$P_{water,inlet}$	88.6 psia
$\dot{Q}_{water}$	9560 gpm

Looking at the calculated air temperatures from the different heat transfer models (figure 36), a tight grouping of temperatures over the bank 0 tubes may be observed. As seen in figure 37, this tight grouping of bank 0 temperatures correlates to a tight grouping of calculated water temperatures; and—as seen in figure 38—an 8% spread in the calculated tube wall temperature.

Again, the sudden change in the curves in figure 36 at tube row number 31 is due to the change in tube type—from smooth tubes in bank 3 to finned tubes in bank 4. The increased available heat transfer area of the finned tubes causes a reduced thermal resistance (i.e. an increased heat transfer coefficient) and acts to increase the cooling rate of the air over those tubes.

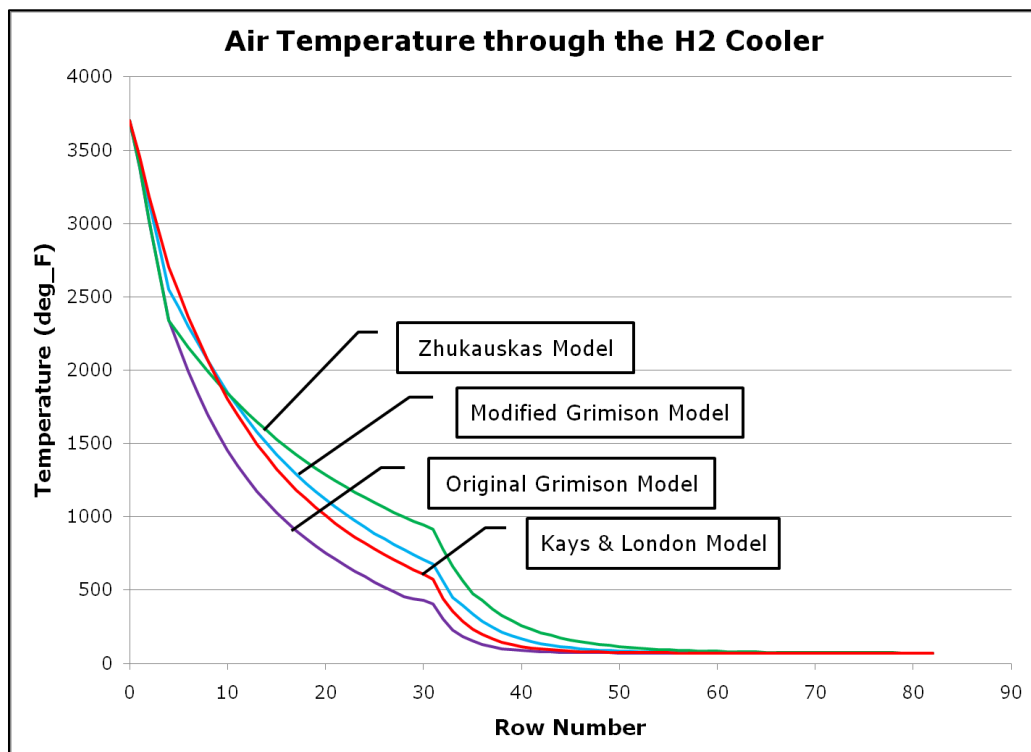


**Figure 36 - Air Temperature v. Axial Distance (Row Number) for Various Heat Transfer Models for H2-031-020**

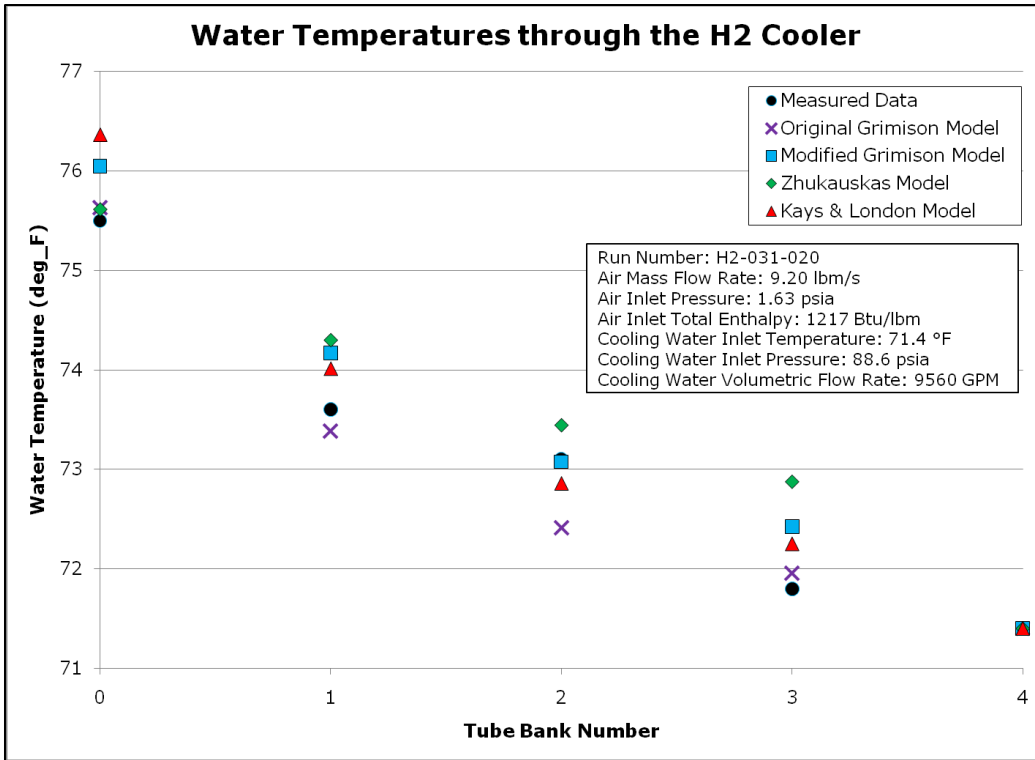


**Figure 37 - Inlet Water Manifold Temperature Comparisons by Heat Transfer Model for Run H2-031-020**

It is notable that for the bank 0 calculation the calculated  $Re_{D,max}$  value approaches the lower bound accepted  $Re_{D,max}$  value of 2000 for the original Grimison model. The Grimison model, as per usual, predicts a higher tube wall temperature than the other models. Because the Reynolds number is nearer the proposed valid operating range for the Grimison model, the calculated temperatures can be seen as being more reasonable and could arguably be used as a "safe-side" prediction of results for this condition. The maximum relative error of the calculated water temperature increase to the measured data is 0.94% and occurs in bank 2. This is expected since the Reynolds number has been much reduced due to the larger flow field area in the intermediate banks.

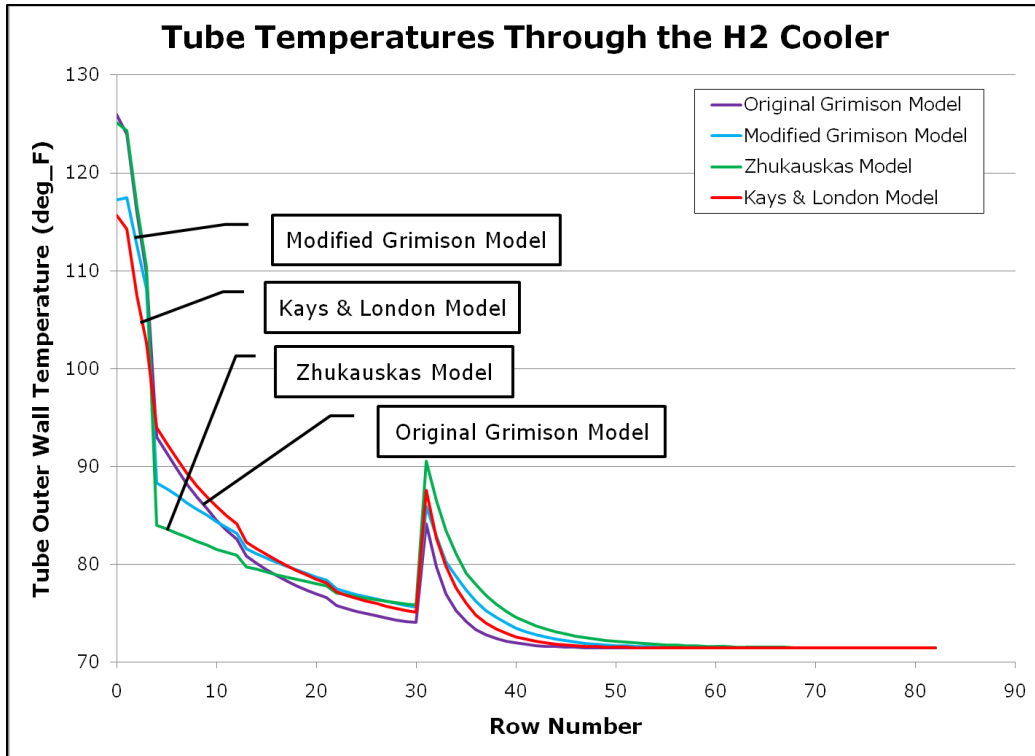


**Figure 38 - Tube Temperatures per Row as Calculated for H2-031-020**

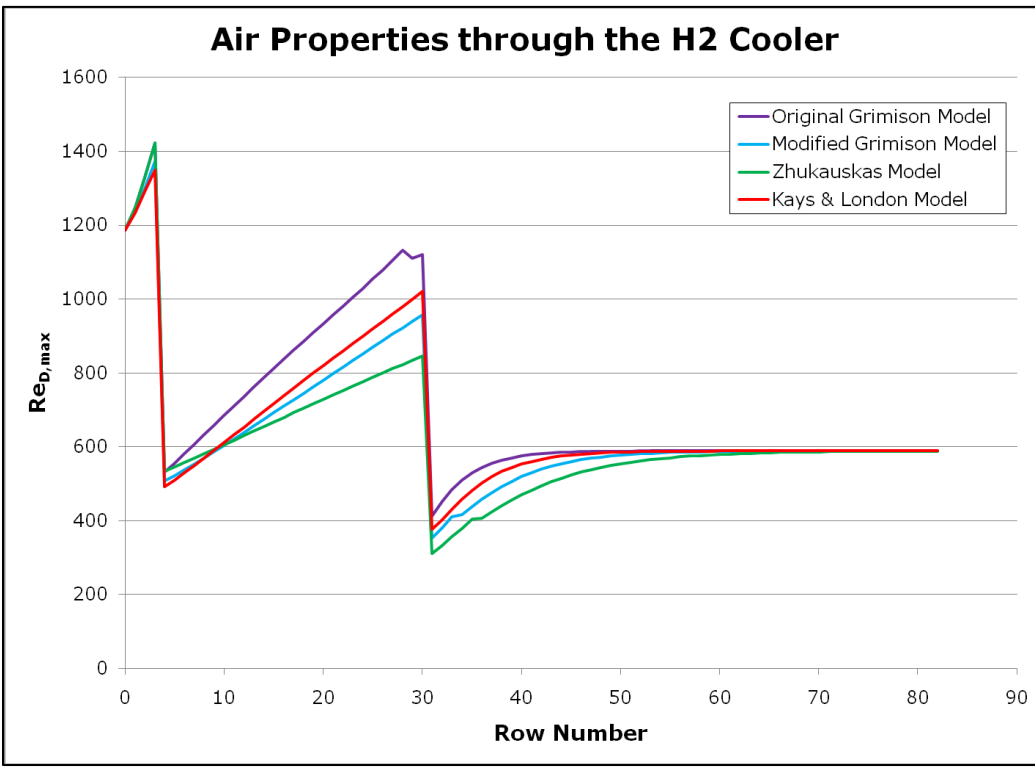


**Figure 39 - Calculated Reynolds Number by Heat Transfer Model for H2-031-020**

The modified Grimison model calculates a lower tube wall temperature than the original Grimison model for a large portion of the upstream tube rows. The model also calculates water temperature rises that vary by, at most, 0.87%. As expected, the modified Grimison model presents profiles that are similar to the Zhukauskas model as evidenced in the preceding figures.

The Zhukauskas heat transfer model does a good job of modeling the water temperature increases, having a maximum relative error of 1.56%. It is interesting to note the calculated tube temperature magnitude and profile similarities of the Zhukauskas model and the original Grimison model over the bank 0 tubes in figure 38. With the exception of the first tube, the calculated temperatures are nearly identical for the following tubes within the first bank.

The Kays & London model, using an overall  $C_h = 0.5$ , yields good agreement with the measured water temperature data. The maximum relative error in the measured water temperatures and the calculated temperature is 1.15%.

The four heat transfer models show that the outlet air temperature is once again equal to the temperature of the inlet cooling water. The exchanger has  $\varepsilon = 1$  for this condition since the outlet air temperature is equal to the inlet water temperature. By the first law of thermodynamics, the calculated heat transfer rate is equal to

$$\begin{aligned}\dot{q} &= \dot{m}_{air}(i_{air,inlet} - i_{air,outlet}) \\ \dot{q} &= \left(9.20 \frac{lb_m}{s}\right) \left(1217 \frac{Btu}{lb_m} - 127.46 \frac{Btu}{lb_m}\right) \\ \dot{q} &= 10,024 \frac{Btu}{s}\end{aligned}$$

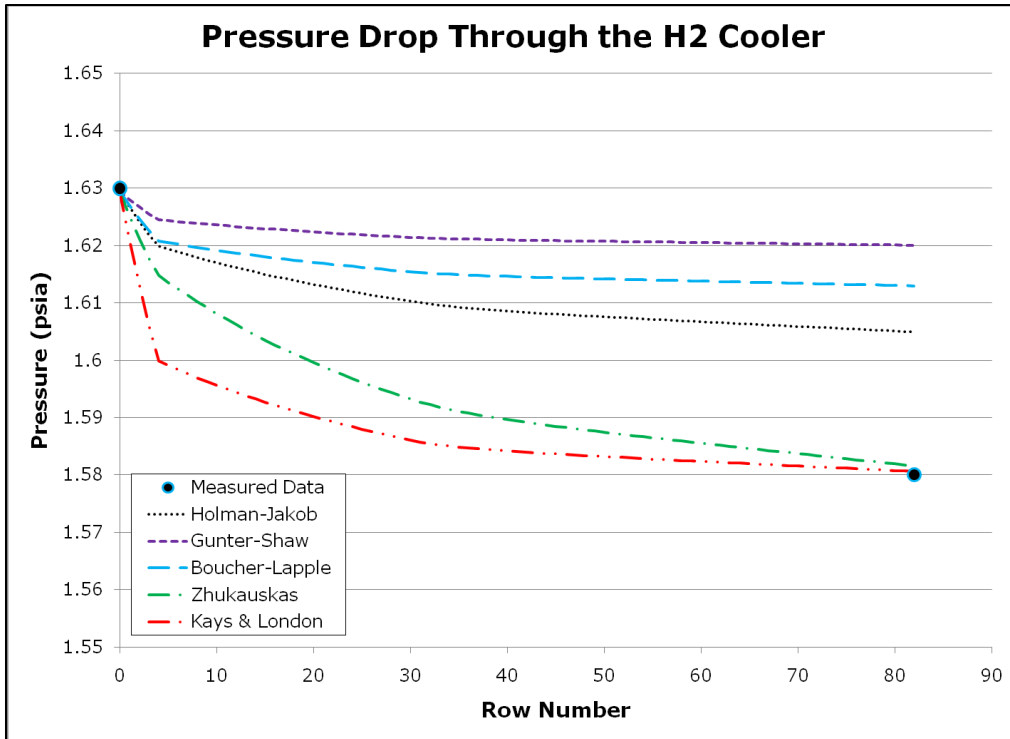


**Figure 40 - Comparison of Pressure Drop Models for H2-031-020**

This calculated heat transfer value is an expected result due to the mass flow rate being approximately 1.7 times that of those runs in Group 2, but having nearly the same inlet enthalpy value.

Figure 40 shows the calculated pressure drop across the heat exchanger. Again the Zhukauskas model is greatly superior to the Holman-Jakob, the Gunter-Shaw, and the Boucher-Lapple correction models in terms of its agreement with the measured data. As with the previous data, the Kays & London model calculates a pressure drop that very closely matches the measured data using an overall  $C_f = 0.8$ .

### **3.4 Group 4**

Of the eight total run conditions within the Group 4 data set, four have the intra-bank water measurements thus far used in the calculation. The others have

inlet and outlet only information, but due to having little variation in inlet temperatures and pressures, the data is much the same for all eight runs. Therefore, consider one characteristic data point within the Group 4 subset using the numerical model inputs given in table 14.

**Table 14 - Program Inputs for Run H2-031-019**

Run Number	H2-031-019
$\dot{m}_{air}$	10.20 lb <sub>m</sub> /s
$p_{air,inlet}$	1.71 psia
$i_{air,inlet}$	1455 Btu/lb <sub>m</sub>
$T_{water,inlet}$	72 °F
$P_{water,inlet}$	84.8 psia
$\dot{Q}_{water}$	9688 gpm

All of the heat transfer models produce comparable temperature profiles as evidenced by figure 41. With the exception of the original Grimison model, the heat transfer models tend to converge on similar values for the calculated water temperature rise as seen in figure 42.

The original Grimison model tends to underpredict the temperature differentials of the intra-bank manifolds for this run condition. Referencing figure 44, it may be seen that for many tube rows the Reynolds number approaches the accepted lower bound Reynolds number for the original Grimison model. This helps the original Grimison model to better match the measured water temperature data, but because the Reynolds number falls with the geometry change between the first and second tube banks, the calculated heat transfer coefficient becomes less than those calculated by the other models.

As may be observed in figure 42, the modified Grimison model produces results that agree rather well with the measured water temperatures. The modified model has a maximum relative error of 0.59% of the measured water temperature (occurring at the bank 2 measurement). The modified Grimison model calculates a maximum tube wall temperature that is also within approximately 8°F of that calculated by the Zhukauskas model.

As seen in figure 42, the Zhukauskas model also agrees with the measured water temperature data—having a maximum relative error of 1.25% of the measured water temperature values. It is interesting to observe that the methods of calculation between the modified Grimison model and the Zhukauskas model are

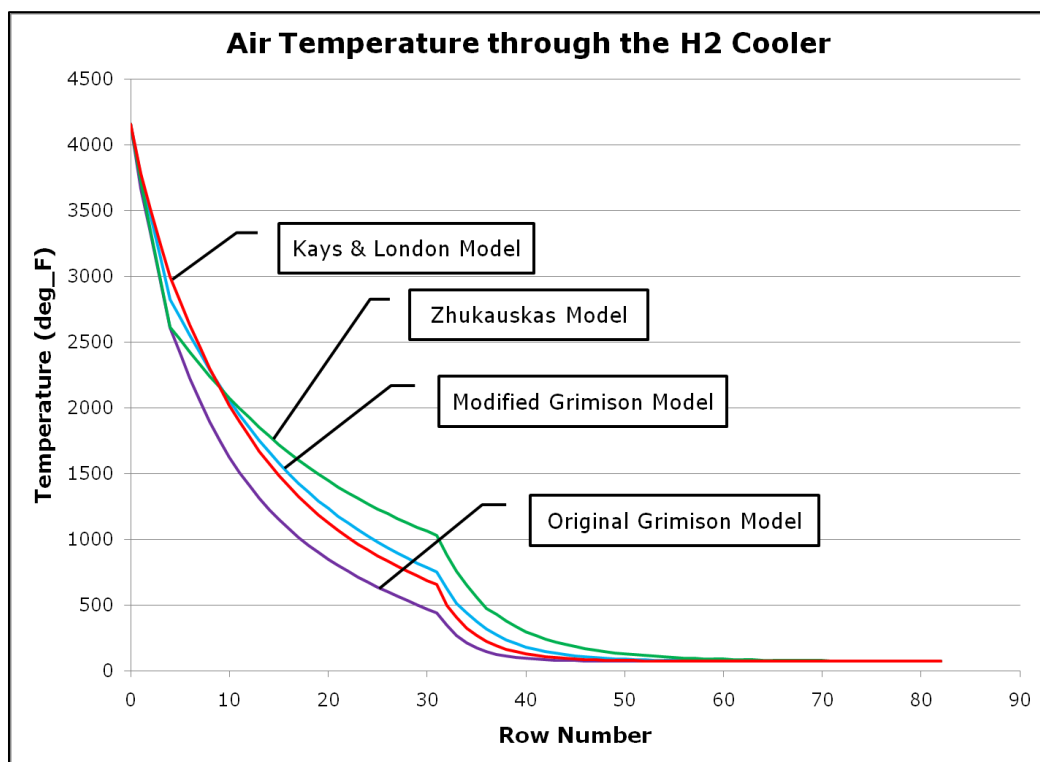


**Figure 41 - Air Temperature v. Axial Distance (Row Number) for Various Heat Transfer Models for H2-031-019**

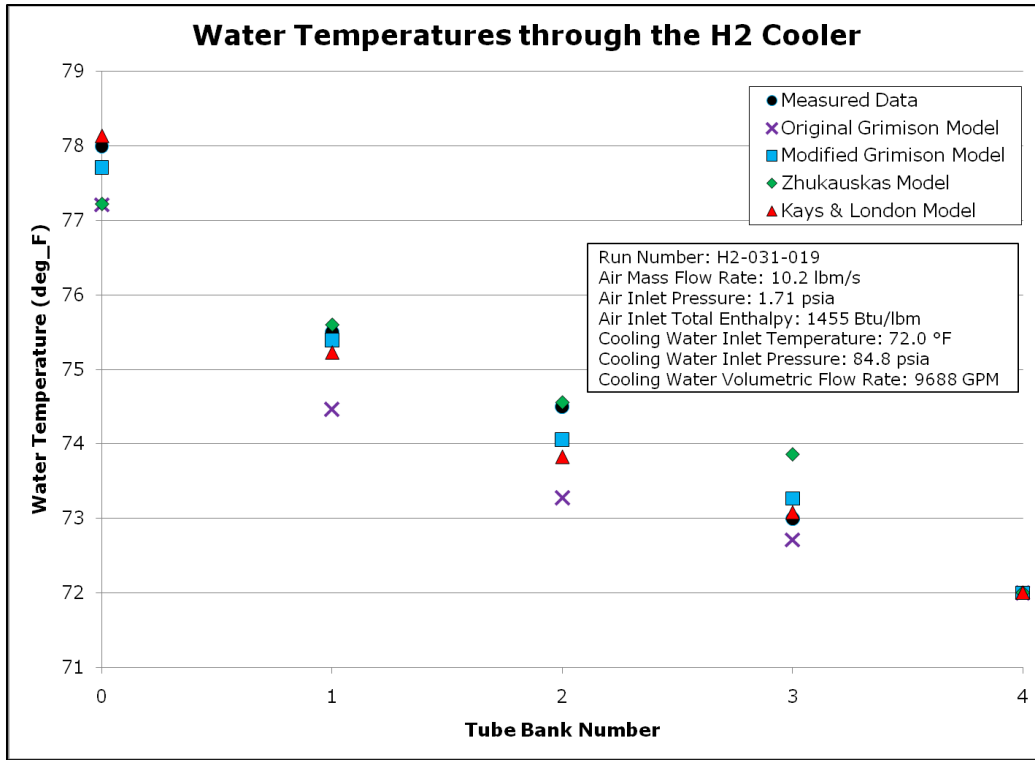


**Figure 42 - Inlet Water Manifold Temperature Comparisons by Heat Transfer Model for Run H2-031-019**

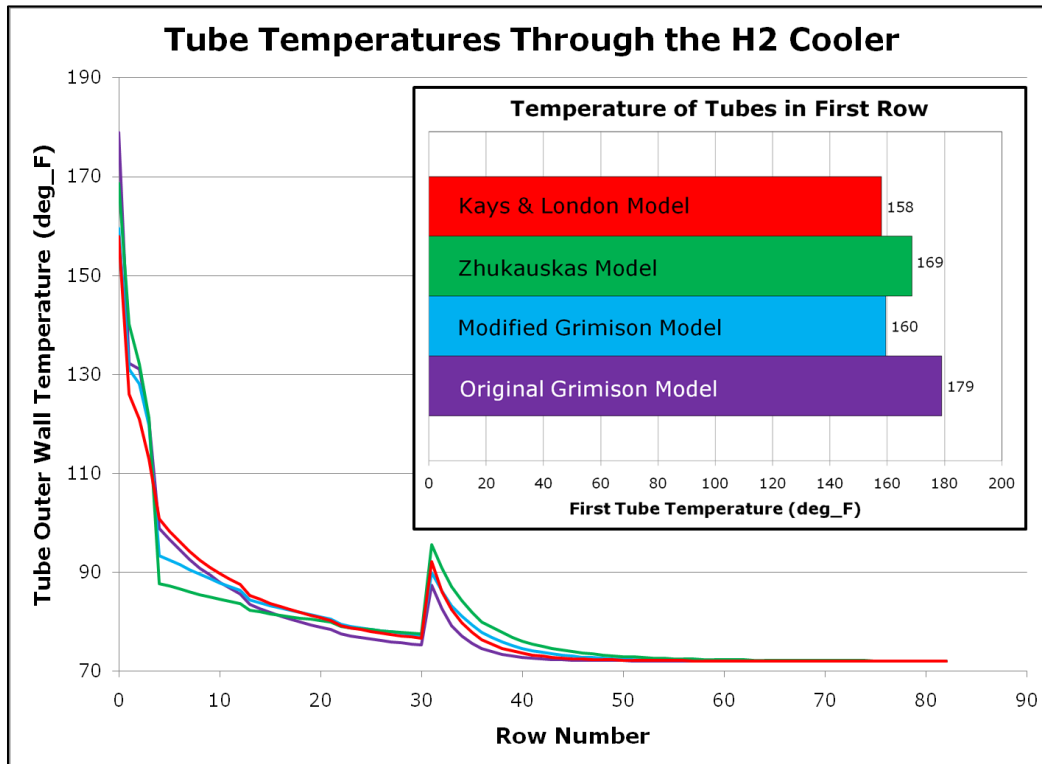


**Figure 43 - Tube Temperatures per Row as Calculated for H2-031-019**

vastly different, yet—for this condition—produce very similar results in most every aspect. The Zhukauskas model does calculate an air temperature that is almost 500°F greater than the other three models for the most downstream (bank 4) inlet. The model also shows that more of the finned tubes in bank 4 are required to cool the flow than the number calculated by the other models (see figure 41).

The Kays & London heat transfer model produces water temperature values that agree well with the measured data. Using an overall  $C_h = 0.5$ , the maximum relative error in the calculated water temperatures is 0.91% of the measured data. It is noteworthy to observe that the Kays & London model appears to remove heat energy from the air at a slower rate than the other models over the bank 0 hot section tube bank. This may be a numerical effect due to having insufficient  $C_h$  for the actual tube geometries present in the cooler, leading to some error propagating into the downstream tube bank calculation. It is assumed that this probable error is later compensated in the downstream tubes due to further geometry changes. Through much of the intermediate banks, the Kays & London model calculates greater tube wall temperatures than the other three models. The Kays & London model did, however, calculate a maximum tube wall temperature that is nearly 20°F cooler than that predicted by the original Grimison model.

The calculated  $Re_{D,max}$  is plotted in figure 44. Observe that the calculated Reynolds numbers are less than the recommended lower bound for the original Grimison model. Recall that the discontinuities in the curves are due to geometry changes between tube banks and that the differences in the calculated  $Re_{D,max}$  of the models are due to the differences in the calculated air density.

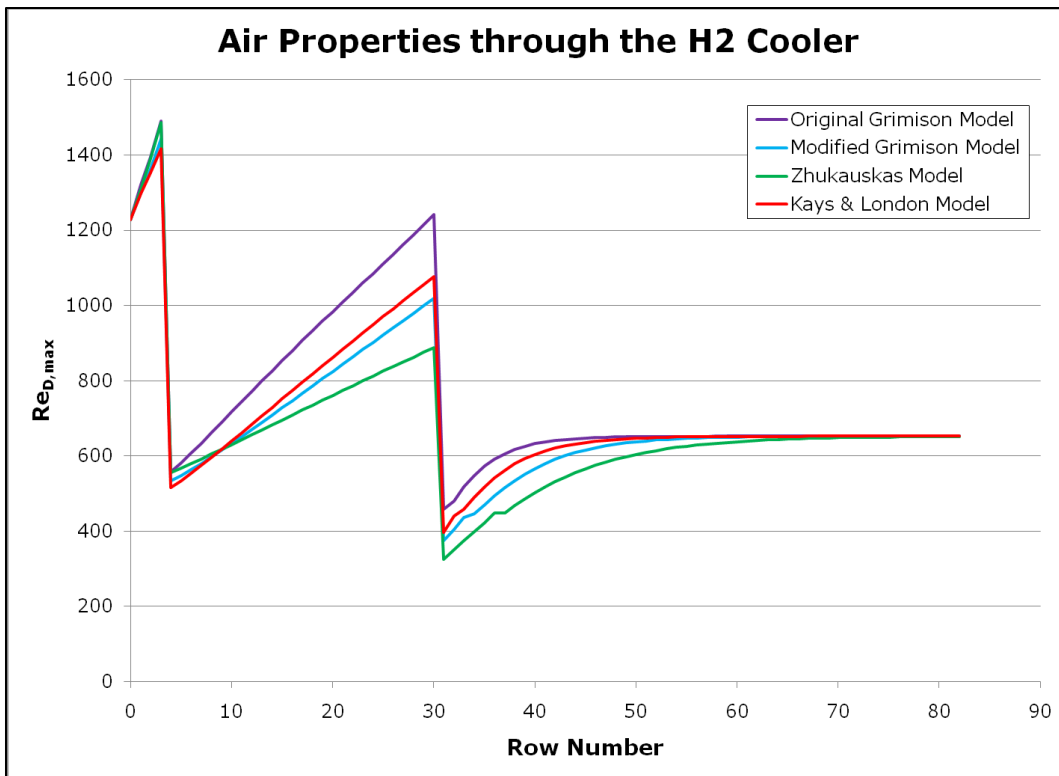


**Figure 44 - Calculated Reynolds Number by Heat Transfer Model for H2-031-019**

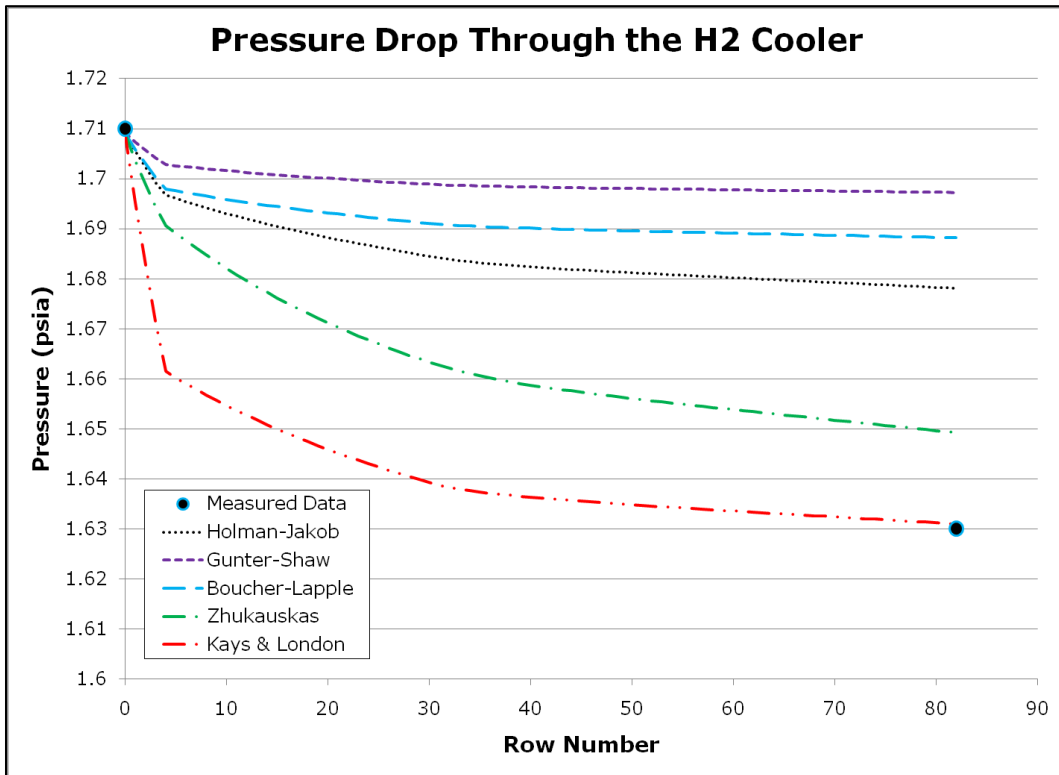


**Figure 45 - Comparison of Pressure Drop Models for H2-031-019**

As observed in figure 45, most of the models underpredict the measured pressure drop for this run condition. Using an overall  $C_f = 1.0$ , the Kays & London model predicts the measured pressure differential. The Zhukauskas model fits within approximately 25% of the measured pressure drop (1.2% of the outlet pressure value). As with previous data, the Holman-Jakob model, the Gunter-Shaw model, and the Boucher-Lapple corrected model underpredict the pressure drop by a significant amount.

The heat transfer models again show that the outlet air temperature is equivalent to the temperature of the inlet cooling water. For the test runs in Group 4, the cooler has  $\varepsilon = 1$  since the outlet air temperature is equal to the inlet water temperature. By the first law of thermodynamics, the calculated heat transfer rate is equal to

$$\dot{q} = 13,540 \frac{\text{Btu}}{\text{s}}$$

### **3.5 Possible Test Condition**

As mentioned previously, the intent of this study is to evaluate possible limitations of the existing heat exchanger. A representative high mass flow rate, high inlet enthalpy condition was chosen as a "worst case" condition. It may be recalled that the primary failure mechanism for this type of condition would be tube wall thermal failure. The inputs for this representative condition are presented in table 15.

It may be seen in figure 46 that the tube wall temperatures are much increased over those observed in the previous test cases. This is especially important as it dictates whether the initial tubes would need to be replaced with a

higher conductance material or if an increased water volumetric flow rate would be sufficient to adequately cool the tubes to prevent thermal failure.

**Table 15 - Input Conditions for Representative High Heat Flux Run**

Run Number	N/A
$\dot{m}_{air}$	15 lb <sub>m</sub> /s
$p_{air,inlet}$	1.7 psia
$i_{air,inlet}$	5000 Btu/lb <sub>m</sub>
$T_{water,inlet}$	72 °F
$P_{water,inlet}$	80 psia
$\dot{Q}_{water}$	9500 gpm

Note that there is a 20% spread in the calculated tube temperatures of the first row tubes. If the original Grimison model is deemed a “safe side” estimate of the tube temperatures (and, indeed, the model could be done so based on the calculated Reynolds numbers as shown in figure 47), then it is evident that the current tubes would need to retain their strength at over 700°F. If it is accepted that the present modified Grimison model is more representative of the convective environment, then the actual tube temperature may only be 585°F.

Though the input mass flow rate is about 50% higher than that presented in the previous section, the Reynolds number still fails to break above 1500 due to the much reduced air density. The much greater input enthalpy implies a greater air temperature. The elevated temperatures (at similar pressures as the previous runs) imply that the density is reduced while the viscosity is actually slightly increased at these temperatures (based on the curve fit data in reference [4]).

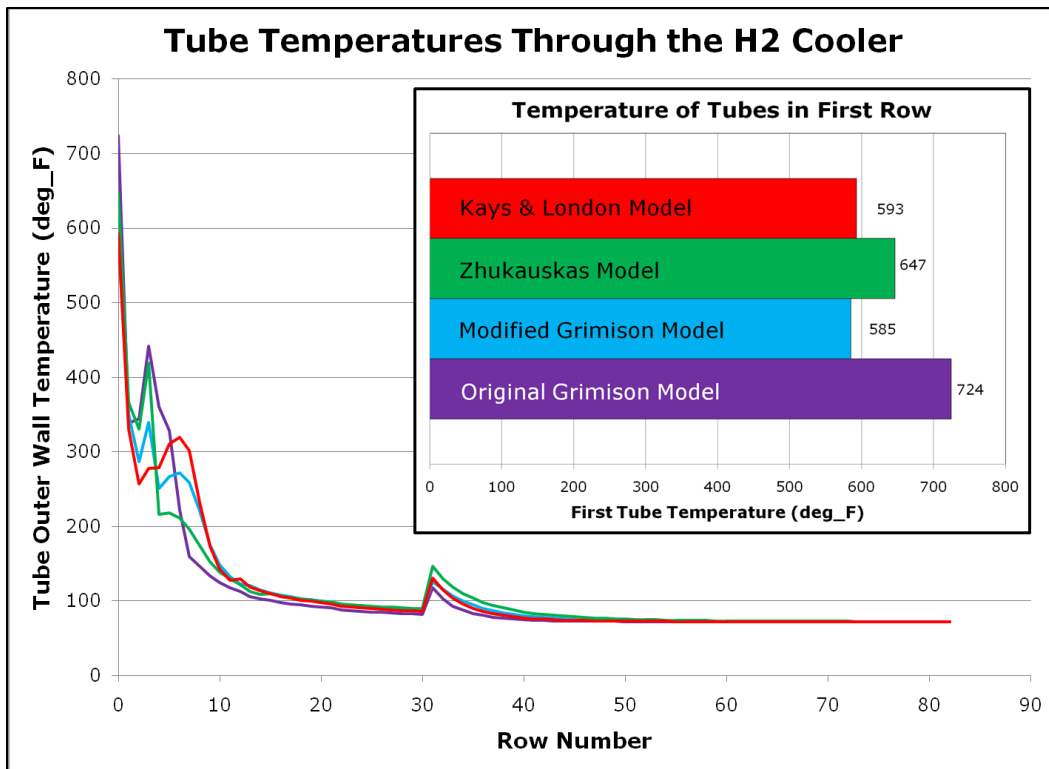


**Figure 46 - Tube Temperatures of Representative High Heat Flux Condition**

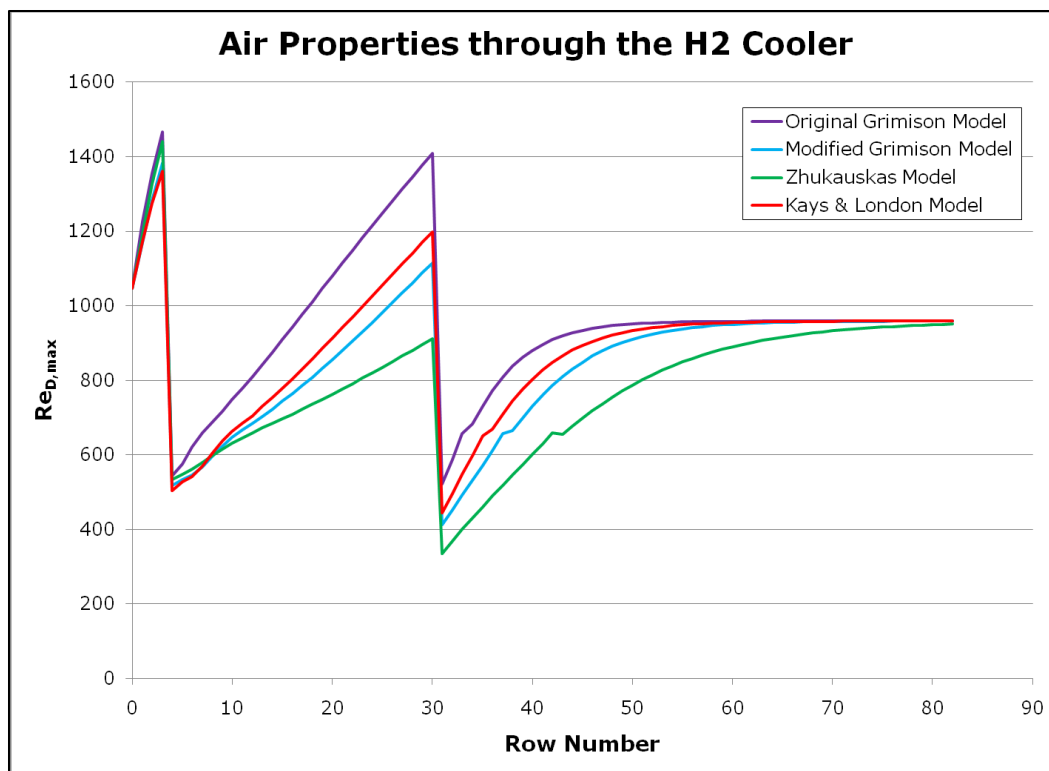


**Figure 47 - Calculated Reynolds Number for Representative High Heat Flux Condition**

This combination works to reduce the calculated Reynolds number for the same freestream velocity and tube diameters.

### **3.6 Influence of Variables**

Over the four heat transfer models, the variable that plays the largest role in the evaluation of the heat transfer rate for the conditions listed is the Reynolds number. As shown in figure 48, the Prandtl number actually has the smallest role in the determination of the Nusselt number calculation.

Note that for the Zhukauskas heat transfer model, the geometry effects are nearly zero for conditions such that  $Re < 100$  or  $Re > 1000$ . The large increase in geometric effects is due to the fact that the tube diameter is used to calculate  $Re_D$

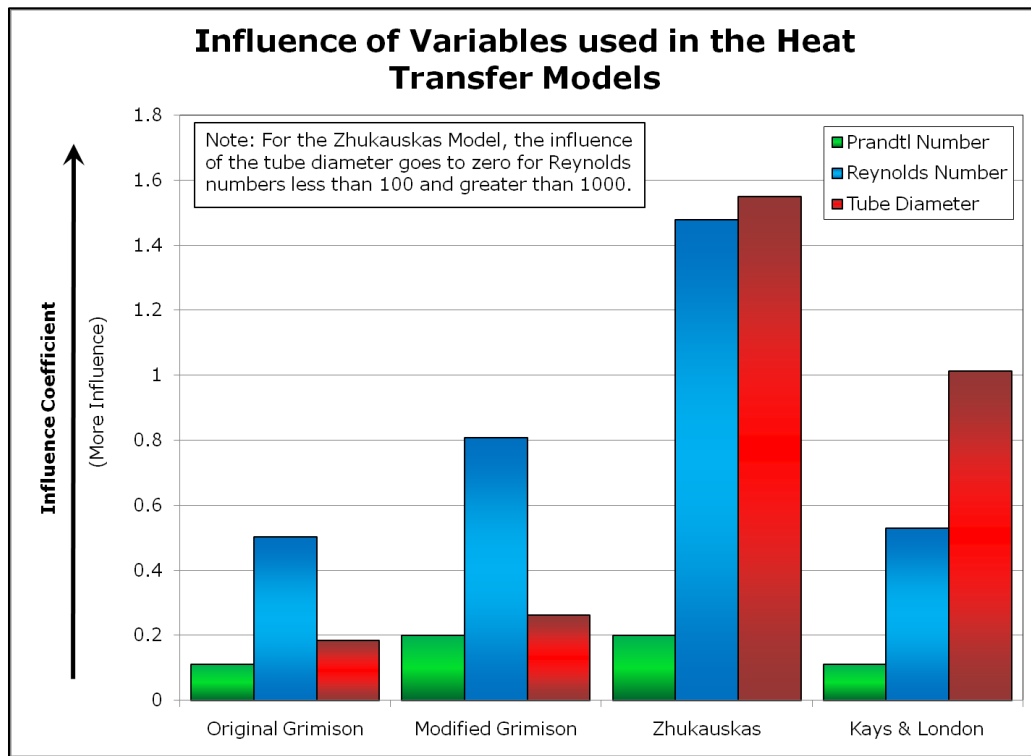


**Figure 48 - Influence Coefficients on the Nusselt Number Calculation for the Four Heat Transfer Models**

based on the freestream velocity since for that the model requires that the system be modeled as a single isolated cylinder for that Reynolds number regime.

Note also that the influence of geometry may be biased high—in the case of the Kays & London model—since some  $C_H$  factors were extrapolated. As mentioned previously, the Kays & London heat transfer relation appears very similar to the original Grimison model but is used for the case of “compact” heat exchangers—implying smaller tube spacings than those used in the H2 staggered tube heat exchanger.

### **3.7 Real Gas Effects**

As mentioned previously, an initial model was developed when the heat exchanger was procured in 1987. This initial model used statically determined properties as given in table 16. From these properties, the specific heat was calculated by

$$c_p = \mathbb{R} \frac{\gamma}{\gamma-1},$$

the air temperature was calculated by

$$T \approx \frac{i}{c_p},$$

the air density was calculated using the ideal gas law (assuming a compressibility of unity), and the air viscosity was calculated using Sutherland’s viscosity law which is given as:

$$\mu = 1.4584 \times 10^{-5} \frac{T^{3/2}}{T+110.33} \quad ([T] = \text{Kelvin}, [\mu] = \text{poise})$$

**Table 16 - Static Thermodynamic Properties used in Original Model**

$\gamma$	1.2
$R$	53.34 $\frac{ft-lb_f}{lb_m - ^\circ R}$
$Pr$	0.71
$k$	0.047 $\frac{Btu}{ft-hr-^{\circ}F}$

It should be evident that these static properties will be acceptable for moderate input enthalpies, but will produce drastically erroneous results for higher input enthalpies. From the heat transfer perspective, the term that will present the largest calculation error is the use of a static specific heat value. Also, Gupta, et. al recommend that Sutherland's viscosity law only be used for temperatures less than 500 K (440°F)<sup>[4]</sup>. The variability of the relevant thermodynamic properties of air at 1.5 psia is presented in Appendix D.

Compare the real gas effects of the two conditions presented for H2-031-020 (table 13) and for the notional, high enthalpy condition (table 15). For the plots shown, the Zhukauskas heat transfer model and the Zhukauskas pressure drop model were used.

Observe from figure 49 that the calculated air temperatures deviate somewhat near the cooler inlet and over the bank 3 tubes. This is due to the calculation of temperature using enthalpy and a static specific heat value. These air temperature deviations produce a calculated tube wall temperature that is approximately 20% less than the temperatures calculated using real gas properties over the first tube bank as seen in figure 50.

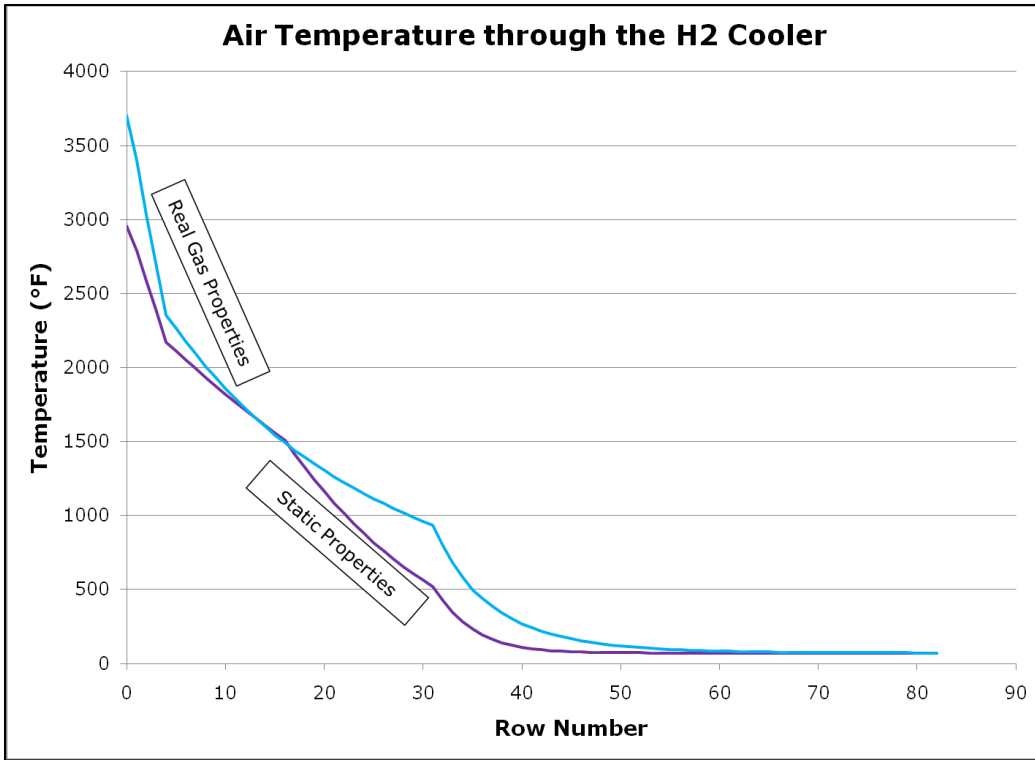


**Figure 49 - Air Temperature Comparisons Using Static Properties and Real Gas Properties for H2-031-020**

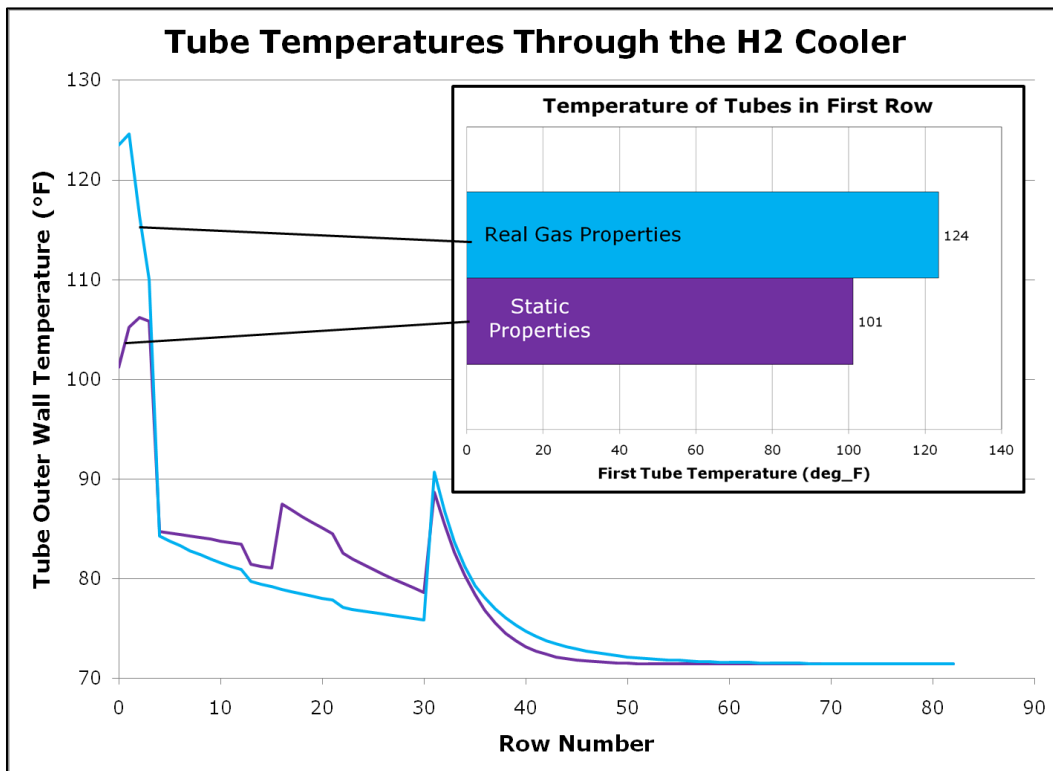


**Figure 50 - Calculated Tube Wall Temperature Comparisons Using Static Properties and Real Gas Properties for H2-031-020**

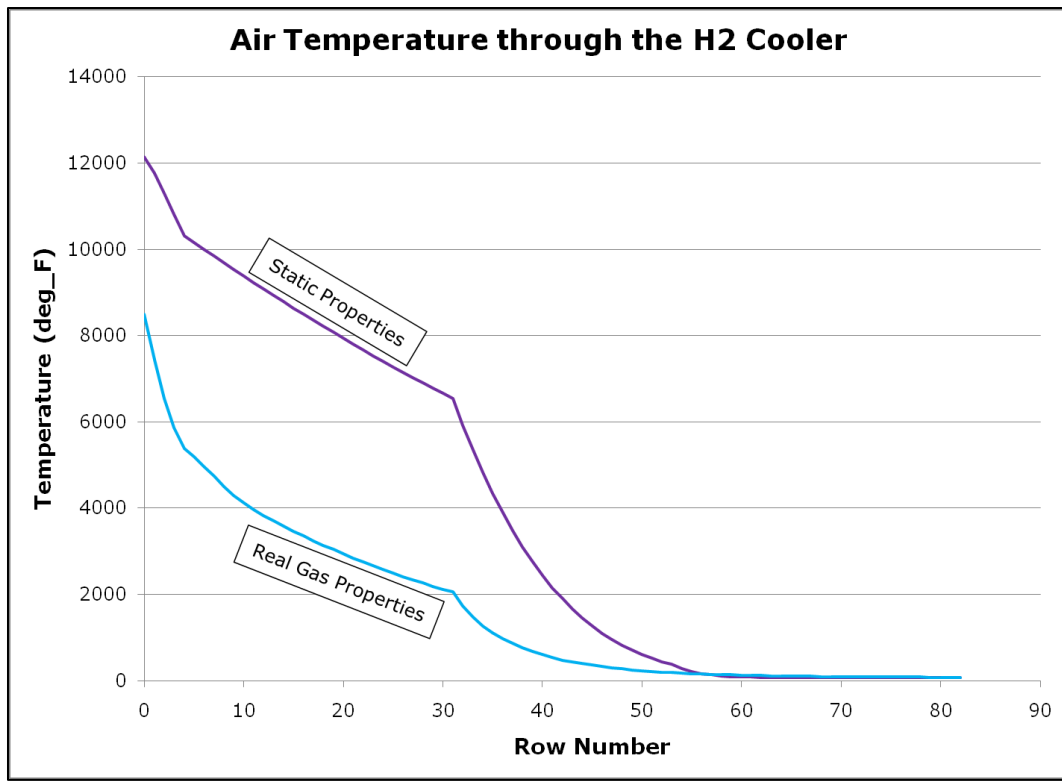


**Figure 51 - Air Temperature Comparison for High Enthalpy, Notional Condition**

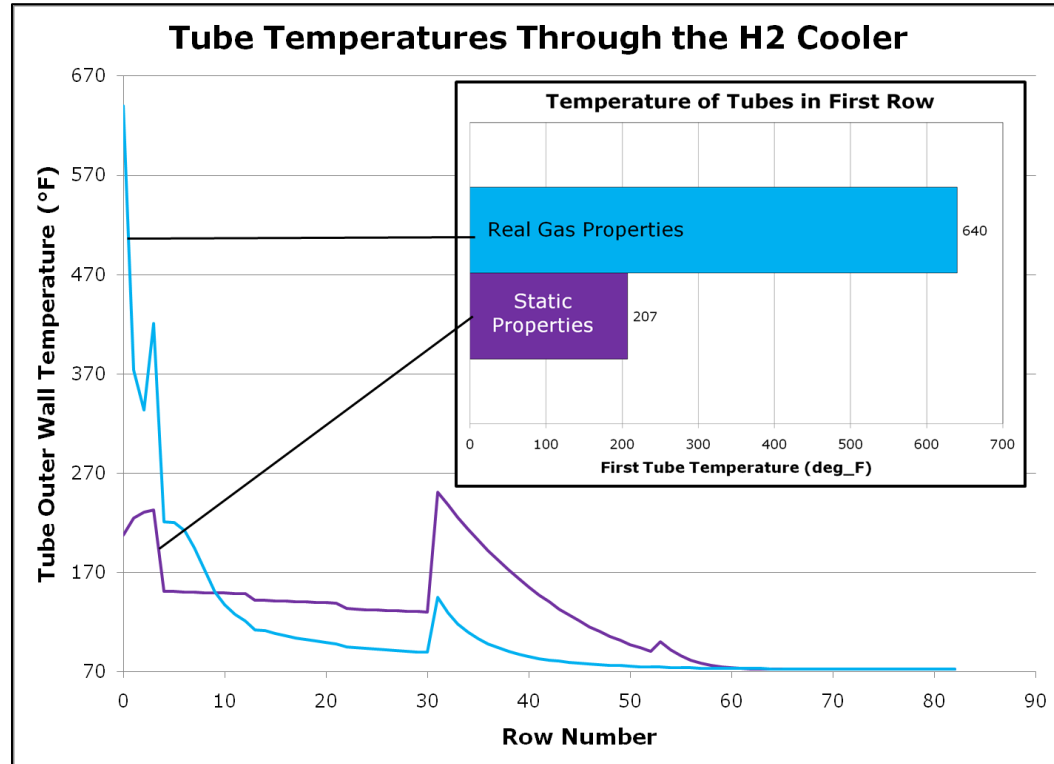


**Figure 52 - Calculated Tube Wall Temperature Comparison for High Enthalpy, Notional Condition**

Observe the effect of increasing the enthalpy as in the notional test condition. In figure 51, it can be seen that the calculated air temperatures deviate by at most 300% at the inlet of the bank 4 finned tube region beginning with tube row number 31.

Figure 52 shows the calculated tube wall temperatures for the notional high enthalpy input condition. Note that using real gas properties to calculate the outer wall temperature of tubes in the first row results in a value that is over three times the value of that calculated using statically determined properties. This shows that pressure and temperature dependent properties must be used when making design considerations; otherwise, catastrophic failure of the exchanger may occur due to vastly under-predicting the flow conditions.

## 4.0 Conclusions

It would seem that for the run conditions specified, the heat transfer models are not as sensitive to Prandtl numbers less than 0.7 as was first suspected. The models seem to exhibit significantly more sensitivity to the Reynolds number. While geometry effects are important to the models, the geometric effects as manifested in the evaluation of  $Re_{D,max}$  seem to play a much larger role than the scalar coefficients that are typical determined based on the bank geometry and tube diameter.

In all presented test cases, the author's modified Grimison heat transfer model is the best at predicting the performance of the H2 air cooler, and has parity with the well-established Zhukauskas model for many conditions. Additionally, it is able to be implemented into computational models with fewer implementation costs than the Zhukauskas model. Though it is the most difficult to implement into code, the Zhukauskas model does perform well.

The Kays & London heat transfer model, though developed for much smaller heat exchanger geometries than the H2 heat exchanger, does present a good fit to the measured data with less complexity than the Zhukauskas model. However, the validity is questionable as to the use of a geometric scaling coefficient ( $C_H$ ) to adjust the "gain" of the model based on Reynolds number as is presented in this paper.

For all the established conditions presented, the heat exchanger exhibits an effectiveness equal to unity. This would imply that the existing cooler may have more tube rows than required to adequately cool the process air for the conditions presented herein. This may also imply that there is some thermal margin

exploitable by taking advantage of the axial length of the heat exchanger for possible upgrades.

The Zhukauskas pressure drop model tends to give the best prediction of matching pressure drop data for the given run conditions without the necessity of trial-and-error coefficient fitting. For most cases, the Zhukauskas model was able to match the pressure drop almost exactly. The Kays & London model could be a better model assuming one accepts that, for the cases presented, the  $C_f$  scaling factor was iterated upon to approach the measured data. Both models far surpass the Holman-Jakob and Gunter-Shaw models; including the Boucher-Lapple corrected model.

In all cases, results computed using temperature and pressure dependent properties are superior to those computed using statically determined properties. Without the use of real gas properties, tube wall temperatures may be grossly underestimated leading to possible thermal failure of the device.

It would seem that, though the fluid temperatures were much hotter than is typically encountered for a standard-industry-application heat exchanger (and by extension, the fluid's inlet enthalpy), the same numerical models may be used to evaluate the heat exchanger's performance provided that some accommodation is made for the reduced calculated Reynolds numbers.

The numerical model that was developed by the author for this effort allowed for the compilation of a suite of performance calculations that give a high confidence in estimating the thermal load limits for the H<sub>2</sub> heat exchanger. This compilation of data as well as the model will influence future decisions on the need

and efficacy of device upgrades and will play a key role in optimization studies for infrastructure enhancement opportunities.

# **References**

## References

- [1] Stepanek, S. A. and W. E. Bruce, "A User's Guide to the H2 Arc Facility," Calspan Corporation/AEDC Operations. AEDC-TMR-88-V32. May 1989 (Revised January 1992). Arnold Engineering Development Center, Arnold Air Force Base, TN.
- [2] Felderman, E. J., D. D. Horn, D. B. Carver, and L. M. Davis, "AEDC Expanded Flow Arc Facility (HEAT-H2) Description and Calibration," Proceedings of the 38th International Instrumentation Symposium, Paper No. 92-0191, April 1992.
- [3] Hammock, Gary. "The Use of Nitrogen as a Test Gas for Arnold Engineering Development Center's Huels H2 Arc Heater Facility," American Institute of Aeronautics and Astronautics. AIAA 2009-4091. 41<sup>st</sup> AIAA Thermophysics Conference. San Antonio, TX. June 2009.
- [4] Gupta, R., K. Lee, R. Thompson, J. Yos. "Calculations and Curve Fits of Thermodynamic and Transport Properties for Equilibrium Air to 30000 K". NASA Reference Publication 1260. October 1991.
- [5] Spang, B. "IAPWS Equations for Transport Properties and Surface Tension of Water and Steam". *The Chemical Engineers' Resource Page*. <http://www.chersources.com/iapwsif97.shtml>. Accessed: 16 Apr 2010.
- [6] *Revised Release on the IAPWS Industrial Formulation 1997 for the Thermodynamic Properties of Water and Steam*. The International Association for the Properties of Water and Steam (IAPWS). Lucerne, Switzerland. August 2007.
- [7] Incropera, F. P., David P. Dewitt. *Fundamentals of Heat and Mass Transfer*. Fifth Edition. John Wiley & Sons, Inc. Hoboken, NJ. 2002.
- [8] Grimison, E. D., "Correlation and Utilization of New Data on Flow Resistance and Heat Transfer for Cross Flow of Gases Over Tube Banks", Transactions of the ASME. Vol. 59, pp. 583-594. 1937.
- [9] Zhukauskas, A., R. Ulinskas. *Heat Transfer in Tube Banks in Crossflow*. Hemisphere Publishing Corporation. New York, NY. 1988.
- [10] Zhukauskas, A., "Heat Transfer from Tubes in Cross Flow", *Advances in Heat Transfer*. Volume 8. Academic Press, New York. 1972.

- [11] Bejan, Adrian. *Convection Heat Transfer*. Third Edition. John Wiley & Sons, Inc. Hoboken, NJ. 2004.
- [12] Kays, W.M., A. L. London. *Compact Heat Exchangers*. Third Edition. McGraw-Hill. New York. 1984.
- [13] Jakob. *Transactions of the ASME*. Volume 60. P. 384. 1938.
- [14] Gunter, A. Y., W. A. Shaw, "A General Correlation of Friction Factors for Various Types of Surfaces in Crossflow". *Transactions of the ASME*. Volume 67. pp. 643-660. 1945.
- [15] Boucher, D. F., C. E. Lapple, "Pressure Drop Across Tube Banks: Critical Comparison of Available Data and of Proposed Methods of Correlation". *Chemical Engineering Progress*. Volume 44, Number 2. pp. 117-134. 1948.

# **Appendices**

## Appendix A

### Calculation of Thermal Resistance for Finned Tubes

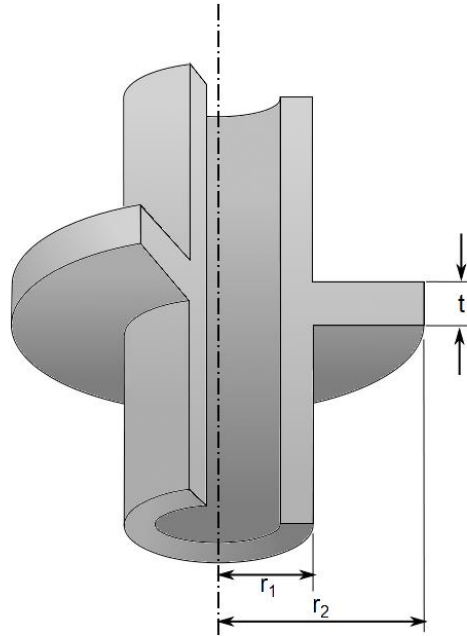


**Figure A.1 – Finned Tube Geometry**

For finned tubes, the thermal resistance is (usually) reduced due to the increased surface area and an alternately calculated convective heat transfer coefficient. The thermal resistance is derived from Newton's Law of Cooling:

$$\dot{q} = hA\Delta T \quad (\text{A.1})$$

However, for radially extended surfaces, equation A.1 incorporates relevant dimensions of the fins as well as a calculated fin efficiency factor. The heat transfer of a radial extended surface is given by equation A.2<sup>[7]</sup>.

$$\dot{q} = hA_T \left[ 1 - \frac{N_f A_f}{A_T} (1 - \eta_f) \right] \Delta T \quad (\text{A.2})$$

where the fin efficiency is calculated by the relation

$$\eta_f = \frac{\frac{2r_1}{m}}{(r_{2c}^2 - r_1^2)} \left\{ \frac{K_1(mr_1) I_1(mr_{2c}) - I_1(mr_1) K_1(mr_{2c})}{I_0(mr_1) K_1(mr_{2c}) + K_0(mr_1) I_1(mr_{2c})} \right\} \quad (\text{A.3})$$

Where:

$$r_{2c} = r_2 + \frac{1}{2}t$$

$$m = \sqrt{\frac{2h}{kt}}$$

Note that  $I_0(x)$  and  $K_0(x)$  are the modified zeroth order Bessel functions of the first and second kind, respectively. Note also that  $I_1(x) = \frac{d}{dx}\{I_0(x)\}$  and  $K_1(x) = \frac{d}{dx}\{K_0(x)\}$ .

The  $r_{2c}$  term is a correction to account for an active (convecting) tip on the fin.

Having calculated  $\eta_f$  and the relevant areas, the thermal resistance may then be calculated using equation A.4.

$$R_{conv,fins} = \frac{1}{hA_T \left[ 1 - \frac{N_f A_f}{A_T} (1 - \eta_f) \right]} \quad (\text{A.4})$$

## Appendix B

### Zhukauskas Pressure Drop Friction Factor Cubic Spline Coefficients

$$f = A(Re - Re_i)^3 + B(Re - Re_i)^2 + C(Re - Re_i) + D$$

$P_T = 1.25$				
Interval	A	B	C	D
$0 < Re \leq 10$	$1.00726 \times 10^{-4}$	0	-0.683987	24.2
$10 < Re \leq 40$	$-5.35359 \times 10^{-5}$	0.00906536	-0.412026	6.4
$40 < Re \leq 100$	$7.57755 \times 10^{-7}$	$-5.71094 \times 10^{-4}$	0.0976302	2.75
$100 < Re \leq 400$	$-7.36544 \times 10^{-8}$	$1.10885 \times 10^{-4}$	-0.0404323	1.1
$400 < Re \leq 1000$	$8.49917 \times 10^{-9}$	$-2.16926 \times 10^{-5}$	0.0130834	0.85
$1000 < Re \leq 2000$	$-7.15801 \times 10^{-10}$	$3.80496 \times 10^{-6}$	$-4.80421 \times 10^{-3}$	0.74
$2000 < Re \leq 4000$	$3.03398 \times 10^{-11}$	$-4.89846 \times 10^{-7}$	$1.82601 \times 10^{-3}$	0.625
$4000 < Re \leq 1 \times 10^4$	$-9.6498 \times 10^{-13}$	$5.62704 \times 10^{-8}$	$-7.75444 \times 10^{-4}$	0.5
$1 \times 10^4 < Re \leq 3.2 \times 10^4$	$4.39193 \times 10^{-14}$	$-7.41829 \times 10^{-9}$	$2.99303 \times 10^{-4}$	0.4
$3.2 \times 10^4 < Re \leq 1 \times 10^5$	$-5.42058 \times 10^{-15}$	$1.54123 \times 10^{-9}$	$-1.00338 \times 10^{-4}$	0.26
$1 \times 10^5 < Re \leq 2 \times 10^5$	$3.5392 \times 10^{-17}$	$-8.49408 \times 10^{-11}$	$4.52917 \times 10^{-5}$	0.218
$2 \times 10^5 < Re \leq 1 \times 10^6$	0	0	0	0.21

$P_T = 1.5$				
Interval	A	B	C	D
$0 < Re \leq 10$	$4.05503 \times 10^{-5}$	0	-0.273162	10
$10 < Re \leq 40$	$-2.16099 \times 10^{-5}$	0.00364953	-0.163676	2.9
$40 < Re \leq 100$	$3.18815 \times 10^{-7}$	$-2.40247 \times 10^{-4}$	0.0408807	1.55
$100 < Re \leq 400$	$-3.09488 \times 10^{-8}$	$4.6687 \times 10^{-5}$	-0.0171873	0.8
$400 < Re \leq 1000$	$3.53843 \times 10^{-9}$	$-9.02083 \times 10^{-6}$	0.0054124	0.61
$1000 < Re \leq 2000$	$-2.9999 \times 10^{-10}$	$1.59446 \times 10^{-6}$	$-2.01397 \times 10^{-3}$	0.54
$2000 < Re \leq 4000$	$1.27227 \times 10^{-11}$	$-2.05476 \times 10^{-7}$	$7.64007 \times 10^{-4}$	0.49
$4000 < Re \leq 1 \times 10^4$	$-4.02937 \times 10^{-13}$	$2.35328 \times 10^{-8}$	$-3.27655 \times 10^{-4}$	0.425
$1 \times 10^4 < Re \leq 3.2 \times 10^4$	$1.81433 \times 10^{-14}$	$-3.06101 \times 10^{-9}$	$1.22725 \times 10^{-4}$	0.316
$3.2 \times 10^4 < Re \leq 1 \times 10^5$	$-2.25043 \times 10^{-15}$	$6.40229 \times 10^{-10}$	$-4.18886 \times 10^{-5}$	0.212
$1 \times 10^5 < Re \leq 2 \times 10^5$	$1.45415 \times 10^{-17}$	$-3.48995 \times 10^{-11}$	$1.86443 \times 10^{-5}$	0.175
$2 \times 10^5 < Re \leq 1 \times 10^6$	0	0	0	0.2

$P_T = 2.0$				
Interval	A	B	C	D
$0 < Re \leq 10$	$2.23049 \times 10^{-5}$	0	-0.125741	5
$10 < Re \leq 40$	$-1.90812 \times 10^{-5}$	$0.00200744$	-0.0655178	1.83
$40 < Re \leq 80$	$2.35615 \times 10^{-6}$	$-2.82301 \times 10^{-4}$	0.00348789	1.2
$80 < Re \leq 125$	$-4.80502 \times 10^{-8}$	$3.57795 \times 10^{-5}$	-0.00760557	1
$125 < Re \leq 400$	$2.64919 \times 10^{-9}$	$-3.86191 \times 10^{-6}$	0.00117177	0.615
$400 < Re \leq 1000$	$-3.50235 \times 10^{-10}$	$9.06631 \times 10^{-7}$	$-6.01397 \times 10^{-4}$	0.5
$1000 < Re \leq 2000$	$2.73707 \times 10^{-11}$	$-1.44073 \times 10^{-7}$	$1.61162 \times 10^{-4}$	0.455
$2000 < Re \leq 4000$	$-1.22867 \times 10^{-12}$	$2.01519 \times 10^{-8}$	$-8.66792 \times 10^{-5}$	0.42
$4000 < Re \leq 1 \times 10^4$	$3.44511 \times 10^{-14}$	$-1.96419 \times 10^{-9}$	$2.2447 \times 10^{-5}$	0.36
$1 \times 10^4 < Re \leq 3.2 \times 10^5$	$-1.79243 \times 10^{-15}$	$3.09581 \times 10^{-10}$	$-1.39545 \times 10^{-5}$	0.27
$3.2 \times 10^5 < Re \leq 1 \times 10^5$	$1.99347 \times 10^{-16}$	$-5.60742 \times 10^{-11}$	$3.28395 \times 10^{-6}$	0.189
$1 \times 10^5 < Re \leq 2 \times 10^5$	$-1.55409 \times 10^{-18}$	$3.72982 \times 10^{-12}$	$-1.95049 \times 10^{-6}$	0.156
$2 \times 10^5 < Re \leq 1 \times 10^6$	0	0	0	0.187

$P_T = 2.5$				
Interval	A	B	C	D
$0 < Re \leq 10$	$1.12632 \times 10^{-5}$	0	-0.0668036	3.06
$10 < Re \leq 40$	$-9.31541 \times 10^{-6}$	$0.00101369$	-0.0363929	1.36
$40 < Re \leq 80$	$8.93887 \times 10^{-7}$	$-1.04161 \times 10^{-4}$	$-1.1772 \times 10^{-5}$	0.93
$80 < Re \leq 125$	$-2.14454 \times 10^{-8}$	$1.65139 \times 10^{-5}$	-0.00395588	0.8
$125 < Re \leq 400$	$8.44713 \times 10^{-10}$	$-1.17852 \times 10^{-6}$	$2.6135 \times 10^{-4}$	0.515
$400 < Re \leq 1000$	$-1.31375 \times 10^{-10}$	$3.41962 \times 10^{-7}$	$-2.40586 \times 10^{-4}$	0.43
$1000 < Re \leq 2000$	$1.0029 \times 10^{-11}$	$-5.21638 \times 10^{-8}$	$4.92113 \times 10^{-5}$	0.4
$2000 < Re \leq 4000$	$-4.80593 \times 10^{-13}$	$8.01052 \times 10^{-9}$	$-3.90951 \times 10^{-5}$	0.37
$4000 < Re \leq 1 \times 10^4$	$1.15545 \times 10^{-14}$	$-6.40143 \times 10^{-10}$	$5.12714 \times 10^{-6}$	0.32
$1 \times 10^4 < Re \leq 3.2 \times 10^5$	$-6.88226 \times 10^{-16}$	$1.22452 \times 10^{-10}$	$-6.26205 \times 10^{-6}$	0.246
$3.2 \times 10^5 < Re \leq 1 \times 10^5$	$6.50174 \times 10^{-17}$	$-1.79457 \times 10^{-11}$	$8.444 \times 10^{-7}$	0.17
$1 \times 10^5 < Re \leq 2 \times 10^5$	$-6.49786 \times 10^{-19}$	$1.55949 \times 10^{-12}$	$-7.94226 \times 10^{-7}$	0.14
$2 \times 10^5 < Re \leq 1 \times 10^6$	0	0	0	0.17

## Appendix C

### Zhukauskas Pressure Drop Correction Factor Cubic Spline Coefficients

$$\mathcal{X} = A(Re - Re_i)^3 + B(Re - Re_i)^2 + C(Re - Re_i) + D$$

$Re = 10^2$				
Interval	A	B	C	D
$0 < P_T/P_L \leq 0.4$	0.121801	0	-0.0484627	1
$0.4 < P_T/P_L \leq 1.18$	-0.0669048	0.285014	0.173848	1.02
$1.18 < P_T/P_L \leq 2.6$	0	0	0	1.65

$Re = 10^3$				
Interval	A	B	C	D
$0 < P_T/P_L \leq 0.428$	0.637575	0	-0.106071	1.04
$0.428 < P_T/P_L \leq 0.6$	-1.03281	0.328989	-0.0494853	1.025
$0.6 < P_T/P_L \leq 0.8$	1.24917	-0.290698	-0.0418272	1.02
$0.8 < P_T/P_L \leq 1.0$	-0.580965	0.458804	-0.00820597	1.01
$1.0 < P_T/P_L \leq 1.18$	-0.0543359	0.145083	0.100494	1.02
$1.18 < P_T/P_L \leq 2.0$	-0.00447733	0.0114172	0.228824	1.17
$2.0 < P_T/P_L \leq 2.85$	0	0	0	1.37

$Re = 10^4$				
Interval	A	B	C	D
$0 < P_T/P_L \leq 0.423$	0.872977	0	-0.507575	1.2
$0.423 < P_T/P_L \leq 0.6$	0.19542	0.463551	-0.425527	1.115
$0.6 < P_T/P_L \leq 0.8$	-0.612611	0.580803	-0.216656	1.05
$0.8 < P_T/P_L \leq 1.0$	-0.256548	0.213237	-0.0578482	1.025
$1.0 < P_T/P_L \leq 1.18$	-0.00959928	0.0747007	-0.00601949	1.02
$1.18 < P_T/P_L \leq 2.0$	-0.0189209	0.0510864	0.0971259	1.06
$2.0 < P_T/P_L \leq 2.9$	0	0	0	1.175

$Re = 10^5$				
<b>Interval</b>	<b>A</b>	<b>B</b>	<b>C</b>	<b>D</b>
$0 < \frac{P_T}{P_L} \leq 0.415$	1.05731	0	-0.792943	1.44
$0.415 < \frac{P_T}{P_L} \leq 0.6$	-0.824442	0.586807	-0.684384	1.3
$0.6 < \frac{P_T}{P_L} \leq 0.8$	0.754133	0.0921426	-0.548594	1.18
$0.8 < \frac{P_T}{P_L} \leq 1.0$	-0.312484	0.544622	-0.421241	1.08
$1.0 < \frac{P_T}{P_L} \leq 1.18$	-0.169018	0.375881	-0.25555	1.02
$1.18 < \frac{P_T}{P_L} \leq 2.0$	0.0177347	-0.039903	0.0199515	0.97
$2.0 < \frac{P_T}{P_L} \leq 2.75$	0	0	0	0.97

## Appendix D

### Thermodynamic Properties of Air at 1.5 psia

#### Source:

Gupta, R., K. Lee, R. Thompson, J. Yos. "Calculations and Curve Fits of Thermodynamic and Transport Properties for Equilibrium Air to 30000 K". NASA Reference Publication 1260. October 1991.

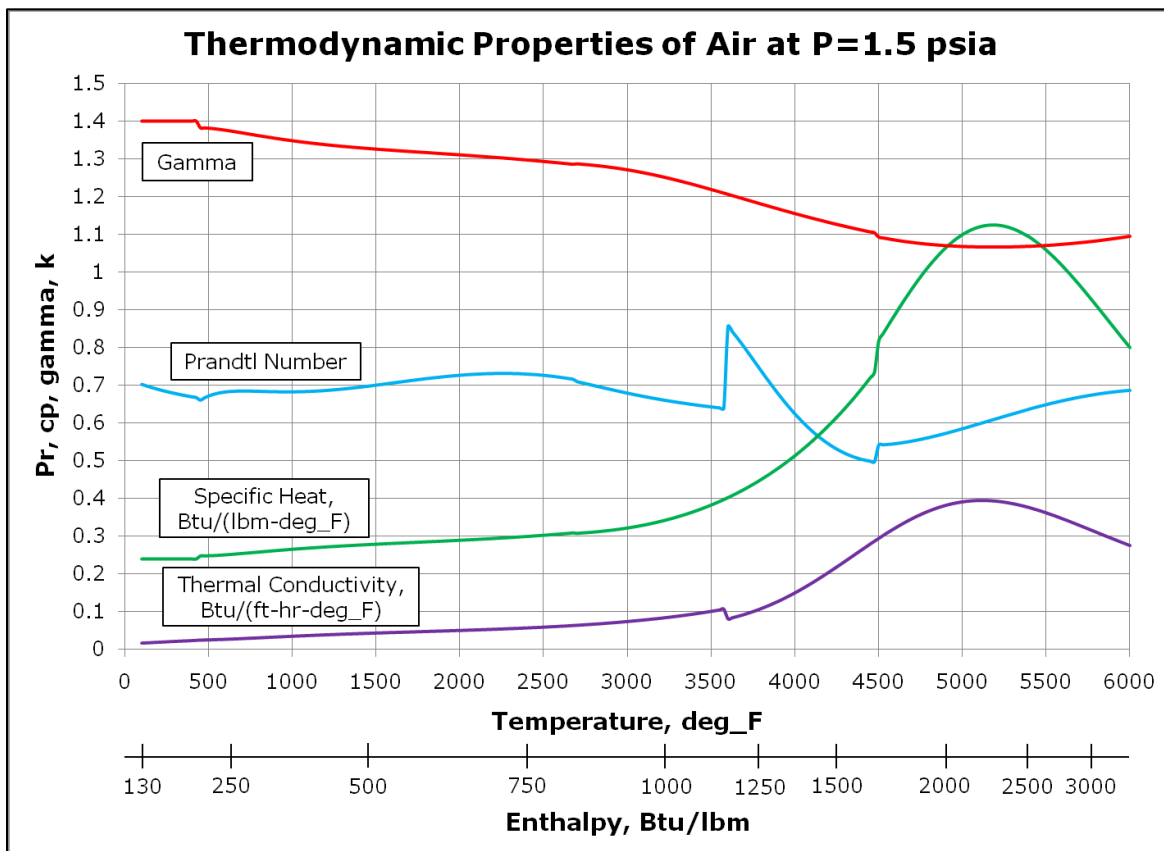


**Figure D.1 – Variation of the Prandtl number, specific heat, specific heat ratio, and thermal conductivity of air with temperature and enthalpy at 1.5 psia**

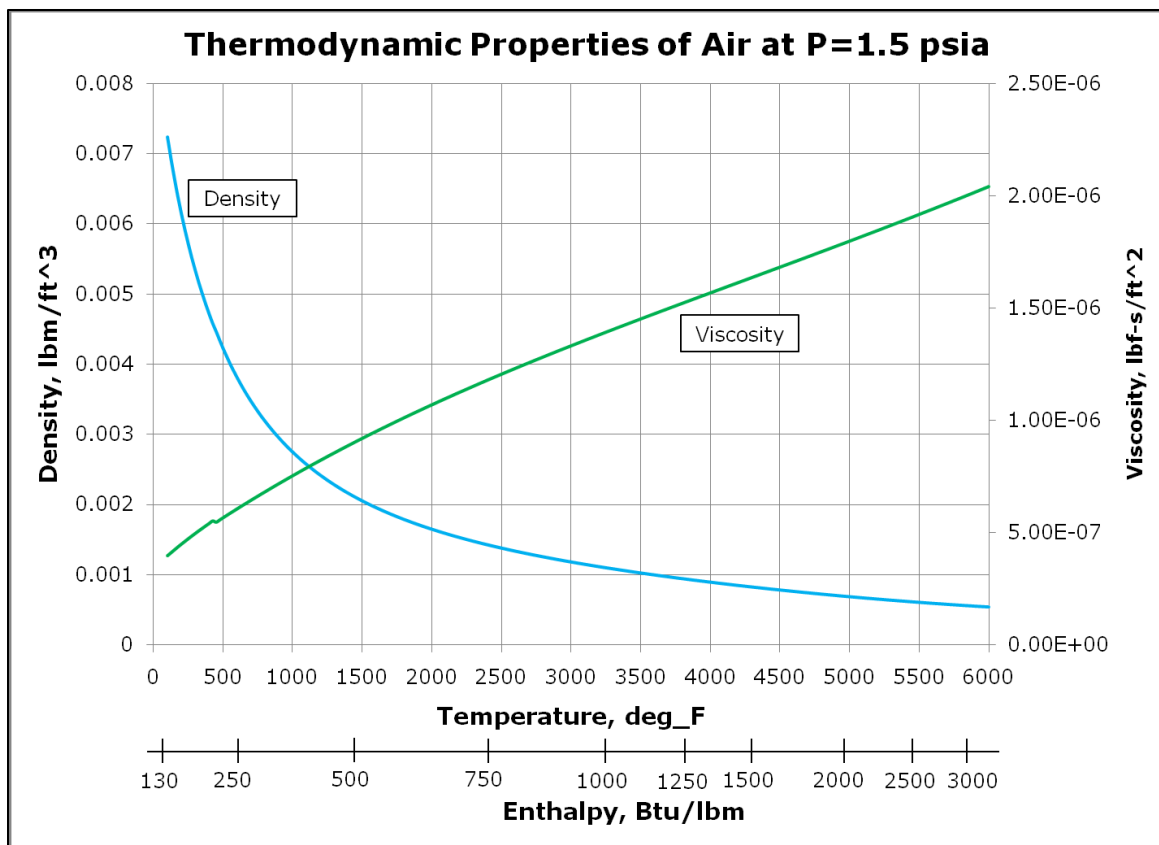


**Figure D.2 – Variation of the density and viscosity of air with temperature and enthalpy at 1.5 psia**

**Table D.1 – Thermodynamic Properties of High Temperature Air at 1.5 psia**

<i>T</i>	<i>i</i>	<i>ρ</i>	<i>k</i>	<i>c<sub>p</sub></i>	<i>γ</i>	<i>μ</i>	<i>Pr</i>
°F	Btu/lb <sub>m</sub>	lb <sub>m</sub> /ft <sup>3</sup>	Btu/ft - hr - °F	Btu/lb <sub>m</sub> - °F	—	lb <sub>f</sub> - s/ft <sup>2</sup>	—
100	134.322	7.23E-03	0.016	0.240	1.40	3.96E-07	0.702
200	158.322	6.14E-03	0.018	0.240	1.40	4.48E-07	0.689
300	182.323	5.33E-03	0.020	0.240	1.40	4.96E-07	0.678
400	206.323	4.71E-03	0.022	0.240	1.40	5.40E-07	0.669
500	233.699	4.22E-03	0.024	0.248	1.38	5.66E-07	0.672
600	256.303	3.81E-03	0.026	0.251	1.38	6.05E-07	0.682
700	281.447	3.47E-03	0.028	0.255	1.37	6.43E-07	0.685
800	308.231	3.19E-03	0.030	0.258	1.36	6.81E-07	0.684
900	336.026	2.95E-03	0.032	0.262	1.35	7.17E-07	0.683
1000	364.379	2.75E-03	0.034	0.266	1.35	7.53E-07	0.683
1100	392.966	2.57E-03	0.036	0.269	1.34	7.88E-07	0.684
1200	421.563	2.41E-03	0.038	0.272	1.34	8.22E-07	0.686
1300	450.02	2.28E-03	0.039	0.275	1.33	8.55E-07	0.690
1400	478.251	2.16E-03	0.041	0.277	1.33	8.88E-07	0.695
1500	506.22	2.05E-03	0.042	0.279	1.33	9.19E-07	0.700
1600	533.927	1.95E-03	0.044	0.281	1.32	9.50E-07	0.706
1700	561.405	1.87E-03	0.045	0.283	1.32	9.81E-07	0.712
1800	588.709	1.79E-03	0.047	0.285	1.32	1.01E-06	0.718
1900	615.913	1.71E-03	0.048	0.287	1.31	1.04E-06	0.723
2000	643.104	1.65E-03	0.049	0.290	1.31	1.07E-06	0.727
2100	670.379	1.59E-03	0.051	0.292	1.31	1.10E-06	0.730
2200	697.845	1.53E-03	0.052	0.294	1.30	1.12E-06	0.731
2300	725.613	1.48E-03	0.054	0.297	1.30	1.15E-06	0.731
2400	753.797	1.43E-03	0.056	0.300	1.30	1.18E-06	0.730
2500	782.518	1.38E-03	0.058	0.303	1.29	1.21E-06	0.726
2600	811.897	1.34E-03	0.061	0.306	1.29	1.23E-06	0.721
2700	842.06	1.29E-03	0.063	0.308	1.29	1.26E-06	0.710
2800	873.133	1.25E-03	0.066	0.311	1.28	1.28E-06	0.699
2900	905.249	1.22E-03	0.070	0.316	1.28	1.31E-06	0.689

**Table D.1 – Thermodynamic Properties of High Temperature Air at 1.5 psia  
(continued)**

<b>T</b>	<b>i</b>	<b><math>\rho</math></b>	<b>k</b>	<b><math>c_p</math></b>	<b><math>\gamma</math></b>	<b><math>\mu</math></b>	<b><math>Pr</math></b>
<b>°F</b>	<b>Btu/lb<sub>m</sub></b>	<b><math>lb_m/ft^3</math></b>	<b><math>Btu/ft - hr - °F</math></b>	<b><math>Btu/lb_m - °F</math></b>	—	<b><math>lb_f - s/ft^2</math></b>	—
3000	938.54	1.18E-03	0.073	0.322	1.27	1.33E-06	0.679
3100	973.145	1.15E-03	0.077	0.330	1.26	1.36E-06	0.670
3200	1009.2	1.12E-03	0.082	0.340	1.25	1.38E-06	0.662
3300	1046.86	1.08E-03	0.087	0.352	1.24	1.40E-06	0.655
3400	1086.28	1.05E-03	0.093	0.366	1.23	1.43E-06	0.648
3500	1127.61	1.03E-03	0.100	0.383	1.22	1.45E-06	0.642
3600	1171.01	9.97E-04	0.080	0.403	1.21	1.47E-06	0.856
3700	1216.67	9.70E-04	0.092	0.425	1.19	1.50E-06	0.799
3800	1264.76	9.44E-04	0.108	0.451	1.18	1.52E-06	0.737
3900	1315.47	9.19E-04	0.127	0.480	1.17	1.54E-06	0.677
4000	1369.02	8.94E-04	0.150	0.514	1.15	1.57E-06	0.624
4100	1425.62	8.71E-04	0.175	0.551	1.14	1.59E-06	0.579
4200	1485.49	8.48E-04	0.204	0.593	1.13	1.61E-06	0.544
4300	1548.88	8.25E-04	0.234	0.640	1.12	1.64E-06	0.519
4400	1616.06	8.04E-04	0.265	0.692	1.11	1.66E-06	0.503
4500	1687.29	7.83E-04	0.295	0.818	1.09	1.68E-06	0.541
4600	1762.89	7.63E-04	0.323	0.890	1.08	1.70E-06	0.545
4700	1843.16	7.43E-04	0.347	0.957	1.08	1.73E-06	0.552
4800	1928.46	7.24E-04	0.368	1.016	1.07	1.75E-06	0.561
4900	2019.14	7.05E-04	0.383	1.064	1.07	1.77E-06	0.572
5000	2115.6	6.88E-04	0.392	1.099	1.07	1.80E-06	0.585
5100	2218.27	6.70E-04	0.396	1.120	1.07	1.82E-06	0.598
5200	2327.6	6.54E-04	0.394	1.125	1.06	1.84E-06	0.611
5300	2444.08	6.38E-04	0.387	1.115	1.07	1.87E-06	0.624
5400	2687.19	6.22E-04	0.376	1.093	1.07	1.89E-06	0.637
5500	2799.6	6.07E-04	0.363	1.058	1.07	1.92E-06	0.649
5600	2902.23	5.93E-04	0.346	1.015	1.07	1.94E-06	0.659
5700	2995.77	5.79E-04	0.329	0.965	1.08	1.97E-06	0.668
5800	3081.02	5.66E-04	0.311	0.911	1.08	1.99E-06	0.676
5900	3158.87	5.53E-04	0.293	0.855	1.09	2.02E-06	0.682
6000	3230.24	5.41E-04	0.276	0.800	1.09	2.04E-06	0.687

## **Vita**

Gary Hammock graduated from Westmoreland High School, in Westmoreland, Tennessee in 2001. He attended Tennessee Technological University from 2001 to 2005, graduating with a Bachelor of Science degree in Mechanical Engineering. After graduating from TTU, he accepted a position working as an engineer analyst and project engineer for Aerospace Testing Alliance at Arnold Air Force Base in 2005. Gary obtained a professional engineering license in 2010. He is continuing his education to obtain a Master of Science degree in Mechanical Engineering from the University of Tennessee. After which, he plans to pursue a graduate degree in computer science.